USGS
science for a changing world

Rocky
8/5/99

GROUND-WATER HYDROLOGY AND SIMULATION OF FIVE REMEDIATION ALTERNATIVES FOR AN AREA AFFECTED BY URANIUM-MILL EFFLUENT NEAR CAÑON CITY, COLORADO

U.S. GEOLOGICAL SURVEY

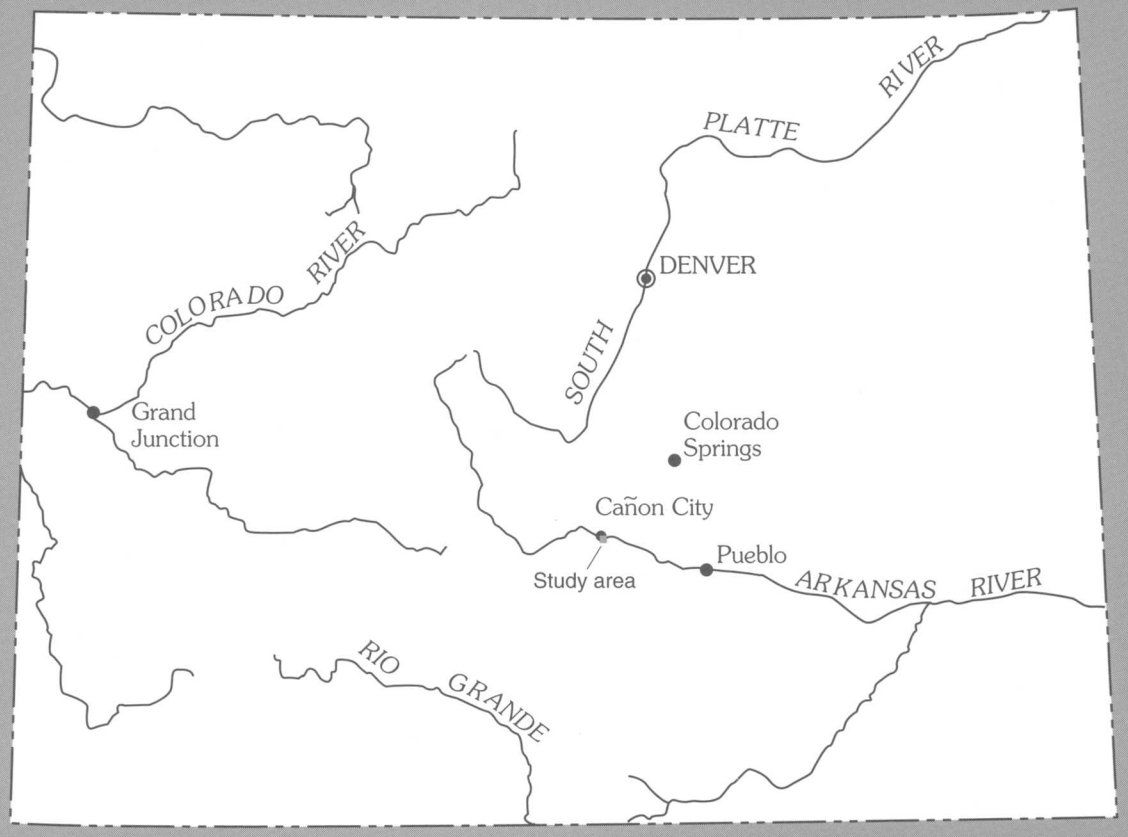

Water-Resources Investigations Report 98–4229

Prepared in cooperation with the
COLORADO DEPARTMENT OF PUBLIC HEALTH AND ENVIRONMENT

Ground-Water Hydrology and Simulation of Five Remediation Alternatives for an Area Affected by Uranium-Mill Effluent near Cañon City, Colorado

By Edward R. Banta and Daniel T. Chafin

U.S. GEOLOGICAL SURVEY

Water-Resources Investigations Report 98–4229

Prepared in cooperation with the
COLORADO DEPARTMENT OF PUBLIC HEALTH AND ENVIRONMENT

Denver, Colorado
1999

U.S. DEPARTMENT OF THE INTERIOR
BRUCE BABBITT, Secretary

U.S. GEOLOGICAL SURVEY
Charles G. Groat, Director

For additional information write to:

District Chief
U.S. Geological Survey
Box 25046, Mail Stop 415
Denver Federal Center
Denver, CO 80225–0046

Copies of this report can be purchased from:

U.S. Geological Survey
Information Services
Box 25286
Federal Center
Denver, CO 80225

CONTENTS

FIGURES

TABLES

CONVERSION FACTORS, VERTICAL DATUM, AND ABBREVIATIONS

Multiply	By	To obtain
acre	0.4047	hectare
centimeter	0.3937	inch
centimeter per month (cm/mo)	0.3937	inch per month
centimeter per second (cm/s)	0.03281	foot per second
cubic foot (ft^3)	0.02832	cubic meter
cubic foot per day (ft^3/d)	0.02832	cubic meter per day
cubic foot per second (ft^3/s)	0.02832	cubic meter per second
cubic foot per second per mile [(ft^3/s)/mi]	0.01760	cubic meter per second per kilometer
cubic meter per kilogram (m^3/kg)	515.2	cubic foot per slug
foot (ft)	0.3048	meter
foot per day (ft/d)	0.3048	meter per day
foot per mile (ft/mi)	0.1894	meter per kilometer
gallon per minute (gal/min)	3.785	liter per minute
inch (in.)	2.54	centimeter
inch per day (in/d)	2.54	centimeter per day
inch per year (in/yr)	2.54	centimeter per year
inverse foot (ft^{-1})	3.281	inverse meter
kilogram per cubic meter (kg/m^3)	0.001941	slug per cubic foot
kilogram per cubic meter per second [(kg/m^3)/s]	0.001941	slug per cubic foot per second
liter per day (L/d)	1.835×10^{-4}	gallon per minute
meter (m)	3.281	foot
meter per second (m/s)	3.281	foot per second
mile (mi)	1.609	kilometer
million gallons (Mgal)	3.785×10^6	liter
square foot (ft^2)	0.0929	square meter
square foot per day (ft^2/d)	0.0929	square meter per day
square meter (m^2)	10.76	square foot
square mile (mi^2)	2.59	square kilometer

Temperature in degrees Celsius (°C) may be converted to degrees Fahrenheit (°F) as follows:

$$°F = (1.8 \times °C) + 32$$

Other abbreviations, terms, and symbols used in this report:

gram per cubic centimeter (g/cm^3)
inverse second (sec^{-1})
microgram per liter (µg/L)
milligram per kilogram (mg/kg)
milligram per liter (mg/L)

Sea level: In this report, "sea level" refers to the National Geodetic Vertical Datum of 1929 (NGVD of 1929)—a geodetic datum derived from a general adjustment of the first-order level nets of both the United States and Canada, formerly called Sea Level Datum of 1929.

Ground-Water Hydrology and Simulation of Five Remediation Alternatives for an Area Affected by Uranium-Mill Effluent near Cañon City, Colorado

By Edward R. Banta *and* Daniel T. Chafin

Abstract

Leakage of water from unlined uranium-mill tailings ponds, operated from 1958 to 1979 near Cañon City, Colorado, resulted in contamination of shallow ground water with uranium and molybdenum. The ground-water system affected by the contamination is in consolidated and unconsolidated rocks ranging in age from Cretaceous to Quaternary. An upgradient area, where the tailings ponds were located, is characterized by consolidated rocks, which are weathered or fractured in places and overlain in places by alluvium. The downgradient area is characterized by alluvium overlying bedrock. In the vicinity of the tailings ponds, solid-phase contaminant concentrations were largest in intervals above the water table. Results of a prior pilot test of a remediation method in which water was injected and withdrawn to flush contaminants from materials in the vicinity of the tailings ponds indicated that solid-phase concentrations did not decrease in proportion to decreases in aqueous concentrations; the difference was ascribed to nonequilibrium between the solid and aqueous phases. The nonequilibrium likely was due, in part, to fracturing in the consolidated materials.

Results of three-dimensional ground-water flow modeling were used as a basis for two-dimensional modeling of contaminant transport in the ground-water system. Modeling of contaminant transport accounted for the nonequilibrium between the solid and the aqueous phases of the contaminants by using a model capable of simulating rate-limited sorption and desorption. The contaminant-transport model was calibrated using contaminant-concentration data for samples collected between 1978 and 1995.

The calibrated contaminant-transport model was used to simulate over 50 years the likely effects of five proposed remediation alternatives in addition to a no-action scenario. The remediation alternatives that were simulated are: (1) Simultaneous injection of municipal water derived from the Arkansas River into wells completed at depths of about 10 to 75 feet and withdrawal of water through gravel-filled trenches in the area of the old, unlined tailings ponds; (2) removal of earth materials from the unsaturated zone in the area of the old, unlined tailings ponds that have uranium or molybdenum concentrations substantially larger than background concentrations; (3) injection of water into wells and withdrawal of water through trenches, as in alternative 1, followed by removal of contaminated earth materials, as in alternative 2; (4) installation of a layered cover system in the area of the old, unlined tailings ponds; and (5) application of a reducing agent to decrease the mobility of the contaminants in the area of the old, unlined tailings ponds.

In all the simulations, including the no-action scenario, uranium and molybdenum concentrations at contaminated sites in the upgradient and downgradient areas were predicted to decrease substantially in response to remedial actions that had been implemented as of 1996. Contaminant concentrations at a

site in the upgradient area were predicted to be strongly affected by the various remediation alternatives. At a site in the downgradient area, however, predicted effects of the remediation alternatives were small. Alternative 3 was predicted to produce the largest decreases in contaminant concentrations at the upgradient site. The predicted relative effectiveness of the other alternatives differed for the two contaminants. The second most effective alternative for uranium remediation was alternative 5, but for molybdenum, alternative 1 was the second most effective.

INTRODUCTION

A uranium-ore processing mill began operating at a site south of Cañon City, Colorado, in 1958. From 1958 through 1979, mill wastes were discharged to a series of unlined tailings ponds adjacent to the mill. In this report, the term "raffinate" refers to liquid wastes discharged directly from the uranium mill and to leachate derived from mill tailings. In 1978, ground water from some wells in Lincoln Park, a suburban community that is immediately south of Cañon City and that is situated between the mill and the Arkansas River, was determined (W.A. Wahler & Associates, 1978) as being affected, as early as 1968, by contaminants presumably originating from the tailings ponds. Uranium and molybdenum were identified as two constituents of particular concern. In 1984, Lincoln Park was placed on the National Priorities List (U.S. Environmental Protection Agency, 1984) required by the Comprehensive Environmental Response, Compensation, and Liability Act of 1980 (CERCLA, Public Law 96–510). Past remedial activities have included: (1) Construction projects designed to decrease the source of contamination or to impose a barrier to ground-water flow, and (2) hydraulic stresses designed to limit or enhance transport of contaminants in ground water. Specific remedial activities that strongly affected the ground-water flow or transport of contaminants are discussed in the "Physical Ground-Water System" section. In 1994, the U.S. Geological Survey, in cooperation with the Colorado Department of Public Health and Environment, began a study to evaluate the geohydrology and geochemistry of the vicinity of the uranium mill and Lincoln Park and to evaluate the effectiveness of several remediation alternatives.

Purpose and Scope

This report: (1) Characterizes the ground-water hydrology and geochemistry of ground water near the uranium mill and the immediately surrounding area, including Lincoln Park; and (2) comparatively evaluates the effects of five remediation alternatives that have been proposed to alleviate the contamination of ground water by uranium and molybdenum. The five alternatives are: (1) Simultaneous injection of municipal water derived from the Arkansas River into wells completed at depths of about 10 to 75 ft and withdrawal of water through gravel-filled trenches in the area of the old, unlined tailings ponds; (2) removal of earth materials from the unsaturated zone in the area of the old, unlined tailings ponds that have uranium or molybdenum concentrations substantially larger than background concentrations; (3) injection of water into wells and withdrawal of water through trenches, as in alternative 1, followed by removal of contaminated earth materials, as in alternative 2; (4) installation of a layered cover system in the area of the old, unlined tailings ponds; and (5) application of a reducing agent to decrease the mobility of the contaminants in the area of the old, unlined tailings ponds.

This report presents a quantitative description of the ground-water hydrology of the unconsolidated deposits and near-surface bedrock of the study area. It also documents the development and calibration of ground-water flow and contaminant-transport models of the study area. In addition to the natural ground-water system, the models simulated remedial actions that had been implemented in the study area as of 1996. The purpose of the numerical models was to serve as tools for comparing the possible effects of the proposed remediation alternatives on uranium and molybdenum concentrations for 50 years from the start of a particular remediation alternative. Conclusions based on the interpretation of the hydrologic system and model results also are presented. Although the geochemistry of the study area is briefly described in this report, a more detailed discussion is contained in Chafin and Banta (1999).

Description of the Study Area

The uranium mill (fig. 1) is located in a structural basin bounded by a hogback-shaped ridge immediately to the south of the mill and a lower ridge situated between the mill and Lincoln Park. The hogback-shaped ridge and the lower ridge were formed by the erosionally resistant Raton Formation of Tertiary and Cretaceous age. In this report, the hogback-shaped ridge south of the mill is referred to as the hogback, and the ridge between the mill and Lincoln Park is referred to as the Raton ridge.

Between the hogback and the Raton ridge, the land surface is moderately rolling and slopes generally northeastward at about 100 ft/mi. In addition to the uranium mill and its associated facilities, this area includes a golf course, which is located north of the mill.

Lincoln Park is on relatively flat land that forms a terrace between the Raton ridge and an escarpment on the south side of the Arkansas River. Land surface in Lincoln Park slopes northeastward at about 80 ft/mi.

The study area extends from the hogback on the south to the escarpment between Lincoln Park and the Arkansas River on the north and approximately from Oak Creek Grade Road on the west to the unnamed ephemeral stream on which the Willow Lakes are located on the east (fig. 1). The areal extent of the study area is 6.2 mi^2.

Previous Work

The site of the uranium mill and the surrounding areas have been the subject of numerous investigations by government agencies and by consulting firms working under contract either to the government agencies or to the owners of the mill. References in this section are to reports that are most pertinent to the purposes of this report.

The geology of the study area was described in reports by Hershey (1977) and by Scott (1977). W.A. Wahler & Associates (1978) and Environ Corp. and others (1991) documented migration of the contaminant plume. A remedial-investigation report was prepared by Geotrans, Inc., and others (1986). Hearne and Litke (1987) discussed potential flow paths for the contaminant plume and hydraulic characteristics and geochemistry of water from several geologic units. Ground-water flow and contaminant-transport models were documented in Adrian Brown Consultants, Inc. (1993), and in Daniel B. Stephens & Associates, Inc. (1993). Extensive compilations of field data are contained in Adrian Brown Consultants, Inc. (1993), Daniel B. Stephens & Associates, Inc. (1993), and Banta (1997). An investigation of the contaminant plume using uranium isotopes was reported by Zielinski and others (1997).

Acknowledgments

The authors thank Richard L. Naff, U.S. Geological Survey, for providing the computer code used in validation of the contaminant-transport-model modifications documented in the "Supplemental Information" section and for assistance in preparation of that section. Conversations with Mary C. Hill and Richard L. Cooley, both of the U.S. Geological Survey, regarding the parameter-estimation methods used in this report were appreciated. Conversations with David L. Parkhurst and Kenneth G. Stollenwerk, also of the U.S. Geological Survey, helped in the interpretation of the geochemistry of the study area.

PHYSICAL GROUND-WATER SYSTEM

Ground-water flow and the associated transport of solutes in the study area are largely controlled by such natural factors as rate of recharge from precipitation, lithology, geologic structure, and fractures. Anthropogenic modifications in the study area have substantially altered the natural ground-water system. This section presents a conceptual model of the ground-water system, including natural and anthropogenic factors.

Geology and Anthropogenic Modifications to Earth Materials

Geology of the study area is shown in figure 2. Two sources of geologic mapping were used to generate this map. The primary source of information was Scott (1977); however, details of

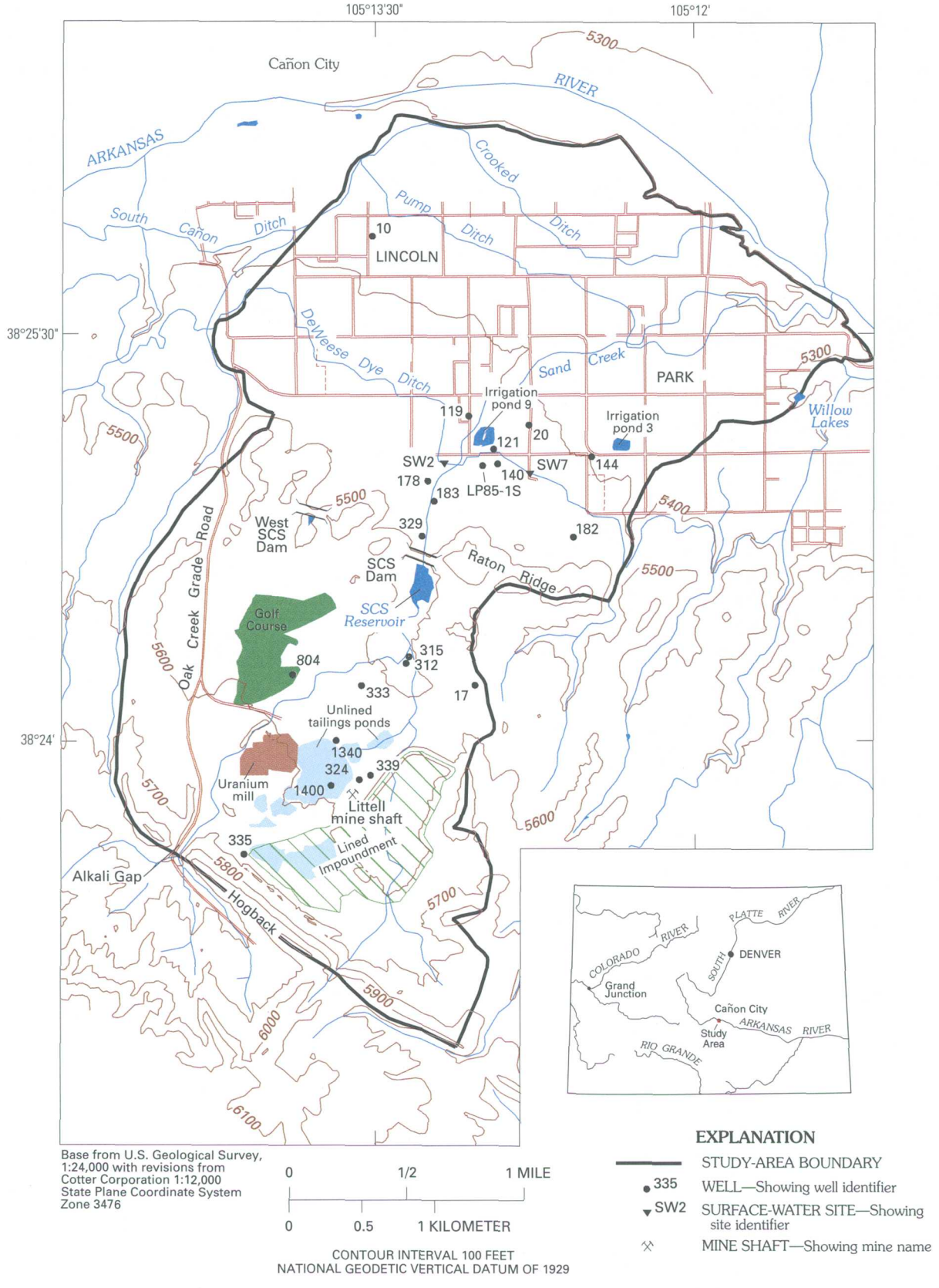

Figure 1. Location of the study area.

the distribution of deposits of Quaternary age along Sand Creek and its tributaries were adapted from Hershey (1977). Evidence that alluvium of Quaternary age is present in areas along Sand Creek is provided by field observations and by Hearne and Litke (1987), who described four wells constructed through alluvium in 1985. Some geologic units that are present only outside the study area were combined to simplify the map. The stratigraphic units of interest in the study area are listed and described in table 1.

Weathered zones and fractures commonly are listed in descriptions of cuttings and cores obtained from near-surface parts of the Poison Canyon Formation of Tertiary age and the Vermejo Formation of Cretaceous age. The Raton Formation also is fractured (Hershey, 1977). The depth to which weathering and fracturing extends below the land surface was characterized using a data file containing lithologic descriptions of intervals in wells and boreholes drilled in the study area (Banta, 1997). For 20-ft-depth classes, the number of descriptions that included references to weathering or fracturing was counted and expressed as a percentage of the total number of intervals in each depth class (table 2). The percentage of total intervals described as weathered or fractured ranged from 2.9 to 5.4 percent in the five depth classes between land surface and 100 ft below land surface. The percentage decreased substantially in the 100- to 120-ft class, and intervals described as weathered or fractured were rare at depths greater than 120 ft.

The uranium mill is situated in a small structural basin formed by the Chandler Syncline (Scott, 1977). The hogback and the Raton ridge, which define the north and south boundaries of the basin, are formed by the hard sandstone of the Raton Formation. Between the hogback and the Raton ridge, bedrock layers from the Pierre Shale of Cretaceous age to the Poison Canyon Formation are folded so that a given stratigraphic horizon is at its lowest altitude approximately under the former location of the old tailings ponds (fig. 3). Northeast of the Raton ridge, the Vermejo Formation, Trinidad Sandstone, and Pierre Shale, all of Cretaceous age, subcrop under the alluvium and terrace alluvium of Quaternary age (fig. 2). Alluvium occupies a narrow band adjacent to Sand Creek, and terrace alluvium underlies most of Lincoln Park. Alluvium-filled channels cut the Raton ridge formed by the Raton Formation at two places. The gap in the Raton ridge through which Sand Creek passes is referred to as the Sand Creek gap in this report. Another gap in the Raton ridge, west of the Sand Creek gap, is called the west gap. For a more detailed discussion of the geology of the study area, the reader is referred to Hearne and Litke (1987).

Mining of coal from the Vermejo Formation has resulted in shafts and underground rooms where the coal has been removed. Chafin and Banta (1999) included a map showing the locations of mines in the study area. The shaft having the most potential effect on ground-water flow in the study area is the Littell mine shaft, which was located near the old tailings ponds (fig. 1); the depth to the coal mine is about 1,000 ft (Hearne and Litke, 1987). The shaft was filled with gravel in 1978 (Geotrans, Inc., and others, 1986).

Earth-moving operations at the study area locally have resulted in substantial changes to the natural physiography. Earth-fill flood-control dams were constructed of locally derived earth fill by the Soil Conservation Service (SCS) [now (1998) the Natural Resources Conservation Service] in the Sand Creek and west gaps in 1971. The dam at the Sand Creek gap is referred to as the SCS dam in this report. The dam at the west gap is referred to as the west SCS dam. Between 1978 and 1980, an impoundment was constructed adjacent to the uranium mill and consists of clay layers, gravel drains, and a synthetic liner to accept mill wastes and tailings from the old tailings ponds (fig. 1). In about 1979, gravel-filled trenches were constructed to intercept ground-water flow in the vicinity of the old tailings ponds and immediately upgradient from the SCS reservoir.

In 1988, a barrier was constructed on the south side of the SCS dam to decrease ground-water flow through Sand Creek gap. Unconsolidated deposits and fractured bedrock along the south side of the dam were removed to allow the base of the barrier to be constructed on the unfractured part of the Vermejo Formation. However, the base of the barrier is on weathered shale of the Vermejo Formation near the east end of the barrier. Locally derived clay-rich material was used to construct the barrier (Preston L. Niesen, Cotter Corporation, oral commun., 1995).

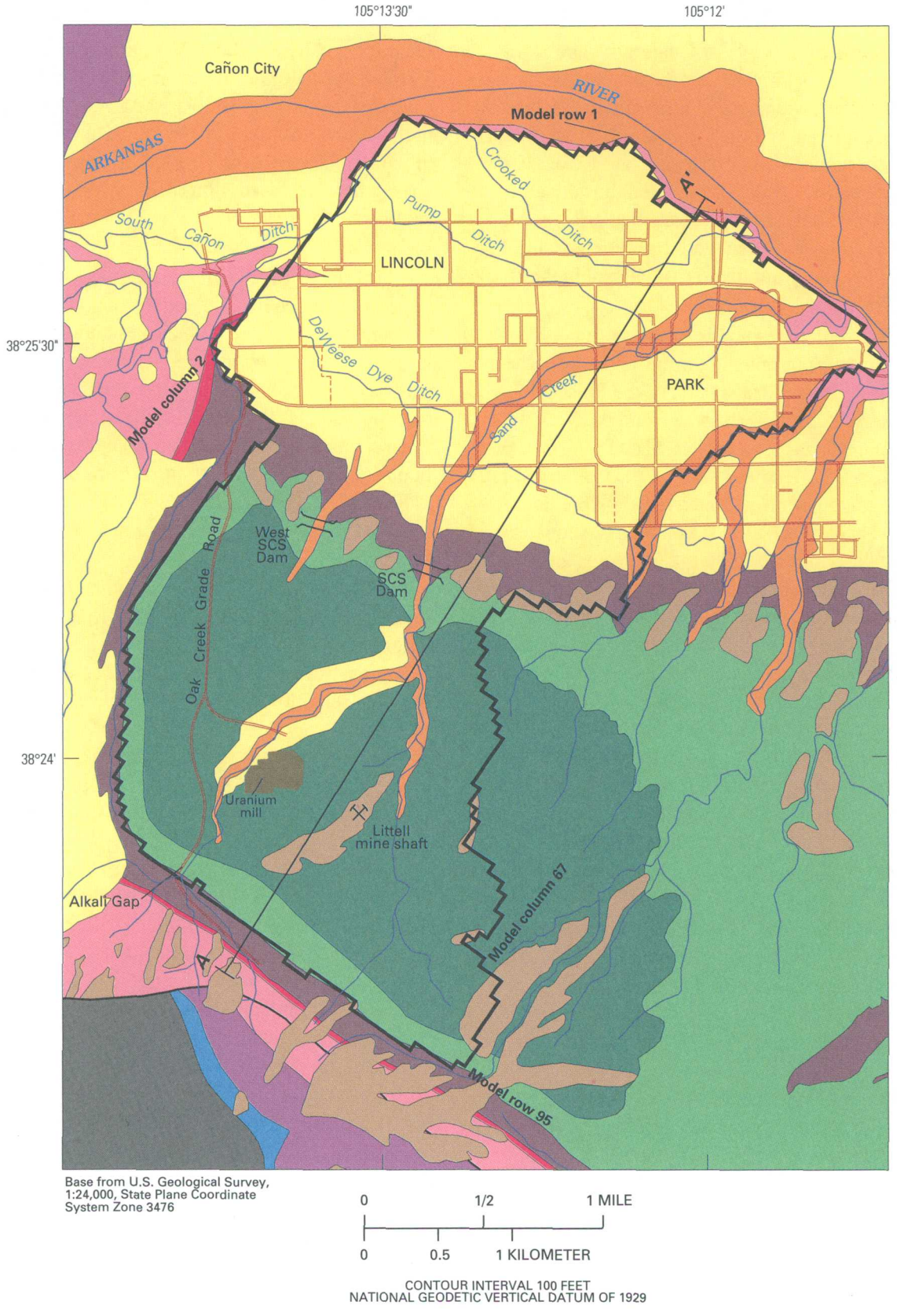

Figure 2. Geology of the study area.

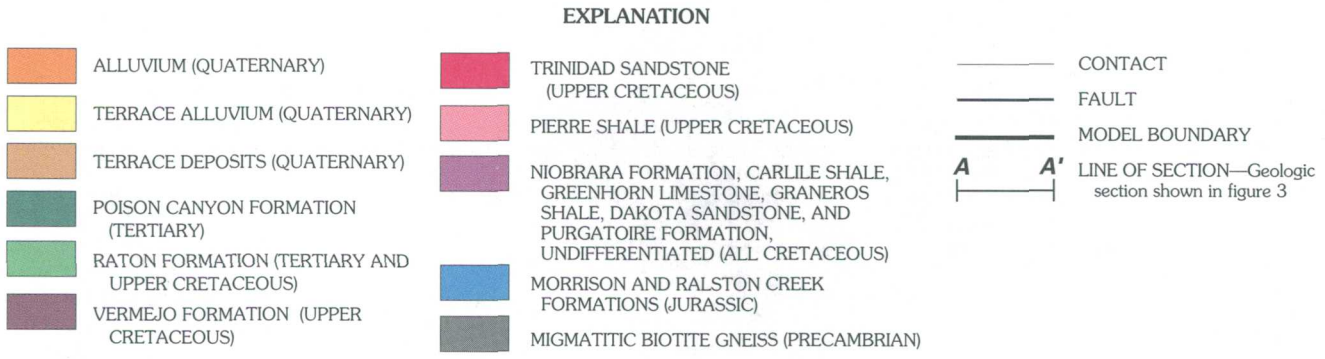

Figure 2. Geology of the study area—Continued.

Hydrology

The area of the ground-water system considered for analysis in this report is bounded on the south by the hogback and on the north by the escarpment between Lincoln Park and the Arkansas River. On the east, the analysis area is bounded from the escarpment to the Raton ridge by the unnamed tributary of the Arkansas River on which the Willow Lakes are located and from the Raton ridge to the hogback by the drainage divide between this unnamed tributary and Sand Creek. On the west, the analysis area is bounded by the limit of the Raton Formation along a low ridge trending approximately northward from the west end of the hogback (fig. 2) to the Raton ridge and approximately by the limit of terrace alluvium near South Cañon Ditch; one section of this boundary is across an area where terrace alluvium is present. In the next two sections, the hydrology is described in terms of (1) the geohydrologic setting and (2) the important hydrologic stresses and processes.

Table 1. Lithologic and hydraulic characteristics of geologic units of interest in the study area

[Lithologic descriptions are modified from Scott (1977)]

System	Series	Geologic unit and thickness	Lithologic and hydraulic characteristics
Quaternary	Holocene	Alluvium, 1–10 feet	Sand and gravel, locally very coarse near the hogback. Hydraulic conductivity is large compared to other units.
	Holocene and Pleistocene	Terrace alluvium, 0–60 feet	Gravel, sand, silt, and clay. Hydraulic conductivity ranges from moderate to large compared to other units. Yields 10 to 400 gallons per minute to wells in Lincoln Park (Daniel B. Stephens & Associates, Inc., 1993).
	Pleistocene	Terrace deposits, 0–20 feet	Alluvial and colluvial gravel; contains some sand, silt, and clay. In places, contains pebbles, cobbles, and boulders. Generally unsaturated.
Tertiary	Paleocene	Poison Canyon Formation, 0–1,000 feet	Claystone, siltstone, and medium-grained to pebbly sandstone; conglomerate in lower part. Hydraulic conductivity ranges from about 1.4×10^{-6} to about 370 feet per day.
Tertiary and Cretaceous	Paleocene and Upper Cretaceous	Raton Formation, 0–500 feet	Hard, medium- to coarse-grained sandstone. Hydraulic conductivity ranges from about 3.7×10^{-3} to about 1.7 feet per day.
Cretaceous	Upper Cretaceous	Vermejo Formation, 0–1,100 feet	Shaly, fine- to medium-grained sandstone interlayered with sandy to clayey shale and coal. In some areas, removal of coal layers by mining has resulted in water-filled voids. Some of the coal beds are fractured. Hydraulic conductivity is variable; it probably is small in the shale or shaly intervals and moderately large in zones of fractured coal compared to other units.
		Trinidad Sandstone, 0–90 feet	Fine- to medium-grained sandstone interlayered with carbonaceous shale. Hydraulic conductivity is unknown, but is likely to be small to moderate compared to other units.
		Pierre Shale, 3,900 feet	Clayey, silty, and sandy shale containing bentonite beds. Hydraulic conductivity is small compared to other units.

Table 2. Well and borehole intervals described as weathered or fractured

Depth class (feet)	Total number of described intervals	Number of intervals described as weathered or fractured	Percentage of total intervals described as weathered or fractured
0–20	1,233	36	2.9
20–40	1,372	74	5.4
40–60	836	40	4.8
60–80	219	7	3.2
80–100	160	7	4.4
100–120	71	1	1.4
120–140	47	0	0
140–160	26	0	0
160–180	14	0	0
180–200	5	0	0
200–1,740	736	2	0.3

Geohydrologic Setting

The ground-water system can be conceptually divided by the Raton ridge into two areas: (1) An upgradient area near the uranium mill, where hydraulic conductivities generally are small and the ground-water flow in the bedrock, although small in magnitude, is an important part of the ground-water regime; and (2) a downgradient area in and near Lincoln Park, where flow in permeable, unconsolidated sediments dominates the ground-water regime. In both areas, the water table is assumed to be the upper limit of the ground-water flow system. The definition of the lower limit of the system differs in the two areas.

In the upgradient area, ground water is in the alluvium; terrace alluvium; Poison Canyon, Raton, and Vermejo Formations; Trinidad Sandstone; and Pierre Shale. Of these geologic units, only alluvium and terrace alluvium are permeable enough to transmit large volumes of ground water at substantial rates. In the bedrock units, which are of Tertiary age and older, the rate of ground-water flow is limited by small hydraulic conductivities (table 1), although fractures in the bedrock, where present, allow small amounts of water to travel at substantial velocities. The base of the ground-water system analyzed in this report in most of the upgradient area is the contact between the Raton Formation and the underlying Vermejo Formation. Below this contact, the Vermejo Formation, because of its content of shale and clayey shale, is considered to be impermeable to flow across the bedding planes.

Geotrans, Inc., and others (1986) estimated the hydraulic conductivity of the material used to fill the Littell mine shaft (fig. 1) as about 100 to 450 ft/d, based on a grain-size analysis. The same report indicates that the head in the mine (well 339) was about 5,425 ft above sea level on April 19, 1985. Well 339 has a total depth of 1,058 ft (Banta, 1997) in the mine workings. On April 24, 1985, the water level in nearby well 324, which was completed in the Poison Canyon Formation between depths of 250 and 350 ft, was 112.2 ft below the measuring point of 5,579.1 ft above sea level (Banta, 1997). The head in well 324, at 5,467 ft, was 42 ft above the head in the mine. Wells 324 and 339 are within 560 ft of the Littell mine shaft (fig. 1). Because of the large hydraulic conductivity of the materials used to fill the Littell mine shaft, it is a conduit through the Vermejo Formation. The difference in hydraulic head between the mine and the materials overlying the mine indicates that the direction of flow in the mine shaft was from the overlying materials to the mine.

At the margin of the upgradient area, the Vermejo Formation directly underlies the terrace alluvium or alluvium. In these areas, because of weathering and fracturing, the upper few tens of feet of the Vermejo Formation is assumed to be permeable enough to be part of the ground-water flow system.

Most of the monitoring wells constructed in the upgradient area were completed in the Poison Canyon Formation and yield only small amounts of water; these wells generally need several hours or overnight to recover when purged for sampling. In contrast, well 333 (fig. 1) has been pumped almost continuously since about 1981. Estimates of hydraulic conductivity from aquifer tests conducted in well 333 range from 4.93 to 49.3 ft/d (Daniel B. Stephens & Associates, Inc., 1993). This range of hydraulic conductivity is characteristic of silt or sand. The location of this well is near the mapped contact between the Poison Canyon Formation and the terrace alluvium; however, the source of most of the water yielded by this well probably is the terrace alluvium.

Estimates of hydraulic conductivity for the Poison Canyon Formation range from about 1.4×10^{-6} to about 370 ft/d (Daniel B. Stephens & Associates, Inc., 1993). Hydraulic conductivity of the Poison

Canyon has no obvious relation with depth below land surface (fig. 4). However, many of the 224 estimates are for core samples, and core sections that are fractured are not readily analyzed for hydraulic conductivity. As a result, the sample distribution probably favors unfractured parts of the Poison Canyon. Despite the possibly skewed sample distribution, the large range in hydraulic-conductivity values is consistent with the variability in rock types of the Poison Canyon Formation (table 1).

The Raton Formation is less variable than the Poison Canyon Formation in its lithology (table 1), and, as a result, the hydraulic conductivity is less variable. Estimates of hydraulic conductivity of the Raton Formation range from about 4×10^{-6} to about 1.7 ft/d (Daniel B. Stephens & Associates, Inc., 1993) (fig. 4). The three smallest values are measurements of vertical hydraulic conductivity of core samples of shale, however. This fact accounts for the apparent separation between these three values and the rest of the values in figure 4, which are for lithologies other than shale and range from about 3.7×10^{-3} to 1.7 ft/d.

Alluvial materials in the Sand Creek gap and, presumably, the west gap form permeable conduits for ground-water flow from the upgradient area to the downgradient area. Emplacement of clay-rich material that forms the barrier on the upgradient side of the SCS dam in the Sand Creek gap in 1988 resulted in a decrease in the rate at which the Sand Creek gap is capable of transmitting ground water.

In the downgradient area, alluvium and terrace alluvium are the principal units capable of transmitting water and yielding water to wells. These unconsolidated units are underlain by either the Vermejo Formation, Trinidad Sandstone, or Pierre Shale. Each of these bedrock units may have an upper part that is weathered or fractured, or both. In this report, the term "alluvial aquifer" is used to refer to the saturated alluvium, terrace alluvium, and underlying

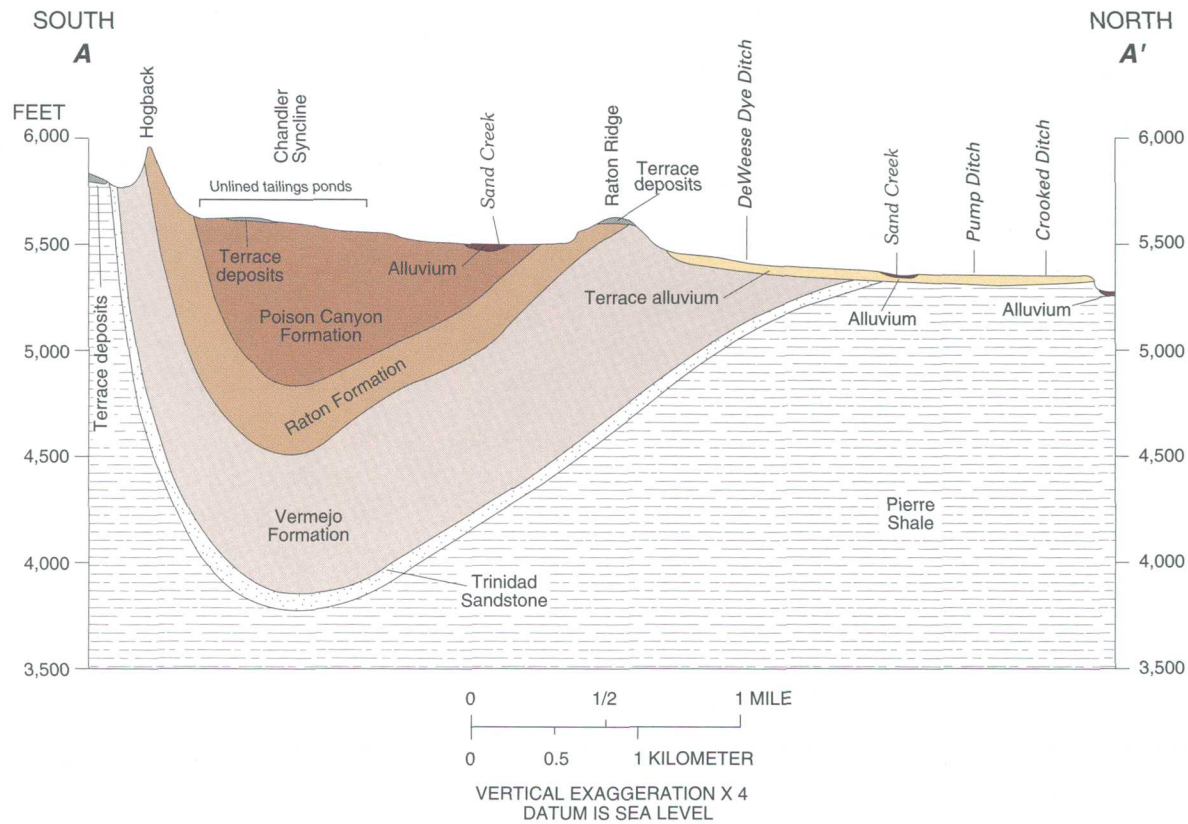

Figure 3. Geologic section A–A'. Line of section is shown in figure 2.

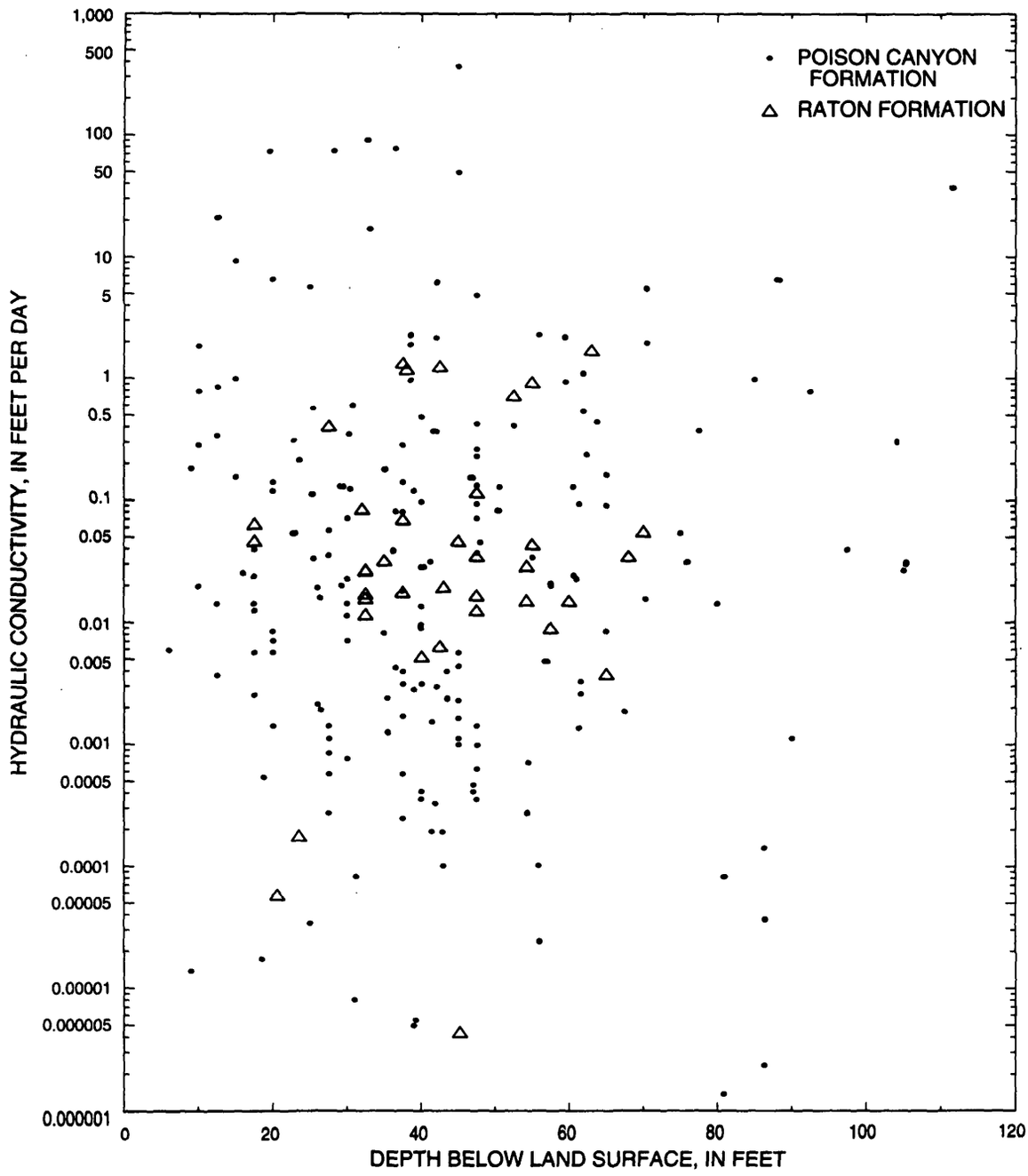

Figure 4. Hydraulic conductivity with depth for the Poison Canyon and Raton Formations.

weathered or fractured bedrock in the downgradient area. This designation corresponds to Hearne's and Litke's (1987, p. 13) "alluvial aquifer near Lincoln Park." The base of the ground-water system in the downgradient area is considered to be the base of the alluvial aquifer, as just defined. The alluvial aquifer yields water to numerous wells in Lincoln Park, which are used mainly for irrigation.

Few estimates of hydraulic conductivity of the alluvium and terrace alluvium in the downgradient area are available. Ten estimates, ranging from 10 to about 250 ft/d, were reported by Preston L. Niesen (Cotter Corporation, written commun., 1994). Galloway (1994) estimated hydraulic conductivity of the terrace alluvium in the vicinity of well 20 to be about 79 ft/d. Hydraulic conductivity of the

alluvium near the SCS dam from two slug tests and an aquifer test conducted during the study ranges from 0.8 to 29 ft/d (table 3).

Slug tests on three wells completed in near-surface parts (shallower than 33 ft) of the Vermejo Formation during the study produced hydraulic-conductivity estimates ranging from 0.007 to 0.02 ft/d (table 3). Two slug tests on intervals of the Vermejo Formation at depths between about 190 and 250 ft produced hydraulic-conductivity estimates of 0.0024 and 0.1 ft/d.

Recharge, Discharge, Ground-Water Flow, and the Water Table

Recharge to the ground-water system in the upgradient area is predominantly by inflow of ground water through Alkali Gap (fig. 1). In the areas mapped as bedrock (Tertiary or older rocks) or as terrace deposits (fig. 2), recharge comes from infiltration of precipitation that exceeds the rate of evapotranspiration. Rates of recharge by these processes are unknown.

Because the two gaps in the Raton ridge provide the major outlets for ground water in the upgradient area, the direction of ground-water flow in the upgradient area generally is toward one of these gaps. Flow downward across the bedding planes of the Poison Canyon, Raton, and Vermejo Formations probably accounts for only a small part of ground-water discharge from the upgradient area because of the generally small hydraulic conductivities of these units. The interbedded nature of the Poison Canyon and Vermejo Formations also would tend to decrease the potential for flow across bedding planes. A major source of discharge from the ground-water system in the upgradient area is well 333 (fig. 1). Between January 1988 and October 1994, 52.2 Mgal of water was pumped from this well to the lined impoundment (Richard Wooten, Cotter Corporation, written commun., 1995) as part of a remediation effort; the average pumping rate was 14.5 gal/min or about 2,800 ft^3/d.

Since construction of the SCS dam, the SCS reservoir upgradient from the dam has provided an area where evaporation and transpiration by wetland vegetation constitute a substantial sink for water from the ground-water system; the Cotter Corporation also pumps water from the SCS reservoir to the lined impoundment at a substantial rate. Between January 1989 and October 1994, 77.5 Mgal of water was pumped from the SCS reservoir (Richard Wooten, Cotter Corporation, written commun., 1995); the average pumping rate was about 25.3 gal/min or 4,860 ft^3/d. The evaporation and transpiration processes were considered together and estimated from a map of mean annual lake evaporation in Dunne and Leopold (1978, p. 118) to be 41 in/yr. The surface area of the SCS reservoir was about 330,000 ft^2. The average rate of evapotranspiration calculated from these values was 3,100 ft^3/d. The long-term average discharge rate, assumed to be the sum of the pumpage rate and the evapotranspiration rate, was about 8,000 ft^3/d.

Table 3. Hydraulic conductivity of alluvium and Vermejo Formation

[--, not determined]

Well	Depth of tested interval	Formation tested	Method of data analysis	Hydraulic conductivity	Storage coefficient
[1]374	10.7–12.7	Alluvium	Bouwer and Rice (1976)	0.8	--
[1]375	21.8–29.2	Alluvium	Bouwer and Rice (1976)	.8	--
[1]376	19.6–24.7	Alluvium	Cooper and Jacob (1946)[2]	29	0.0037
182	197–247	Vermejo Formation	Cooper, Bredehoeft, and Papadopulos (1967)	.0024	--
183	191–246	Vermejo Formation	Cooper, Bredehoeft, and Papadopulos (1967)	.1	--
329	18.0–32.9	Vermejo Formation	Bouwer and Rice (1976)	.009	--
[1]377	24.3–28.7	Vermejo Formation	Bouwer and Rice (1976)	.007	--
[1]378	21.3–25.7	Vermejo Formation	Bouwer and Rice (1976)	.02	--

[1]Location is between well 329 and the SCS dam (fig. 1). Exact locations are in Banta (1997).
[2]Time of pumping for this test was 5 hours, 26 minutes.

Recharge to the alluvial aquifer in Lincoln Park is from infiltration of excess irrigation water, from seepage from irrigation ditches and ponds, and from infiltration of excess precipitation. Water also enters the alluvial aquifer through the two gaps in the Raton ridge as ground water contained in alluvium-filled channels. The rate of ground-water discharge through the Sand Creek gap was estimated by Chafin and Banta (1999) as 1,900 to 12,000 L/d or 67 to 420 ft^3/d in 1996. The rate of ground-water discharge through the west SCS gap is unknown.

The alluvial aquifer discharges water to Sand Creek, which is perennial for about 0.5 mi upstream from its mouth. Discharge in Sand Creek just upstream from the mouth was 2.41 ft^3/s on May 11, 1995, just before the start of the irrigation season and was 4.43 ft^3/s on August 10, 1995 (Banta, 1997). The average of these values, 3.42 ft^3/s or 295,000 ft^3/d, is assumed to represent the average discharge of Sand Creek. The aquifer also discharges water to a series of springs and seeps at the contact between the terrace alluvium and the Pierre Shale at the escarpment along the Arkansas River. Substantial evapotranspiration, indicated by abundant vegetation on the embankment between Lincoln Park and the flood plain of the Arkansas River, is another important discharge process. At the boundary of the study area near South Cañon Ditch, the alluvial aquifer is in hydraulic connection with the saturated terrace alluvium outside the study area. As a result of this connection, ground water can flow across the study-area boundary. The water table in the terrace alluvium on the northwest side of this boundary is substantially lower than the water table in the alluvial aquifer on the southeast side of the boundary (fig. 5). The difference in water-table altitude produces a potential for ground-water flow in the terrace alluvium out of the downgradient area across the study-area boundary toward the northwest.

Saturated thickness of the alluvial aquifer ranges from 0 ft along the Raton ridge to about 60 ft (Colorado State Engineer's Office, written commun., 1995). The saturated thickness varies seasonally; it is largest during the irrigation season and decreases during the nonirrigation season. Some wells that are completed to bedrock near DeWeese Dye Ditch, such as wells LP85–1S and 121 (fig. 1), generally are dry in the nonirrigation season, but they contain about 8 to 16 ft of water late in the irrigation season (Banta, 1997).

The water table in the downgradient area fluctuates substantially with the irrigation cycle. The irrigation season begins in about early to mid-May and ends in late September or early October. During the nonirrigation season, water levels in wells completed in the alluvial aquifer approach an annual minimum as discharge from the aquifer exceeds recharge from infiltration of precipitation. During the irrigation season, leakage from irrigation ditches and ponds and excess irrigation water supplement the water recharging the aquifer from precipitation, and the water table rises substantially, especially near the irrigation ditches and irrigation ponds. In the upgradient area, water-table fluctuations do not correspond to the irrigation cycle in Lincoln Park; however, the water table does respond to ground-water injection and withdrawal associated with remedial activities. The water levels used to generate the water-table map (fig. 5) are medians of water levels (Banta, 1997) not affected by pumping. The wells shown on the water-table map are completed in zones near the local water table without regard to lithology or geologic unit. Wells used to develop the water-table map were completed in water-yielding zones no deeper than 100 ft.

During three pilot tests of methods proposed for flushing contaminants from the ground-water system in the upgradient area in 1991–92, water was injected through wells and trenches in the area of the old tailings ponds at rates ranging from 2 to about 43 gal/min (Adrian Brown Consultants, Inc., 1993). For two pilot tests where water was injected at trenches, water was simultaneously withdrawn from wells completed at depths between about 10 and 55 ft. For one pilot test where water was injected through wells completed in varying depth zones between about 10 and 75 ft, water was withdrawn from gravel-filled trenches.

In a remedial action referred to as the dam-to-ditch flush, water was injected into two injection trenches constructed in 1990 about 500 ft north-northeast of the crest of the SCS dam. Water injection was timed to coincide approximately with the irrigation seasons in 1990 through 1994. In 1990, the injection rate initially ranged from 75 to 100 gal/min, but after 3 months of operation, the rate was decreased to about 30 gal/min (Cotter Corporation, written commun., 1991). During 1991 through 1994, the injection rate was approximately 30 gal/min (Cotter Corporation, written commun., 1992, 1993, 1995).

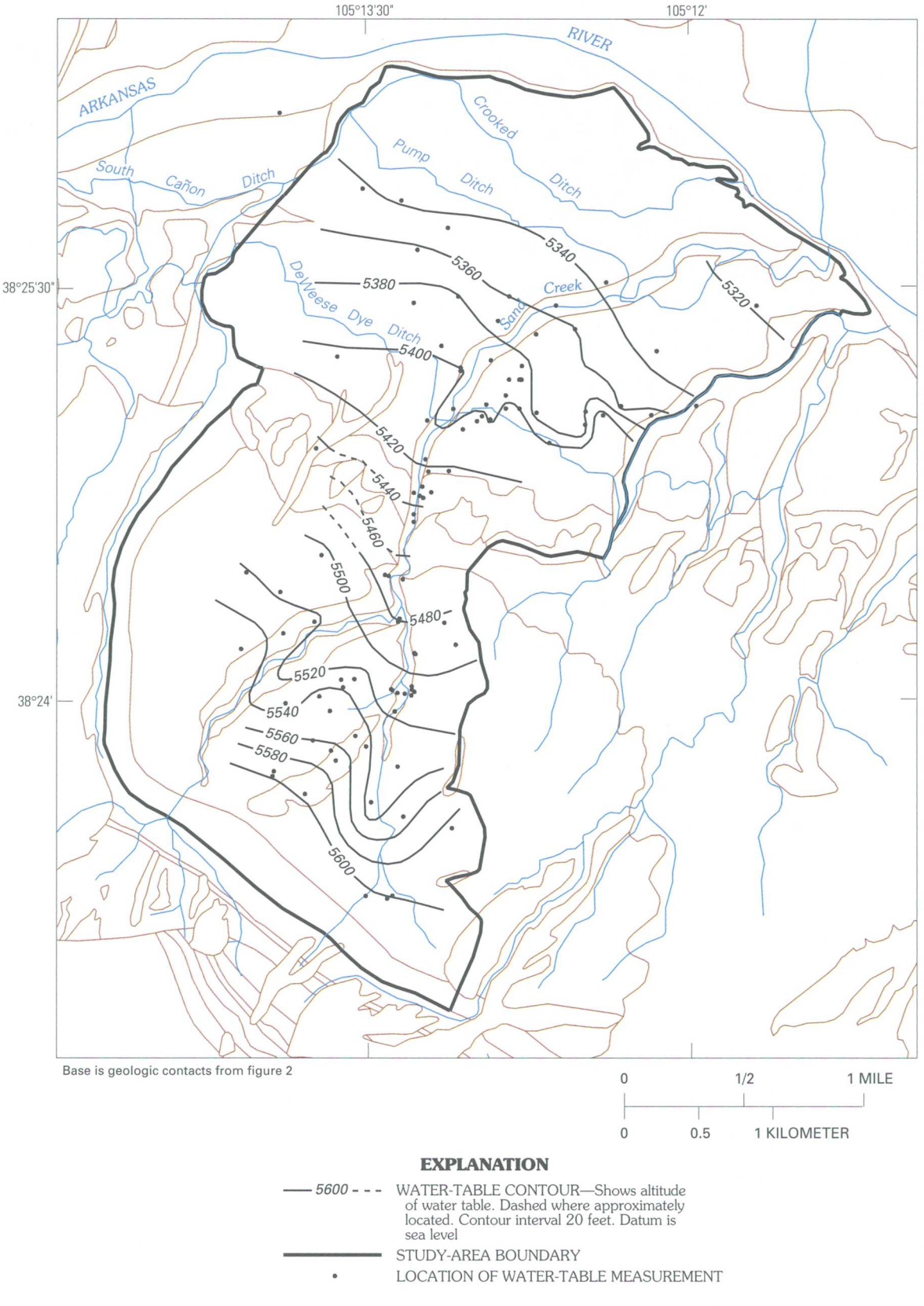

Figure 5. Median static altitude of the water table in the study area.

Leakage from irrigation pond 9 (fig. 1) was investigated by monitoring surface-water inflow and outflow and water levels in pond 9 during filling of the pond and during a period when surface-water flow into and out of the pond was close to zero. The reader is referred to Banta (1997) for surface-water discharge data. During the initial filling of irrigation pond 9 on May 14, 1995, for the irrigation season, discharge in the diversion ditch from DeWeese Dye Ditch to the pond was 6.2 ft^3/s. On the same day, the water level in irrigation pond 9 was 6.38 ft, compared to an arbitrary datum, at 3:55 p.m.; the level was 6.43 ft at 5:00 p.m.; and the level was 6.44 ft at 5:08 p.m. Between 2:45 p.m. and 4:40 p.m., the perimeter of irrigation pond 9 was surveyed; the area of the pond was about 161,000 ft^2. Assuming no change in pond area between the first and last stage measurements, the change in water volume in the pond was 9,660 ft^3 over 73 minutes, and the rate of change of water volume in the pond during this time was 2.2 ft^3/s. The leakage rate was calculated as the difference between the fill rate (6.2 ft^3/s) and the rate of change of volume (2.2 ft^3/s), or 4.0 ft^3/s. This rate was assumed to represent an initial leakage rate, which would apply at the start of the irrigation season, when the soil underlying the pond was essentially dry.

On May 15, 1995, a bank of the DeWeese Dye Ditch failed at a location downstream from the area where leakage from the ditch and irrigation pond 9 was being investigated. In response to this failure, the company that operates the ditch shut off the flow of water into the ditch at a location outside the study area, and gates controlling diversion of water from the ditch to irrigation ponds were closed (Honey Moschetti, DeWeese Dye Ditch and Reservoir Company, oral commun., 1995). During repair of the DeWeese Dye Ditch, inflow to irrigation pond 9 was zero, and outflow was negligible. Operation of the ditch resumed about June 5, 1995. On May 18, 1995, surface-water flow out of irrigation pond 9 was estimated to be less than 0.05 ft^3/s, and flow into the pond was zero. On that day, the stage in the pond was 3.88 ft at 11:28 a.m. and 3.84 ft at 1:27 p.m.; stage in the pond was declining at 0.48 ft/d. Over the pond area, this rate of decline in stage produced a leakage rate of 78,000 ft^3/d or 0.90 ft^3/s. This rate was assumed to be characteristic of the leakage rate that would apply during most of the irrigation season, when the soil underlying the pond was saturated or nearly saturated.

To quantify the rate of leakage from the DeWeese Dye Ditch, a gain-loss investigation was conducted on August 9, 1995, on a 0.425-mi reach of the ditch, from site SW2 to site SW7 (fig. 1). Operating conditions in the ditch and the stage height at site SW2 were constant during the investigation. Discharge was 17.8 ft^3/s at site SW2 and 14.4 ft^3/s at site SW7 (Banta, 1997); the difference was 3.4 ft^3/s, or 2.9×10^5 ft^3/d. The only detectable surface-water discharge from the ditch in the investigation reach was in the diversion ditch to irrigation pond 9, where discharge was estimated as less than 0.05 ft^3/s. This discharge rate was negligible compared to the estimated maximum error in the discharge measurements, which was reported as more than 8 percent (Banta, 1997), so the difference in discharge was assumed to be due entirely to leakage. On a per-mile basis, the leakage rate in the investigation reach was 8.0 (ft^3/s)/mi. A hydrograph for well 178 (fig. 1), an observation well located about 500 ft south of DeWeese Dye Ditch, shows the response of the water table in the alluvial aquifer to leakage from the ditch (fig. 6). Additional illustrations of the effects of leakage from the ditch on water levels in the alluvial aquifer are shown in Banta (1997).

An attempt was made to establish a relation (rating curve) of stage height to discharge at the flume located on the DeWeese Dye Ditch at site SW2. However, stage height at the flume is controlled principally by operating conditions in the ditch (positions of diversion gates and temporary dams); therefore, there is no consistent relation of stage height to discharge.

The rate at which water is applied for irrigation was estimated by estimating the area potentially irrigated from irrigation pond 9; estimating the average delivery rate of water to pond 9; using the estimated leakage rate from pond 9; and calculating the application rate as the difference between the delivery rate and the leakage rate, divided by the potentially irrigated area. The area of Lincoln Park potentially irrigated by water from irrigation pond 9 was the area bounded approximately by a line from irrigation pond 3 to pond 9, along Sand Creek, along Pump Ditch (fig. 1), along the escarpment between Lincoln Park and the Arkansas River, and along a line estimated to separate the area potentially irrigated from pond 9 from the area potentially irrigated from pond 3.

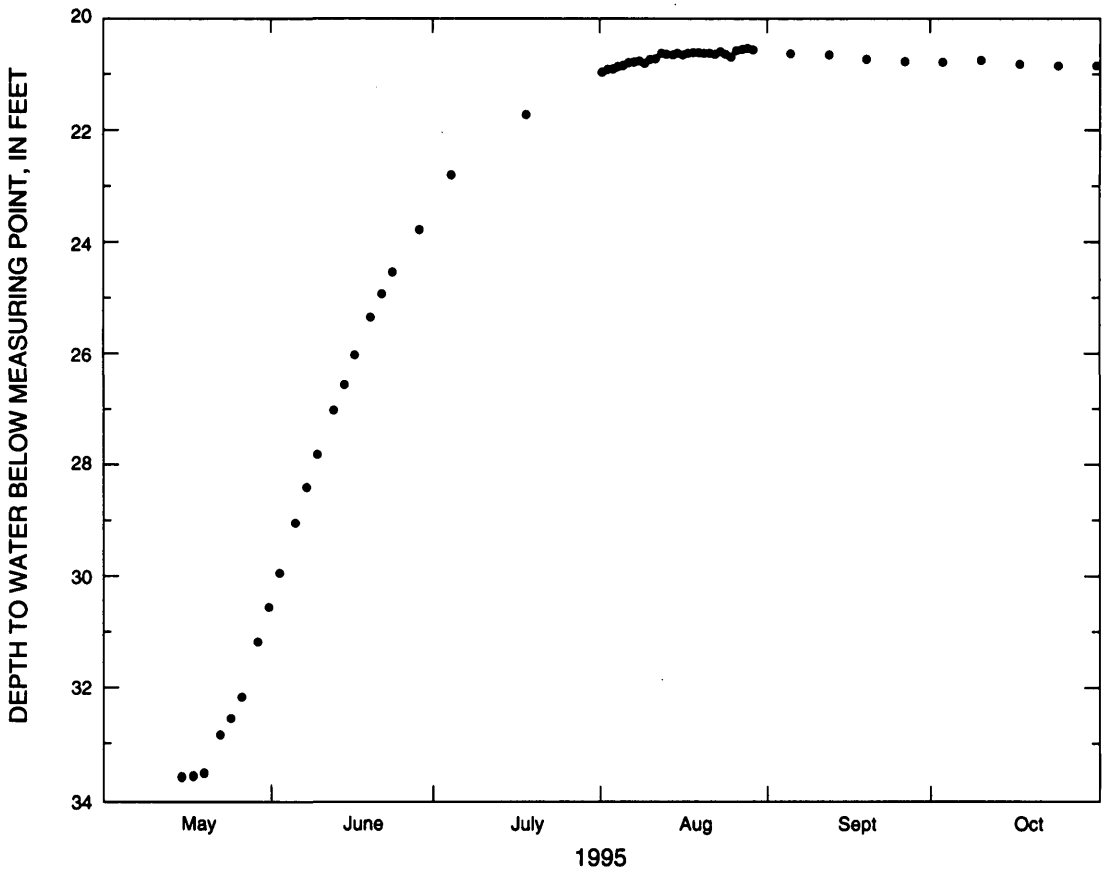

Figure 6. Hydrograph showing the effects of leakage on water-level measurements in well 178.

This area is about 9.16×10^6 ft^2. Pond 9 is filled intermittently according to the weekly DeWeese Dye Ditch irrigation schedule; filling occurs during 16 of 28 6-hour periods in a week, or 57 percent of the time during the irrigation season. If the fill rate is assumed to be 6.2 ft^3/s, which was measured on May 14, 1995, then the fill rate averaged 3.6 ft^3/s during the irrigation season. The leakage rate determined on May 18, 1995, when the area of pond 9 was substantially smaller than normal, was 0.6 ft^3/s. Adjusting the leakage rate for the pond 9 surveyed area resulted in a leakage rate of 0.9 ft^3/s. The delivery rate, which was calculated as the difference between the average fill rate and the leakage rate, was 2.7 ft^3/s. The application rate for the potentially irrigated area was 2.7 ft^3/s divided by 9.16×10^6 ft^2, resulting in 0.025 ft/d, or 0.31 in/d. This application rate includes any leakage from lateral ditches leading from pond 9 to irrigated fields. During the irrigation season, which was assumed to last 5 months (153 days), approximately 46 in. of water was available for use by plants and for recharge to the alluvial aquifer when averaged over the potentially irrigated area. A substantial part of the 46 in. probably leaked out of the lateral ditches before reaching irrigated fields—if the results of the leakage investigation for DeWeese Dye Ditch can be generalized to the lateral ditches.

Water Budget

A comprehensive estimate of the water budget for the study area is not presented because data to estimate substantial components of the budget are lacking. However, data are available to estimate some components of the water budget, and reasonable assumptions can be made to estimate some components.

Approximately 41 percent of the study area is north of DeWeese Dye Ditch. Based on visual inspection of an aerial photograph, which was taken

sometime between 1971 and 1978 and shows part of this area, approximately one-half of the area north of DeWeese Dye Ditch was being irrigated. As the hydrographs in figure 6 and in Banta (1997) show, the water table in the alluvial aquifer rises substantially during the irrigation season. The water-table rise results from deep percolation of water applied in excess of the requirements of crops and from leakage from the irrigation ditches and ponds. In the area south of DeWeese Dye Ditch, recharge to the ground-water system largely is limited to deep percolation of precipitation that neither runs off as surface water nor is evapotranspired. Because the climate of the study area is semiarid, the rate of recharge from precipitation is assumed to be small compared to the rate of recharge from irrigation water.

The rate at which the alluvial aquifer was recharged by water that entered the study area in the irrigation ditches was estimated as the difference between the rate at which water flowed in the irrigation ditches into the study area and the rate at which water evapotranspired from crops and open surface water.

In 1995, three discharge measurements were made in DeWeese Dye Ditch at a flume located about 290 ft west of the point where the ditch crosses Sand Creek (Banta, 1997); the average of these discharges was 10.7 ft^3/s. As discussed in the "Recharge, Discharge, Ground-Water Flow, and the Water Table" section, the rate of leakage from the ditch was 8.0 $(ft^3/s)/mi$ when discharge at the flume was 17.8 ft^3/s. If the rate of leakage is assumed to have been proportional to the discharge in the ditch, when the discharge at the flume was 10.7 ft^3/s, the rate of leakage was 4.8 $(ft^3/s)/mi$. Using this leakage rate to extrapolate upstream along DeWeese Dye Ditch to the point where it enters the study area, the rate of flow of water in DeWeese Dye Ditch into the study area can be estimated. The length of DeWeese Dye Ditch from the point where it enters the study area to the flume is 7,330 ft. However, for 1,320 ft of this length, the water is carried in underground pipes, which are assumed not to have leaked. The length of the ditch, between the study-area boundary and the flume, that is assumed to have leaked is 6,010 ft. If this reach of the ditch leaked water at 4.8 $(ft^3/s)/mi$, then the rate of flow of water into the study area in DeWeese Dye Ditch is [10.7 + (4.8 × 6,010 / 5,280) =] 16 ft^3/s. This amount of water was available to irrigate the area bounded by DeWeese Dye Ditch, South Cañon Ditch, Pump Ditch, Sand Creek, and the study-area boundary, which measures 4.47×10^7 ft^2, or to leak from the irrigation ditches and ponds.

South Cañon Ditch supplies water to Pump Ditch and Crooked Ditch. These ditches potentially can irrigate a 2.52×10^7 ft^2 area. The flow in South Cañon Ditch as it enters the study area was assumed to be proportional to the flow in DeWeese Dye Ditch as the area potentially irrigated from South Cañon, Pump, and Crooked Ditches is proportional to the area potentially irrigated from DeWeese Dye Ditch. The resulting estimate of flow in South Cañon Ditch as it enters the study area was 9.0 ft^3/s.

The flow of water into the study area by way of the irrigation ditches during the irrigation season was estimated as the sum of the estimated flows in DeWeese Dye and South Cañon Ditches, which was 25 ft^3/s. The irrigation season was assumed to be 5 months long, so the total amount of water that entered the study area in the irrigation ditches was estimated to be 3.3×10^8 ft^3; averaged over a year, the daily rate was 900,000 ft^3/d.

The amount of water lost through evapotranspiration during the irrigation season was estimated using the Thornthwaite method (Dunne and Leopold, 1978). The Thornthwaite formula is:

$$E_t = 1.6\left[\frac{10T_a}{I}\right]^a$$

where

E_t = standard potential evapotranspiration, in centimeters per month;

T_a = mean monthly air temperature, in degrees Celsius;

$$I = \sum_{i=1}^{12}\left[\frac{T_{ai}}{5}\right]^{1.5}; \text{ and}$$

$$a = 0.49 + 0.0179I + 0.0000771I^2 + 0.67 \times 10^{-6}I^3.$$

Mean temperatures for months from 1980 through 1996 for Cañon City (National Oceanic and Atmospheric Administration, 1980–96) were averaged to determine mean monthly air temperatures (table 4). The standard potential evaporation rate was multiplied by a factor that corrects for day length and number of days in a month and varies with latitude (Dunne and Leopold, 1978, table 5–2) to calculate the corrected potential evapotranspiration rate. For estimating evapotranspiration in Cañon City, the actual evapotranspiration rate was assumed to equal the corrected potential evapotranspiration rate for the irrigation season (May through September), and the actual evapotranspiration rate for the nonirrigation months was assumed to equal zero. The annual amount of water lost by evapotranspiration in irrigated areas of Lincoln Park was, therefore, estimated to be 54.09 cm. The estimated depth of water lost through evapotranspiration was multiplied by one-half the potentially irrigated area to provide an estimate of the total volume of water annually lost through evapotranspiration in the study area; the resulting estimate was 6.2×10^7 ft^3. Expressed as a daily rate averaged over the year, this amount is 170,000 ft^3/d.

The difference between the rate at which water enters the study area in the irrigation ditches (900,000 ft^3/d) and the evapotranspiration rate (170,000 ft^3/d), which equals 730,000 ft^3/d, approximates the average, long-term rate at which water recharges the alluvial aquifer. This estimate neglects irrigation water that returns to surface-water drains and exits the study area, and it neglects evapotranspiration during the nonirrigation season. The evaporation rate from free water surfaces (irrigation ditches and ponds) was assumed to be the same as the corrected potential evapotranspiration rate. Recharge from precipitation was assumed to be small compared to recharge from irrigation water.

All major processes that result in flow of water into or out of the ground-water system of the study area are listed in table 5. Where sufficient data were available to justify estimation of a volumetric rate of flow, the estimate is listed. Where a recharge or discharge process is known or strongly suspected to have occurred, but insufficient data were available to justify estimation of a rate, "unknown" is entered in the table. Of the features and processes with flow listed as "unknown" in table 5, "springs and evapotranspiration near the Arkansas River" were the most visible. The springs and evapotranspiration by abundant vegetation along the Arkansas River represented a substantial discharge of water from the ground-water system, although the rate of discharge by these processes was not quantified. The other processes listed as "unknown" in table 5 also are not quantified, but the interpretation of the direction of flow in each case is supported by water-level data (fig. 5) (Banta, 1997).

Table 4. Mean monthly air temperature (National Oceanic and Atmospheric Administration, 1980–96) and potential evapotranspiration at Cañon City

Month	Number of years of data	Mean air temperature (degrees Celsius)	Standard potential evapotranspiration (centimeters per month)	Correction factor (dimensionless; Dunne and Leopold, 1978, table 5–2)	Corrected potential evapotranspiration (centimeters per month)
January	14	1.3	0.31	0.80	0.25
February	14	2.5	.70	.89	.62
March	13	6.3	2.19	.99	2.17
April	13	10.7	4.25	1.10	4.67
May	14	15.0	6.55	1.20	7.86
June	13	20.1	9.48	1.25	11.85
July	14	23.2	11.33	1.23	13.94
August	14	22.0	10.60	1.15	12.19
September	13	17.5	7.93	1.04	8.25
October	13	11.8	4.84	.93	4.50
November	14	5.5	1.84	.83	1.53
December	15	1.8	.47	.78	.37

Table 5. Estimated components of the average annual ground-water budget of the study area

Feature or process	Estimated flow into the ground-water system of the study area (cubic feet per day)	Estimated flow out of the ground-water system of the study area (cubic feet per day)
Recharge from excess irrigation and leakage from irrigation ditches and ponds	730,000	0
Recharge from infiltration of precipitation	unknown	0
Ground-water flow across hogback at Alkali Gap	unknown	0
Discharge to Sand Creek	0	295,000
Pumpage and evaporation from the SCS reservoir	0	8,000
Springs and evapotranspiration near the Arkansas River	0	unknown
Discharge to unnamed creek where Willow Lakes are located	0	unknown
Ground-water flow across study-area boundary near South Cañon Ditch	0	unknown
Ground-water flow through Littell mine shaft	0	unknown

Geochemistry of Uranium and Molybdenum

This section describes the aspects of the geochemistry of uranium and molybdenum that are pertinent to solute-transport modeling of the study area. The near-surface ground-water environment of the study area is oxidizing, as is indicated by measurable dissolved-oxygen concentrations in near-surface wells (Chafin and Banta, 1999, table 8), and has relatively neutral pH between 7 and 8 (Banta, 1997; Chafin and Banta, 1999, table 8). Below the oxidizing near-surface ground-water environment south of the Raton ridge, the geochemical environment probably grades into reducing conditions. Evidence that reducing conditions generally occur at greater depths in the Poison Canyon Formation consists of carbonized wood fragments (Banta, 1997), remnant pyrite, and textures indicating replacement of pyrite in the near-surface Poison Canyon Formation (George Breit, U.S. Geological Survey, written commun., 1996). Deeper in that formation (below the zone of near-surface fracturing), sluggish water flow probably has prevented substantial oxidation of pyrite and organic matter, favoring reducing conditions.

A pilot test of a remediation method in which water was injected in wells completed below the zone of contamination and withdrawn in 3-ft-deep, gravel-filled trenches was conducted for 11 months in 1992 in an area referred to as the third test area (Adrian Brown Consultants, Inc., 1993). Water samples were collected from a designated point where drainage occurred from the trenches. Results of this pilot test are discussed in the "Uranium" and "Molybdenum" sections that follow.

Uranium

Natural uranium consists of several isotopes, and the weakly radioactive ^{238}U (half-life 4.5 billion years) is predominant (Hem, 1985, p. 148). Because of the extreme insolubility of minerals bearing reduced U^{4+}, most uranium transport occurs in oxidizing surface and ground water. In such environments, U^{6+} forms uranyl ions (UO_2^{2+}) or uranyl complexes with fluoride, phosphate, or carbonate (Langmuir, 1979, p. 85). Chafin and Banta (1999) concluded, on the basis of thermodynamic calculations on analyses of ground-water samples collected for this study, that uranium phases were undersaturated at all sites in the oxidizing near-surface ground-water environment and that sorption remained the only plausible geochemical mechanism for downgradient decreases in dissolved-uranium concentrations. Ticknor (1994, p. 235) concluded that uranium is sorbed by selected geologic materials in the general order: gray granite < biotite < chlorite = palygorskite < goethite < kaolinite = hematite. Ticknor also concluded that uranium sorption was lessened as concentrations of dissolved solids and bicarbonate or carbonate anions increased. Hsi and Langmuir (1985) reported that dissolved uranyl species were strongly adsorbed onto all iron oxide materials when pH was greater than 5 to 6, but that adsorption was greatest onto amorphous ferric oxyhydroxide and least onto well-crystallized specular hematite. Therefore, in

the near-surface ground-water environment of the study area, uptake of dissolved uranium primarily is onto iron oxides (especially amorphous ones) in the matrices of the aquifers; however, because of their abundance, clays possibly also sorb important quantities of uranium. The hypothesis that reducing conditions occur below the near-surface oxidizing environment south of the Raton ridge is supported by small concentrations of dissolved uranium in wells completed at depths greater than 100 ft. Wells 17 (gravel pack 113–140 ft deep in the Poison Canyon Formation), 315 {gravel pack 215–350 ft in the Poison Canyon Formation; using only the last year of record, 1987, because of aquifer contamination during drilling in 1979 [Runnells and others (1983)]}, 324 (screened 250–350 ft in the Poison Canyon Formation; records from 1990 through February 1995), and 335 (gravel pack 110–220 ft in the Raton Formation; records from 1986 through February 1995) (fig. 1) had maximum dissolved-uranium concentrations ranging from 2 to 5 µg/L. Available information indicated that most raffinate-derived uranium that might migrate downward into the deeper reducing environment would be immobilized by precipitation of insoluble reduced-uranium phases or sorption.

Solid-phase concentrations of uranium in the third test area, tabulated by Adrian Brown Consultants, Inc. (1993), indicated a trend of decreasing concentration with depth (fig. 7). In the depth interval 0 to 5 ft below the land surface, the median solid-phase uranium concentration was about 7.8 mg/kg; below 15 ft, solid-phase uranium concentrations were less than 2.4 mg/kg. Also, below 15 ft, solid-phase concentrations were similar to the average abundances for uranium indicated by Levinson (1980) for shale (4 mg/kg) and soil (1 mg/kg). Characteristic

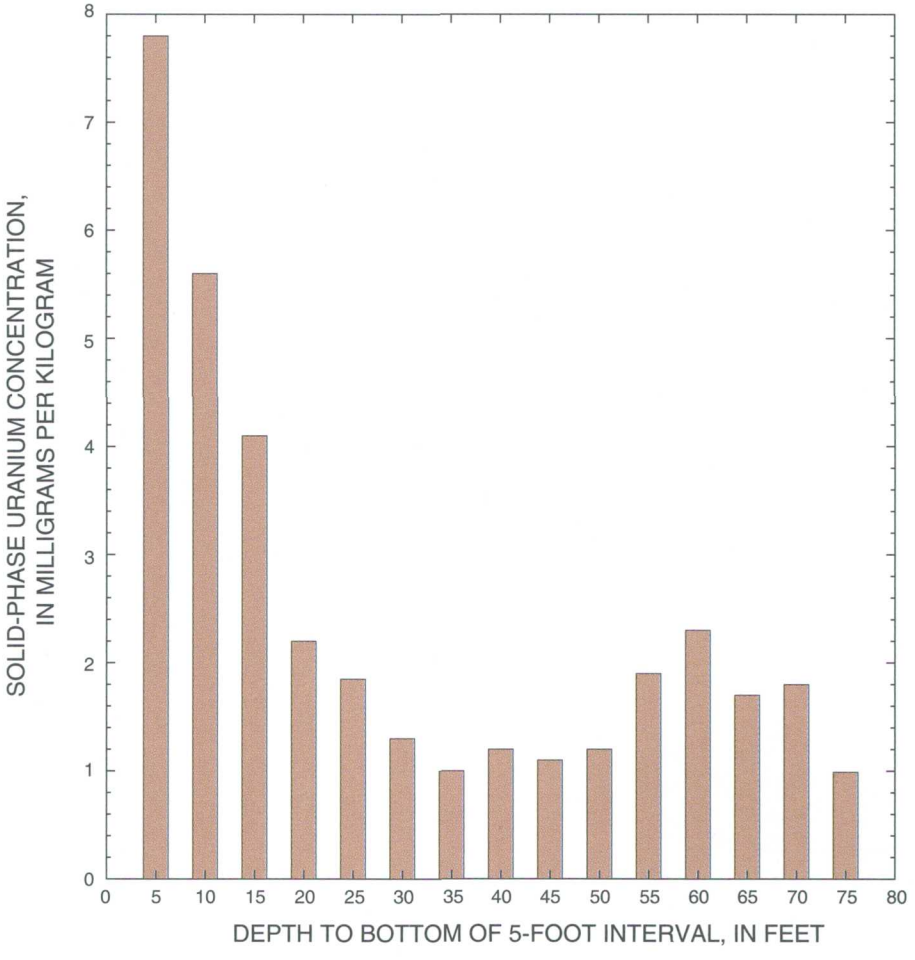

Figure 7. Solid-phase uranium concentration with depth at the third test area.

solid-phase uranium concentrations in sandstone, another rock type in the study area, range from 0.45 to 3.2 mg/kg (Levinson, 1980). These measurements indicate that the intervals where solid-phase uranium concentrations are substantially larger than the naturally occurring concentrations tend to be above the water table.

During the pilot test (Adrian Brown Consultants, Inc., 1993), water samples collected from the trenches and cuttings from boreholes were analyzed for uranium. After an initial increase in the uranium concentration, the concentration peaked at 7.4 mg/L. At the end of the injection and withdrawal period, the uranium concentration in water from the trenches had decreased to 0.91 mg/L (about 12 percent of the peak concentration). In contrast to the change in aqueous uranium concentrations during the pilot test, the solid-phase concentrations were basically unchanged (fig. 8). The difference between changes in aqueous concentrations and changes in solid-phase concentrations indicates that removal of uranium from the contaminated materials by flushing with water was not a process where equilibrium between aqueous and solid-phase uranium was instantaneous.

Molybdenum

The most common oxidation states of molybdenum in dissolved and solid phases are Mo^{4+} and Mo^{6+}; Mo^{6+} predominates in oxidizing environments. In dissolved species, Mo^{6+} forms molybdate (MoO_4^{2+}) ions, which become protonated at pH less than 5 (Hem, 1985). The relatively neutral pH of ground water in the study area implies that the unprotonated molybdate anion is the form of dissolved molybdenum present in the near-surface ground-water environment of the study area. The mobility

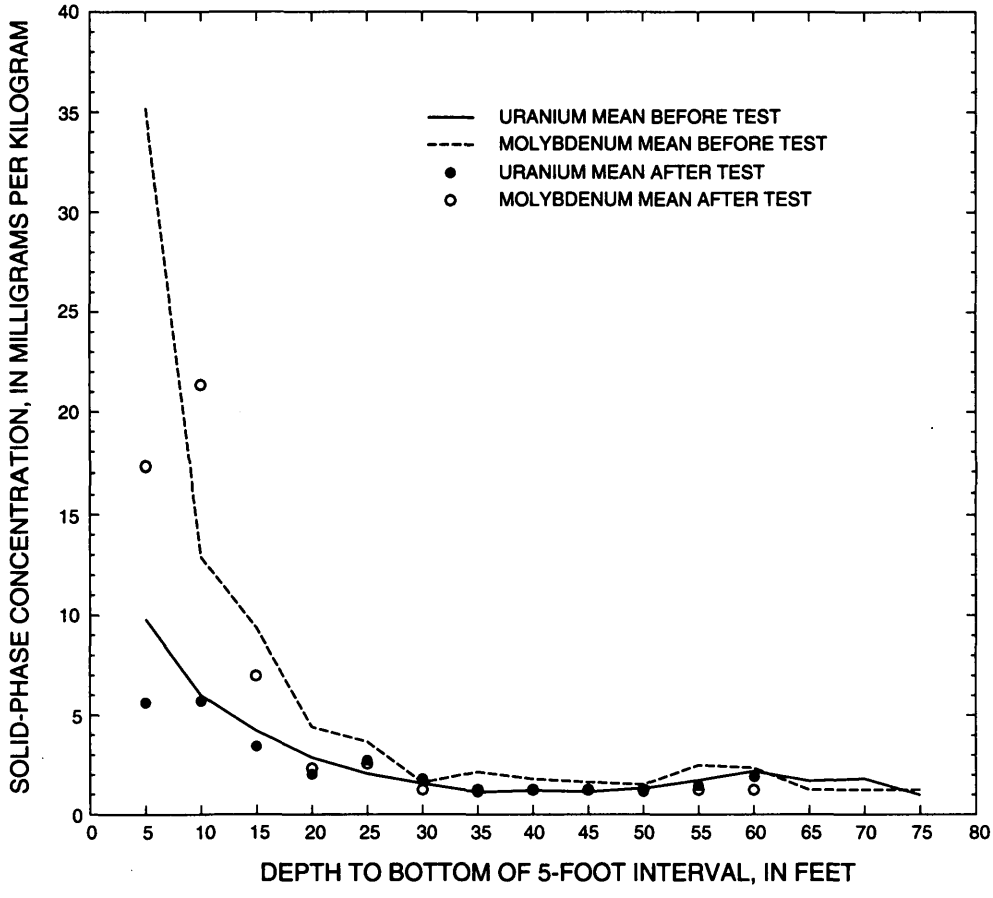

Figure 8. Solid-phase uranium and molybdenum concentrations with depth before and after test at the third test area.

of dissolved molybdenum in near-surface ground water is limited and retarded by sorption (anion exchange) and mineral precipitation. In general, the anion-exchange capacities of aquifer materials (primarily clays) are smaller than the cation-exchange capacities (Grim, 1968, p. 226). Theng (1971) reported that MoO_4^{2+} was optimally sorbed from NaCl solutions by three New Zealand soils that had a pH near 4, but sorption decreased steeply as pH increased, and minor sorption occurred above pH 7. Stollenwerk (1995) reported that MoO_4^{2+} was sorbed strongly from dilute NaCl solutions that had pH less than 5 by alluvial-aquifer materials at Cape Cod, Massachusetts, but very little sorption occurred above pH 7. Furthermore, sorption of MoO_4^{2+} decreased as ionic strength and concentrations of PO_4^{3-}, SO_4^{2+}, and divalent cations increased. Therefore, the relatively neutral pH, predominance of the SO_4^{2+} anion, and relatively large ionic strengths upgradient from the DeWeese Dye Ditch (Banta, 1997; Chafin and Banta, 1999, table 8) imply that sorption of MoO_4^{2+} is minor in the near-surface ground-water environment of the study area, especially upgradient from the DeWeese Dye Ditch, where molybdenum concentrations are greatest. Vlek and Lindsay (1977, p. 42) concluded that, in the absence of lead minerals, powellite ($CaMoO_4$) and ferrimolybdite [$Fe_2O_3(MoO_3)3.52{:}10.4H_2O$] (Kaback and Runnells, 1980) control the solubility of molybdenum in soils. Chafin and Banta (1999) determined by thermodynamic calculations that powellite, but not ferrimolybdite or any other molybdenum phases, was oversaturated in all raffinate-affected near-surface ground-water samples collected for this study upgradient from the DeWeese Dye Ditch. Therefore, because appreciable sorption of molybdate ions was lacking, dissolution and precipitation of powellite were the primary geochemical mechanisms controlling the transport of molybdenum in the study area. Near and downgradient from the DeWeese Dye Ditch, where dissolved-molybdenum, dissolved-sulfate, and dissolved-solids concentrations are smaller than concentrations upgradient from the ditch largely because of dilution of raffinate-affected water by water from the DeWeese Dye Ditch (Banta, 1994; Chafin and Banta, 1999), sorption (and desorption) of molybdenum may be more important in controlling the transport of molybdenum. However, to simplify solute-transport modeling, sorption and desorption of powellite were used as the sole geochemical mechanism regulating concentrations of dissolved molybdenum in the study area. Low concentrations of dissolved molybdenum in wells completed deeper than 100 ft in the Poison Canyon and the Raton Formations (Banta, 1997) were consistent with reducing conditions: well 17 had a maximum concentration of 10 µg/L, well 324 had a maximum concentration of 7 µg/L, and well 335 had a maximum concentration of 12 µg/L (see fig. 1 for well locations; well depths and periods of record are cited in the "Uranium" section). Mechanisms that limit concentrations of reduced molybdenum include precipitation of molybdenum sulfide, coprecipitation with iron sulfides, and sorption onto illite and montmorillonite (a smectite) (Bertine, 1972). Therefore, most raffinate-derived molybdenum that might migrate into the deeper, reducing zones of the ground-water system would be immobilized by these mechanisms.

Solid-phase concentrations of molybdenum in the third test area, tabulated by Adrian Brown Consultants, Inc. (1993), indicated a trend of decreasing concentration with depth (fig. 9). In the depth interval 0 to 5 ft below the land surface, the median solid-phase molybdenum concentration was about 25 mg/kg; below 20 ft, solid-phase molybdenum concentrations were less than the detection limit of 2.5 mg/kg. More than 15 ft below the land surface, solid-phase concentrations were similar to the average abundances for molybdenum provided by Levinson (1980) for shale (3 mg/kg) and soil (2 mg/kg). Characteristic solid-phase molybdenum concentrations in other rock types in the study area also were provided by Levinson (1980): sandstone, 0.2 mg/kg; soils in temperate regions, 1 to 5 mg/kg; and soils in arid regions, 2 to 5 mg/kg. In the third test area, depth to the water table in the absence of artificial hydraulic stress was about 12 to 18 ft (Adrian Brown Consultants, Inc., 1993). These comparisons indicate that the intervals where solid-phase molybdenum concentrations were substantially larger than the naturally occurring average or characteristic concentrations tended to be above the water table.

After an initial increase in the molybdenum concentration during the pilot test (Adrian Brown Consultants, Inc., 1993), the concentration peaked at 14 mg/L. At the end of the injection and withdrawal

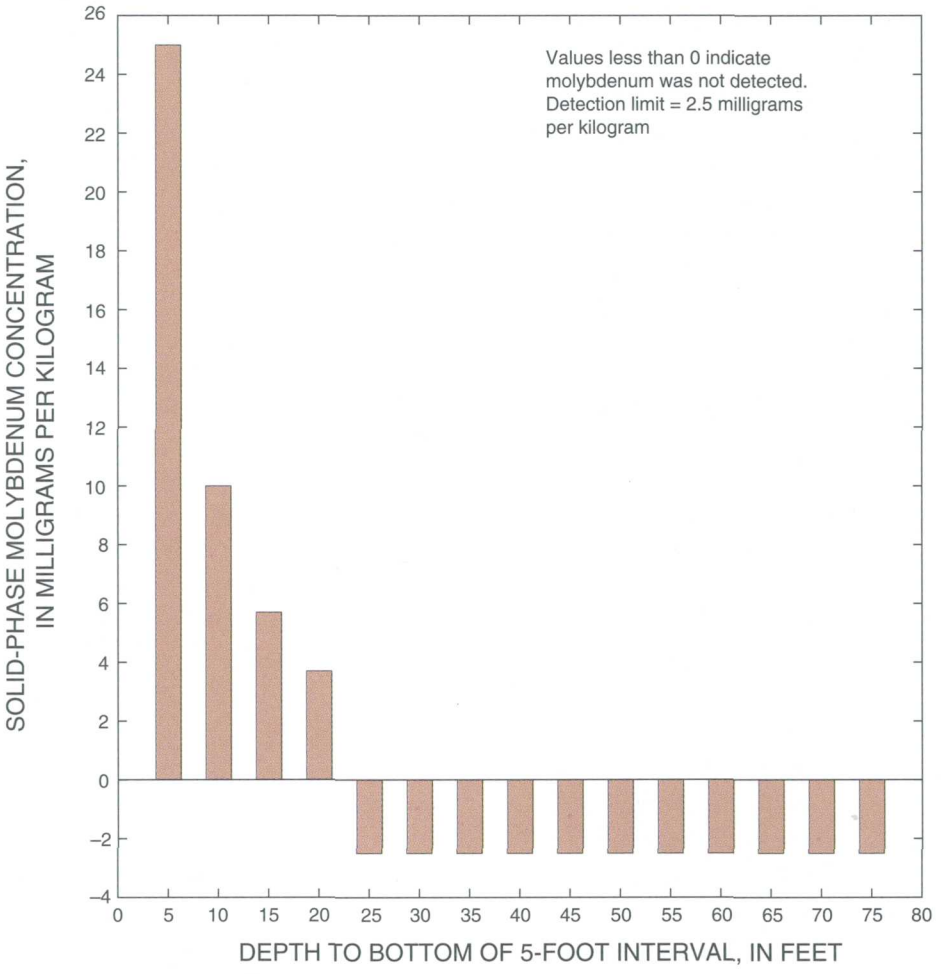

Figure 9. Solid-phase molybdenum concentration with depth at the third test area.

period, the molybdenum concentration in water from the trenches had decreased to 3.3 mg/L (about 24 percent of the peak concentration). Although subsequent samples from the test area were not available, solid-phase molybdenum concentrations in samples from 5-ft intervals in 31 boreholes constructed before the test and 4 boreholes constructed after the test were available. In contrast to the change in aqueous molybdenum concentration during the pilot test, the solid-phase concentrations were basically unchanged (fig. 8). The difference between changes in aqueous concentrations and changes in solid-phase concentrations indicated that removal of molybdenum from the contaminated materials by flushing with water was not a process where equilibrium between aqueous and solid-phase molybdenum was instantaneous.

SIMULATED GROUND-WATER SYSTEM

Two numerical models were developed to comparatively evaluate five remediation alternatives that have been proposed for the study area. The remediation alternatives are listed in the "Purpose and Scope" section. Ground-water flow in the study area was simulated in three dimensions using a finite-difference approach. Transport of contaminants from the vicinity of the unlined tailings ponds was simulated in two dimensions using a finite-element approach. Simulated flows of water across boundaries of the ground-water flow model were used to define, in part, the boundary conditions of the contaminant-transport model. Construction and calibration of the models are described in the following sections.

Parameter-estimation techniques were used during the calibration process. In accordance with common usage in the parameter-estimation literature, in this report, the term "observation" is used to refer to an input to a parameter-estimation computer program that is compared to a model-calculated value.

Ground-Water Flow Model

Hydraulic stresses and the water balance for the ground-water system were analyzed using MODFLOWP (Hill, 1992), a ground-water flow-modeling program based on the program MODFLOW (McDonald and Harbaugh, 1988) and designed for estimating model-input parameters. The purpose of this analysis was to develop a quantitative understanding of the ground-water flow system and to establish boundary conditions for the contaminant-transport modeling phase of the project.

As in MODFLOW, MODFLOWP uses finite-difference methods to set up and solve the equations of ground-water flow for a system discretized in one, two, or three dimensions. In addition to solving the system of equations representing ground-water flow, MODFLOWP uses an iterative approach to optimize model-input parameters to provide a best fit of model-calculated values to field measurements of hydraulic head and ground-water flow into or out of the system being modeled.

Model Description

A six-layer, three-dimensional model was constructed to represent the geohydrologic units of the study area from the water table to the base of the ground-water system, as defined in the "Geohydrologic Setting" section. A grid of square cells, 200 ft on a side, in 100 rows and 70 columns, was superimposed on the study area to define areal discretization of the ground-water system. Model layers were defined to represent all materials between the water table and the base of the ground-water system. Grid cells were defined as active where they corresponded to a part of the ground-water system in the study area. Model layer 1 is the uppermost layer, and model-layer numbers increase downward.

In the upgradient area, model-layer boundaries were defined partly on the basis of depth below the water table. This method of defining the correspondence between model layers and earth materials was used for three reasons: (1) Hydraulic conductivity of the mostly fine-grained Tertiary and Cretaceous rocks in the upgradient area was expected to be strongly affected by weathering and fracturing, which are related to depth (table 2); (2) fractures were expected to be the dominant transport conduit for contaminants at depths less than 100 ft below the land surface; and (3) transport of contaminants generally did not extend deeper than 100 ft below the land surface as a result of immobilization of the contaminants due to reducing conditions (Chafin and Banta, 1999). Although transport of uranium and molybdenum generally was limited to depths less than 100 ft, the same was not true of ground-water flow. In the upgradient area, earth materials deeper than 100 ft below the water table were simulated to ensure proper accounting for ground-water flow between the upper 100 ft of the ground-water system and the base of the system. In the downgradient area, the model layers corresponded to geologic units.

The areal distribution of active model cells in the six layers is shown in figure 10. The top of the uppermost active cell in any stack of cells is at the water table. Model-layer bottom boundaries are defined by a combination of geologic boundaries and specified layer thicknesses. The selection of active cells was such that cells in three to six model layers are active in the upgradient area, depending on the thickness of the interval between the water table and the top of the Vermejo Formation; cells in one model layer are active in the Raton ridge area; and cells in two model layers are active in the downgradient area (fig. 10).

Boundaries of the volume of earth materials represented by the flow model, in general, are simulated as no-flow boundaries. However, in areas where cross-boundary flow occurs, model boundaries are simulated as head-dependent boundaries (where a specified head is external to the model) or specified-flux boundaries (fig. 11). Although the model contains no specified-head cells, the head-dependent-boundary cells (drain, evapotranspiration, general-head-boundary, and river cells) serve much the same purpose as specified-head cells would serve—provision of a set of fixed heads that allows the solution algorithm to converge on a unique solution for a given set of model parameters. The no-flow boundary at the top of

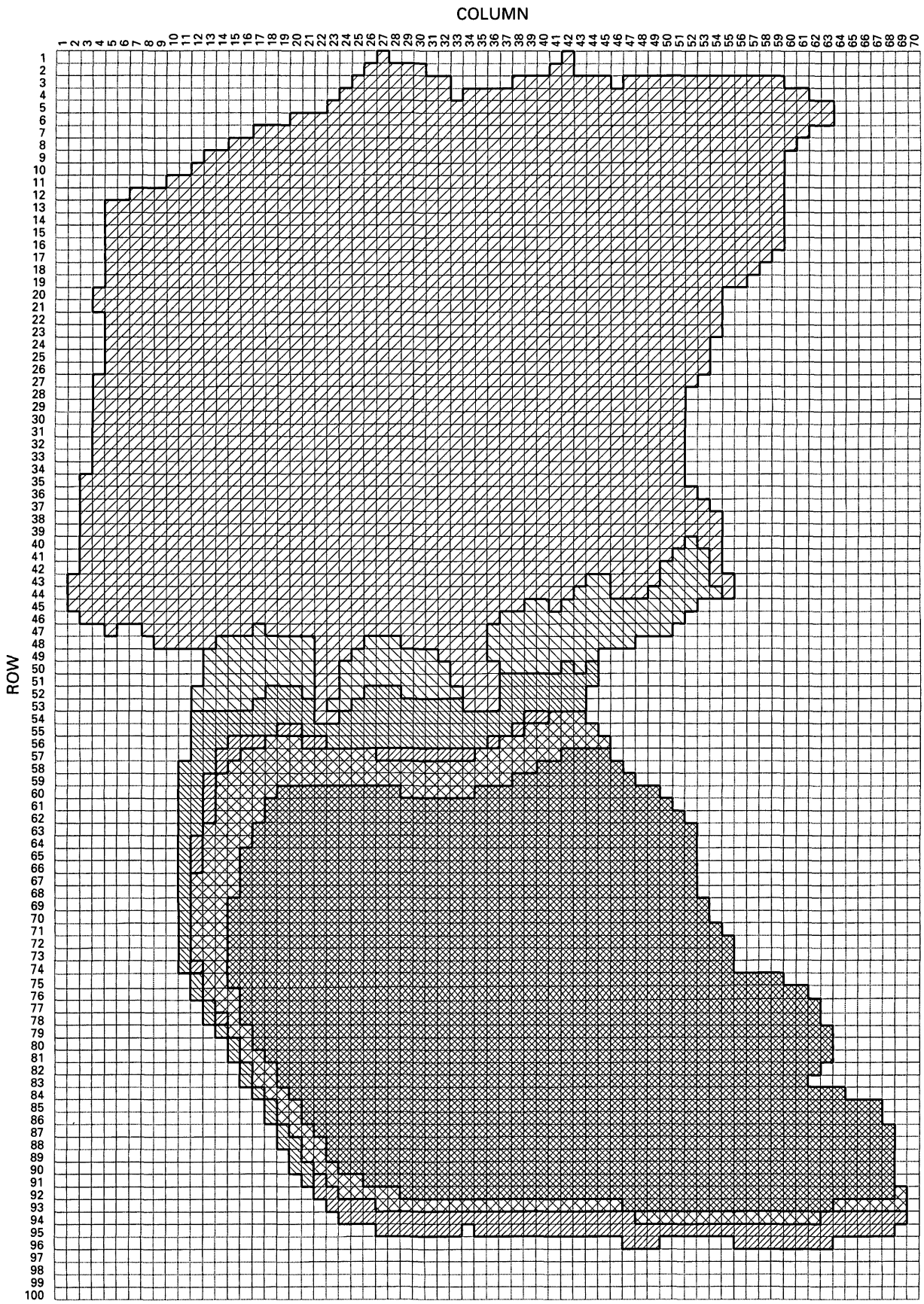

Figure 10. Distribution of active cells in all layers of the flow model. Model-grid location is shown in figure 2.

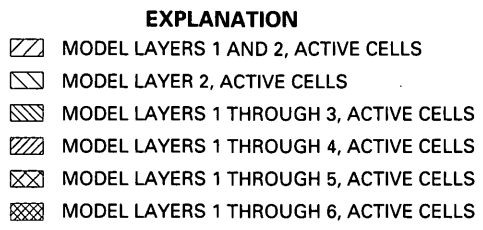

Figure 10. Distribution of active cells in all layers of the flow model. Model-grid location is shown in figure 2—Continued.

the system represents the water table. The base of the modeled system in the upgradient area is at the contact between the Raton Formation and the underlying Vermejo Formation. In the downgradient area, the no-flow boundary at the base of the model represents the base of the weathered and fractured zone of bedrock. The no-flow boundary along the southwest boundary of the modeled area and along the west side from the hogback to the Raton ridge coincides with the maximum extent of the geologic units modeled (fig. 2). The northwest edge of the model area is represented as a no-flow boundary where Pierre Shale crops out and as a head-dependent boundary where saturated terrace alluvium provides a hydraulic connection between the terrace alluvium in the modeled area and the terrace alluvium outside the modeled area. Along the north and northeast edges of the modeled area, the numerous springs and seeps and evapotranspiration by abundant vegetation are simulated as head-dependent boundaries (drains) that simulate flow out of the model. Along the drainage where the Willow Lakes are located, from near the mouth of the unnamed creek to Raton ridge, head-dependent boundaries (drains) are used to represent the potential for discharge from the system where the head in the alluvial aquifer rises above land surface in the channel. The remainder of the eastern edge of the modeled system, along the Raton ridge and the surface-water divide between the Sand Creek drainage and the drainage of the unnamed creek where the Willow Lake are located, is modeled as a no-flow boundary. Assignment of a no-flow boundary along this segment relies on the assumption that a ground-water divide approximately coincides in location with the surface-water divide. Inside the modeled area, head-dependent boundaries are used to represent the potential for discharge to Sand Creek where hydraulic heads are above land surface, to represent the potential for recharge from irrigation ditches and ponds, to represent recharge through Alkali Gap, to represent discharge from the SCS reservoir, and to represent discharge through the Littell mine shaft to the Wolf Park Mine.

In the downgradient area, layer 1 represents alluvium or terrace alluvium of variable thickness (fig. 12); in the upgradient area, layer 1 represents a 15-ft-thick zone of material, the top of which coincides with the water table (fig. 5). This zone includes the parts of the Poison Canyon Formation that are most likely to have been affected by fracturing, the alluvium, and the terrace alluvium. In the area of the Raton ridge, which separates the upgradient area from the downgradient area, saturated, unconsolidated material is absent, and the cells of layer 1 are defined as inactive.

All cells in layer 2 that are in the study area are defined as active in the model. In the downgradient area, layer 2 represents the zone of weathered and fractured bedrock immediately below the base of the alluvium or terrace alluvium. For model input, the thickness of this zone was assumed to be 15 ft; however, model calculations are based on transmissivity, which is the product of thickness and hydraulic conductivity. Because hydraulic conductivity is one of the estimated parameters, no substantial limitations on model accuracy are imposed by assuming a certain thickness for the weathered and fractured zone. In the upgradient area, layer 2 represents a 15-ft-thick zone primarily composed of weathered and fractured Poison Canyon Formation below the base of layer 1. In the Raton ridge area, layer 2 represents a 30-ft-thick zone, which consists mainly of unweathered consolidated material of the Raton and Vermejo Formations.

Layers 3 through 6 are inactive in the downgradient area and in the area of the Raton ridge. In the upgradient area, layer 3 represents a zone that has a thickness of 30 ft, except at the margin of the area where the thickness of the interval between the base of layer 2 and the top of the Vermejo Formation is less than 30 ft; in these areas, the base of layer 3 is the top of the Vermejo. Layer 4 is active only where the thickness of the interval from the base of layer 2 to the top of the Vermejo exceeds 30 ft. In these areas, the base of layer 4 is 40 ft below the base of layer 3 or is the top of the Vermejo, where the top of the Vermejo is less than 40 ft below the base of layer 3. Layer 5 is present only where the thickness of the interval between the base of layer 2 and the top of the Vermejo exceeds 70 ft. Where the thickness of the interval from the base of layer 4 to the top of the Vermejo exceeds

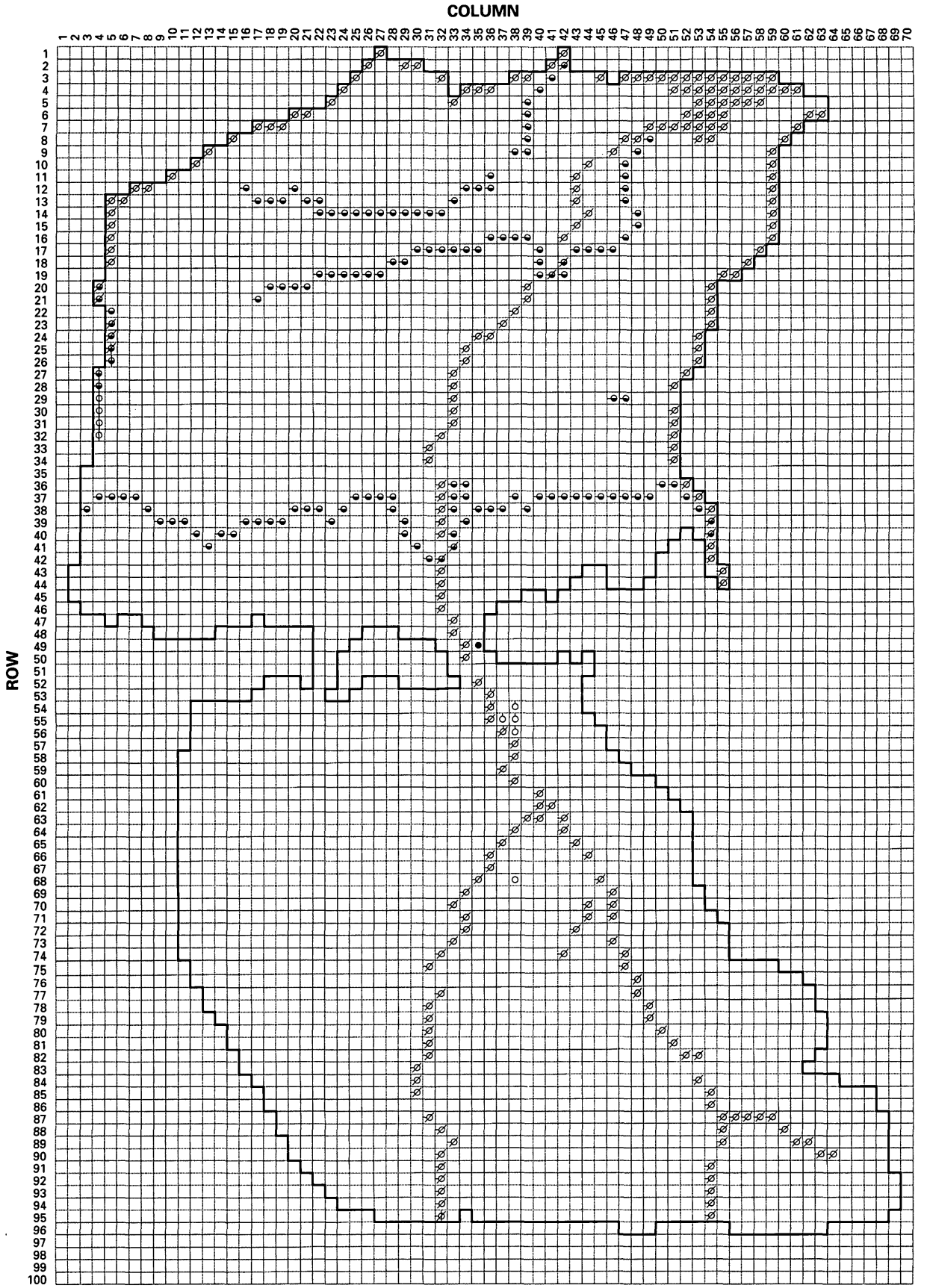

Figure 11. Boundary conditions for layer 1 of the flow model. Model-grid location is shown in figure 2.

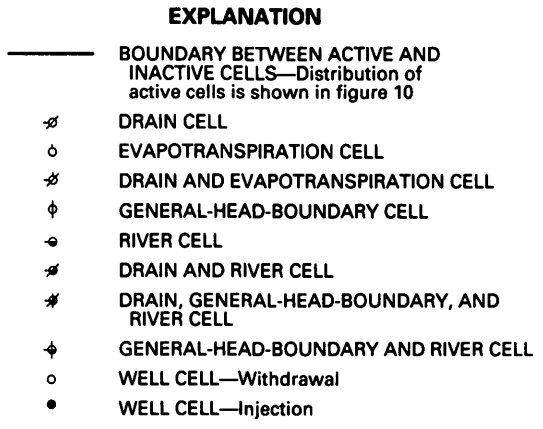

Figure 11. Boundary conditions for layer 1 of the flow model. Model-grid location is shown in figure 2—Continued.

200 ft, the thickness of layer 5 (fig. 13) is one-half the thickness of this interval; where this interval is less than 200 ft thick, the base of layer 5 is the top of the Vermejo. Layer 6 is active only where the interval between the base of layer 2 and the top of the Vermejo exceeds 270 ft; in this area, the top of layer 6 is the base of layer 5, and the base of layer 6 is the top of the Vermejo (fig. 14). A schematic section through the model along column 40 showing active cells in each layer is shown in figure 15.

Water flow into and out of the model was simulated using several types of boundary conditions. A fixed-rate source of water was used to simulate areally distributed recharge from precipitation that percolated through the unsaturated zone to the water table. Recharge was simulated in the uppermost active model cell in each stack of cells in the grid. Simulated, areally variable recharge was distributed according to zones described in table 6 and shown in figure 16. Withdrawal and injection at wells and injection at trenches were simulated as fixed-rate sinks or sources. Head-dependent boundaries enabled simulation of recharge or discharge for which the rate is determined by the difference in head between the model cell and a hypothesized external source or sink of water. The head-dependent-boundary condition was used to simulate recharge through Alkali Gap, discharge to such surface-water bodies as the SCS reservoir and Sand Creek, discharge to springs along the northern edge of the alluvial aquifer, recharge from irrigation ditches, discharge across the northwestern boundary of the study area near South Cañon Ditch, leakage out of the ground-water system to the Wolf Park Mine through the Littell mine shaft, and discharge to withdrawal trenches. No cells were specified as constant-head cells.

Head-dependent and specified-flux boundaries were specified in layers 1 and 6. The distribution of cells in model layer 1 where boundary conditions were simulated is shown in figure 11; areally distributed recharge and injection and withdrawal during the pilot tests are not shown. Injection during the pilot tests is described in the "Model Calibration" section of the "Ground-Water Flow Model" section. Leakage through the Littell mine shaft was simulated in layer 6, row 76, column 44 using the general-head-boundary package (McDonald and Harbaugh, 1988).

Transmissivities were assigned to model cells as the product of layer thickness and hydraulic conductivity. The active cells in layers 1 through 3 were divided into a series of zones for assigning spatially variable hydraulic-conductivity values. For layers 4 through 6, hydraulic conductivity was assumed to be constant in each layer.

The distribution of hydraulic-conductivity zones for model layers 1 through 3 was based on an interval-by-interval interpretation of lithologic logs from wells and boreholes. A data base of available lithologic logs for wells and boreholes in the study area was developed by Banta (1997). For each described interval, an integer code was assigned based on the predominant rock type and any modifiers or accessory rock types in the description. The purpose for assigning the codes, which are called lithology codes in this report, was to group similar rock types in a manner that would allow quantitative analysis and not directly to assign hydraulic-conductivity values.

The basis for the integer code was a diagram in Freeze and Cherry (1979, table 2.2). The diagram indicated ranges of hydraulic conductivity for various unconsolidated deposits and consolidated rocks as bars corresponding to a logarithmic scale. Ranges of hydraulic conductivity interpreted from the diagram in Freeze and Cherry for the deposit and rock types that occur in the study area are listed in table 7. For a given deposit or rock type, an initial lithology code that was equal to the exponent of 10 corresponding to the approximate (logarithmic) center of the range was assigned. For example, the range for sandstone extends from 1×10^{-8} cm/s to 2×10^{-4} cm/s; the (logarithmic) center of the range is at about 10^{-6} cm/s. For an interval described in a lithologic description merely as "sandstone,"

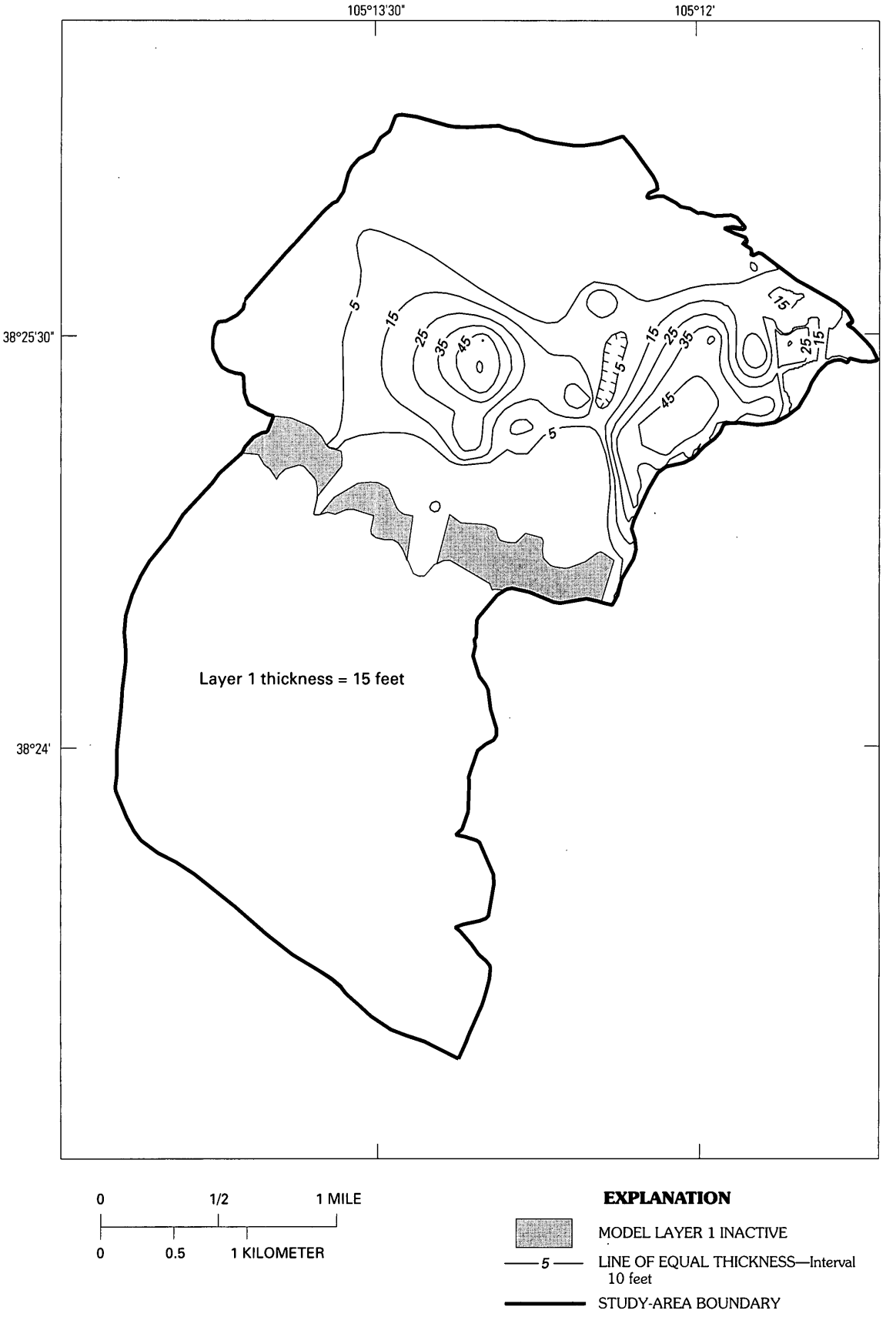

Figure 12. Thickness of model layer 1.

Figure 13. Thickness of model layer 5.

Figure 14. Thickness of model layer 6.

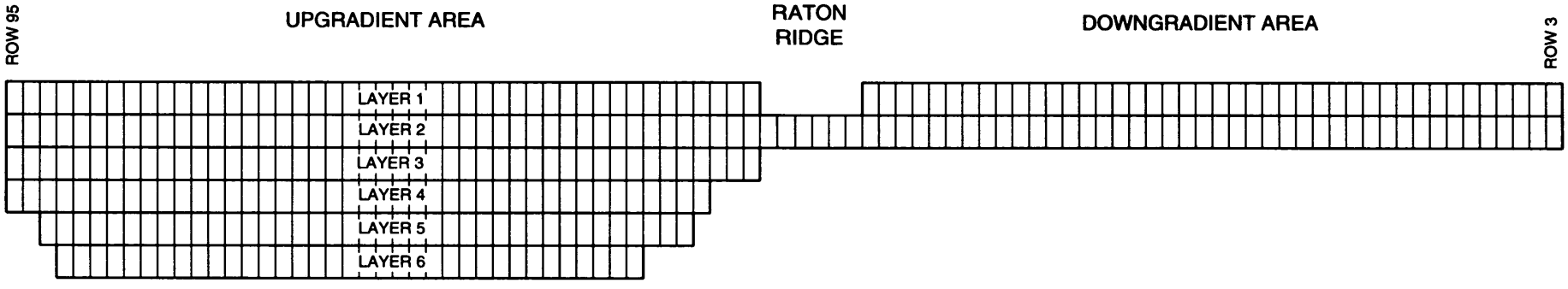

Figure 15. Section of flow model along column 40 showing active cells.

a lithology code of –6 was assigned. Where the lithologic description for an interval included a modifier that tended to indicate either substantially larger or smaller hydraulic conductivity, the lithology code was adjusted upward or downward within the range. For example, intervals listed in a lithologic description as "sandstone, silty" were assigned a lithology code of –7; those intervals described as "sandstone, very fine grained interlaminated with shale" were assigned a code of –8; intervals described as "sandstone, coarse grained" were assigned a lithology code of –5, and intervals described as "sandstone, conglomeratic" were assigned a lithology code of –4. The assignment of lithology codes was subjective, but consistent.

Table 6. Ground-water recharge zones of the flow model

[Distribution of ground-water recharge zones in model is shown in figure 16]

Recharge zone	Basis for recharge zone
1	Alluvial aquifer in Lincoln Park downgradient from DeWeese Dye Ditch
2	Alluvial aquifer in Lincoln Park upgradient from DeWeese Dye Ditch
3	Upgradient area, unmodified
4	Raton ridge (west of west SCS dam)
5	Raton ridge (between west SCS dam and SCS dam)
6	Raton ridge (east of SCS dam)
7	Upgradient area, irrigated area of golf course
8	Upgradient area, overlain by impoundment with synthetic liner
9	Upgradient area, former site of old tailing ponds
10	Upgradient area, former site of old tailings ponds, overlain by impoundment with synthetic liner

After a lithology code was assigned to each interval, the section of each well or borehole corresponding to each model layer was assigned a weighted average of the lithology codes in the section. The codes were weighted based on the length of each interval in the section. At the end of this process, a data point was available for each model layer at every location where the materials represented by the model layer were penetrated by a well or borehole.

Once the data sets for the weighted-average lithology codes were developed, each of the data sets for layers 1 through 3 was analyzed by ordinary kriging using the method by McBratney and Webster (1986) as implemented in the kriging function of ARC/INFO version 7 (Environmental Systems Research Institute, Inc., 1994). For the analysis of the weighted-average lithology code for layers 1 and 2, the study area was divided into two areas corresponding to the upgradient and downgradient areas. The semivariogram of the weighted-average lithology codes for each model layer was analyzed assuming a normal (Gaussian) distribution. The resulting interpolated values were rounded down to integers to generate a distribution of lithology-code zones for each layer. Because the zonation scheme in MODFLOWP requires zones to be identified by positive integers and because many of the integers generated by rounding the interpolated lithology codes were less than zero, the integers were increased by an arbitrary amount to produce a set of zones identified by integers greater than or equal to 1. Zones corresponding to the distribution of Quaternary geologic units in the upgradient area and of Quaternary alluvium in the downgradient area (fig. 2) were superimposed on the lithology-code distribution. The resulting zone maps for layers 1 through 3 (figs. 17–19) were used to distribute hydraulic-conductivity values among model cells. An unusually large, sustained pumpage rate at well 333 indicated a need for a separate zone (zone 15 in fig. 17) in the vicinity of that well. A small number of other areas required separate zones because of site-specific considerations. The characteristics for each zone are listed in table 8.

Model Calibration

One flow model was used for steady-state and for transient-state simulations. The ground-water flow model was calibrated using an initial steady-state period and a subsequent transient-state period, which simulated major stresses on the hydraulics of the ground-water system from May 1, 1978, to May 1, 1996. Initial conditions for the transient-state period of the simulation were generated by simulation of the steady state using the same set of model-input parameters as was used for the transient-state simulations, except for the transient-stress data. The transient-state period was divided into 49 stress periods; during each stress period, hydraulic stresses on the ground-water system were modeled as constant. The length of the stress periods ranged from 2 to 224.5 days. Stresses on the ground-water system during each stress period are listed in table 9.

The ground-water flow model was calibrated by varying model-input parameters and comparing model-calculated hydraulic heads and flows (simulated recharge and discharge across model boundaries) to observed (measured) hydraulic heads and flows. The parameter-estimation capability of MODFLOWP (Hill, 1992) was used to optimize the model-input parameters to obtain a best fit of model-calculated hydraulic heads and flows to observed heads and flows. The difference between a model-calculated head or flow and an observed head or flow is termed a residual.

A measure commonly used to quantify the degree to which a model reproduces observations is the sum of squared, weighted residuals. The sum of squared, weighted residuals can be expressed as:

$$SSWR = \sum_{i=1}^{N} \left[\frac{(y_i - \hat{y}_i)^2}{w_i} \right]$$

where

$SSWR$ is the sum of squared, weighted residuals;

N is the number of observations;

y_i is i^{th} observation;

$\hat{y}_i$ is the model estimate corresponding to the i^{th} observation;

w_i is the (estimated) variance associated with the i^{th} observation; and

$(y_i - \hat{y}_i)$ is the residual for the i^{th} observation.

For each model run during the calibration process, SSWR was calculated. As calibration progressed, smaller values of SSWR indicated better agreement between model results and observations. To obtain a best fit, MODFLOWP attempts to minimize SSWR (Hill, 1992).

To compare model results with observations that may differ in accuracy or in units of measure, each observation was assigned a variance; observations that were relatively accurate were assigned small variances, and observations that were relatively inaccurate were assigned large variances. For example, water levels measured at wells for which the altitude of the measuring point had been surveyed were more accurate than water levels measured at wells where the measuring-point altitude was estimated from a topographic map. In the modeled area, observed hydraulic heads ranged from about 5,300 to about 6,000 ft above sea level, whereas observed flows ranged in absolute value from 100 to 383,000 ft^3/d. To make a comparison between hydraulic heads and flows meaningful, large variances were assigned to observed flows near the upper end of the range of observations, and small variances were assigned to observed flows at the lower end of the range, so that the quotients of the observations of head or flow divided by the variances were comparable in magnitude.

Hydraulic-head observations for 199 wells and boreholes were used in the calibration. Water-level observations that were expected to be representative of steady-state conditions for 197 of these sites were used for the steady-state model period; the median of water levels observed during non-stress conditions for each site was considered to be representative of the steady state (table 10). Because of seasonal irrigation in the downgradient area, the head observations did not represent a true steady state. However, calibration of a steady-state period was required to provide a starting point for the transient-state part of the simulations. Results for the steady-state period of the flow model represented a hypothetical steady-state characteristic of average conditions and were not characteristic of the true dynamic ground-water system. During the transient-state part of the simulation, 1,675 head observations for 97 sites were used in the calibration. Head observations are summarized in table 10. Distribution of head-observation sites is shown in figure 20; locations of specific sites are listed in Banta (1997).

Eight discharge observations were used in calibration of the flow model. Measurements of discharge in Sand Creek just upstream from the mouth were used as observations for the transient calibration. These measurements were 2.1×10^5 ft^3/d on May 11, 1995, which was just prior to the start of the irrigation season, and 3.8×10^5 ft^3/d on August 10, 1995, which was during the irrigation season (Banta, 1997). To provide an observation of discharge from Sand Creek for the steady-state part of the calibration, these two discharge measurements were averaged. Three measured discharges from withdrawal trenches during the 1992 test of an injection and withdrawal system in the third test area were selected for use as discharge observations; these discharges were 900 ft^3/d on February 27, 100 ft^3/d on April 1, and 2,000 ft^3/d on November 1 (Adrian Brown Consultants, Inc., 1993). The loss of 2.9×10^5 ft^3/d, which was calculated for the gain-loss investigation along a reach of DeWeese Dye Ditch on August 9, 1995, and the leakage of 78,000 ft^3/d from irrigation pond 9 on May 18, 1995, also were used as observations.

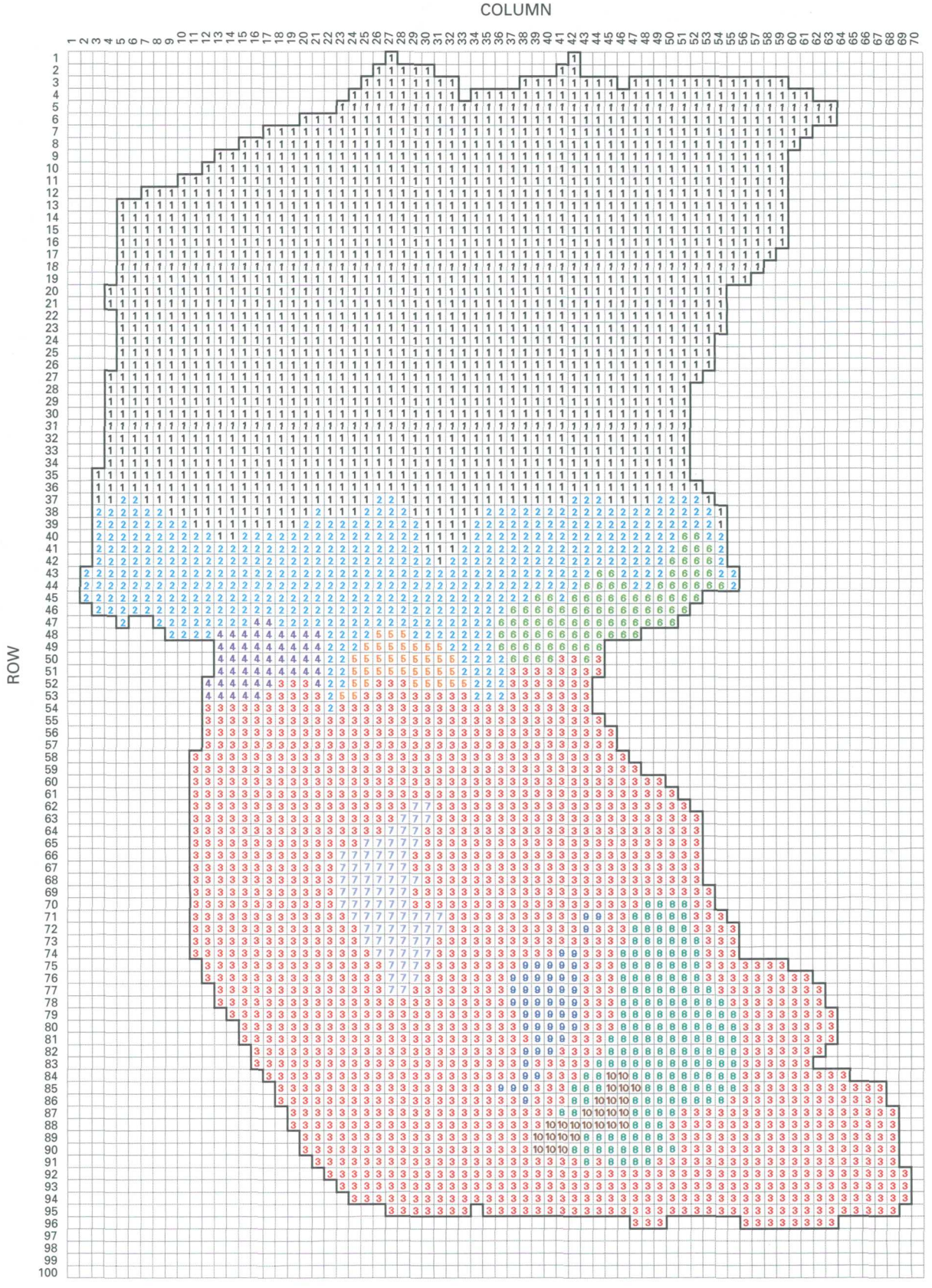

Figure 16. Ground-water recharge zones for the flow model.

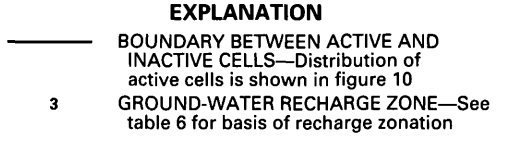

Figure 16. Ground-water recharge zones for the flow model—Continued.

For optimization of model-input parameters, some of the zones listed in tables 6 and 8, which represented areas having similar hydraulic characteristics, were combined to decrease the number of parameters to be estimated. Other model inputs that were not areally divided into zones were added to the list of parameters to be estimated (table 11). Because simulation of a steady-state period required an assumption of a hypothetical steady state in the alluvial aquifer, some simplifying assumptions were made concerning the definition of parameters. For example, recharge in the area north of the DeWeese Dye Ditch was assumed to be entirely due to infiltration of excess irrigation water. The irrigation season was assumed to be 5 months long. The ratio of the annual rate of recharge in this area (R1SP0, table 11) to the rate during the irrigation season (R1IRR, table 11) was assumed to be 5:12. Irrigation ditches and ponds were simulated using head-dependent boundaries. To simulate a hypothetical steady-state leakage rate from the ditches and ponds, the hydraulic conductance between the model cells that were designated as head-dependent boundaries was assumed to be 5/12 times the hydraulic conductance for the irrigation seasons simulated during the transient-state periods.

The flow-model parameters were estimated using MODFLOWP and are listed in table 12. Sensitivity of each model parameter is indicated by the composite scaled sensitivity. The composite scaled sensitivity is a measure of the degree to which each parameter affects model-calculated heads and flows corresponding to observed heads and flows. The composite scaled sensitivity for parameter j, (CSS_j) is calculated as:

$$CSS_j = \left\{ \left[\sum_{i=1}^{N} w_i \left(\frac{\delta \hat{y}_i}{\delta b_j} \right)^2 b_j^{\,2} \right] / N \right\}^{1/2}$$

where

b_j is the j^{th} parameter (D'Agnese and others, 1997).

Changes in parameters that have large composite scaled sensitivities produce large changes in model-calculated heads and flows, and changes in parameters that have small composite scaled sensitivities produce small changes in model-calculated heads and flows. A frequency histogram of residuals for the calibrated flow model (fig. 21) indicates the size of errors that are inherent in the model.

The water budget for the steady-state period simulated by the calibrated model is listed in table 13. The flow-model results quantified all components of the water budget of the simulated ground-water system. However, the categorization of the model-calculated water budget differs from the categorization of the estimated water budget (table 5). Areal recharge in the model-calculated water budget included recharge in the potentially irrigated area north of the DeWeese Dye Ditch and in the nonirrigated area south of the DeWeese Dye Ditch. Recharge in the area north of the DeWeese Dye Ditch was simulated as about 105,000 ft^3/d, and recharge in the area south of the DeWeese Dye Ditch was simulated as about 4,000 ft^3/d. Estimated recharge from excess irrigation and leakage from irrigation ditches and ponds (table 5) was 730,000 ft^3/d. The comparable quantity from the model-calculated water budget is the sum of the model-calculated recharge in the area north of the DeWeese Dye Ditch (105,000 ft^3/d)

Table 7. Hydraulic-conductivity ranges for earth materials in the study area

[Hydraulic conductivities from Freeze and Cherry (1979, table 2.2)]

Deposit or rock type	Hydraulic conductivity (values are approximate)	
	Minimum (centimeters per second)	Maximum (centimeters per second)
Gravel	1×10^{-1}	9×10^{1}
Clean sand	2×10^{-4}	9×10^{-1}
Silty sand	8×10^{-6}	7×10^{-2}
Silt	1×10^{-7}	2×10^{-3}
Unweathered marine clay	5×10^{-11}	2×10^{-7}
Sandstone	1×10^{-8}	2×10^{-4}
Shale	7×10^{-12}	7×10^{-8}

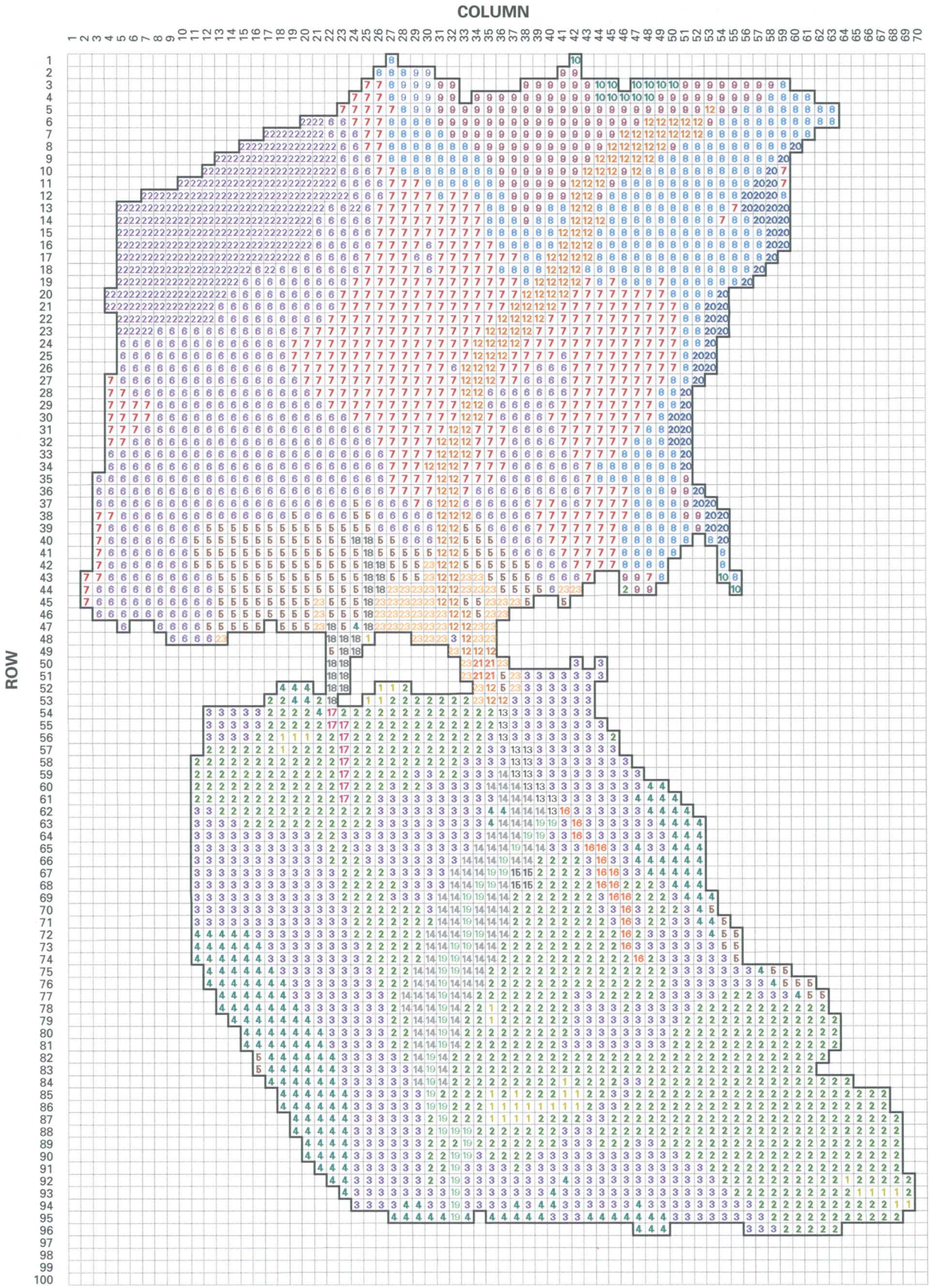

Figure 17. Hydraulic-conductivity zones for layer 1 of the flow model. Model-grid location is shown in figure 2.

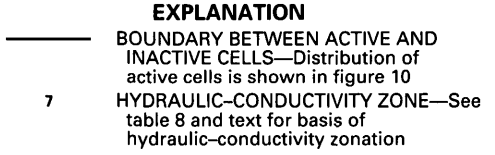

Figure 17. Hydraulic-conductivity zones for layer 1 of the flow model. Model-grid location is shown in figure 2—Continued.

and the net leakage from irrigation ditches and ponds (about 661,000 ft^3/d, table 13); this sum is 766,000 ft^3/d. The difference between the two estimates of recharge to the alluvial aquifer from irrigation water is about 5 percent. In the model, pumpage plus evapotranspiration from the SCS reservoir was simulated as 6,750 ft^3/d (table 13). The estimated rate of pumpage plus evapotranspiration from the SCS reservoir was 8,000 ft^3/d (table 5). The difference between these values is about 16 percent. Discharge to Sand Creek was estimated to be 295,000 ft^3/d (table 5). The model-calculated discharge to Sand Creek was about 289,000 ft^3/d (table 13). The difference between the two values is about 2 percent. The components of the water budget that can be compared between the estimated budget and the model-calculated budget do not represent the entire water budget of the ground-water system of the study area. However, these components undoubtedly represent a large part of the water budget; in the model simulation, they represent 97 percent of the simulated flow into the model and 38 percent of the simulated flow out of the model.

The model-calculated water table (fig. 22) for layer 1 compared reasonably well with the water-table map interpreted from observed water levels (fig. 5). The agreement between the observed water table and the model-calculated water table was best in the central part of the downgradient area and in the northern part of the upgradient area. However, the model did not well represent the undulations of the observed water-table contours in much of the upgradient area. Discrepancies between the two sets of contours likely resulted from (1) inadequate representation of the heterogeneity of the ground-water system, and (2) inability to accurately estimate a steady-state head distribution for the downgradient area, which was seasonally affected by recharge from irrigation water.

Comparison of model-calculated heads with observed heads at specific wells over time indicated variable agreement between the two. In the upgradient area, during the pilot tests, the model overestimated the changes in head at wells 1340 and 1400 (fig. 23). At the same time, observed and model-calculated heads at well 804 changed little, although the model-calculated heads were about 2 to 4 ft lower than the observed heads. In the downgradient area, agreement between model-calculated heads and observed heads was moderately good at well 119 and fair at wells 10, 20, and 329 (fig. 24). The annual fluctuations in head at wells 10, 20, and 119 are the result of seasonal irrigation. Well 329 is near the dam-to-ditch injection trenches; water levels at this well increased at the start of injection in 1990 and fluctuated annually in response to seasonal injection. In the downgradient area, in general, the seasonal fluctuations in the model-calculated heads tended to underestimate the amplitude of the seasonal fluctuations in observed heads, except at well 119, where the agreement is good.

Despite the inaccuracies in the match between model-calculated and observed hydraulic heads in some areas, the model-calculated head gradient and overall orientation of the model-calculated contours reproduced the observed water-table map sufficiently well that the flow model can be considered adequate for its intended use in this study. The relatively good agreement between the model-calculated water-budget components (table 13) and the estimated water-budget components (table 5) provides support for the intended use of the flow model.

Contaminant-Transport Model

Results of the third pilot test, discussed in the "Geochemistry of Uranium and Molybdenum" section and described by Adrian Brown Consultants, Inc. (1993), indicated that the solid and aqueous phases of uranium and molybdenum were not in equilibrium during the test. However, an assumption commonly used in developing models for simulation of transport and sorption of solutes in ground water is that equilibrium between the aqueous phase and the solid phase occurs essentially instantaneously; that is, within the time period represented by one model time step. To account for nonequilibrium in

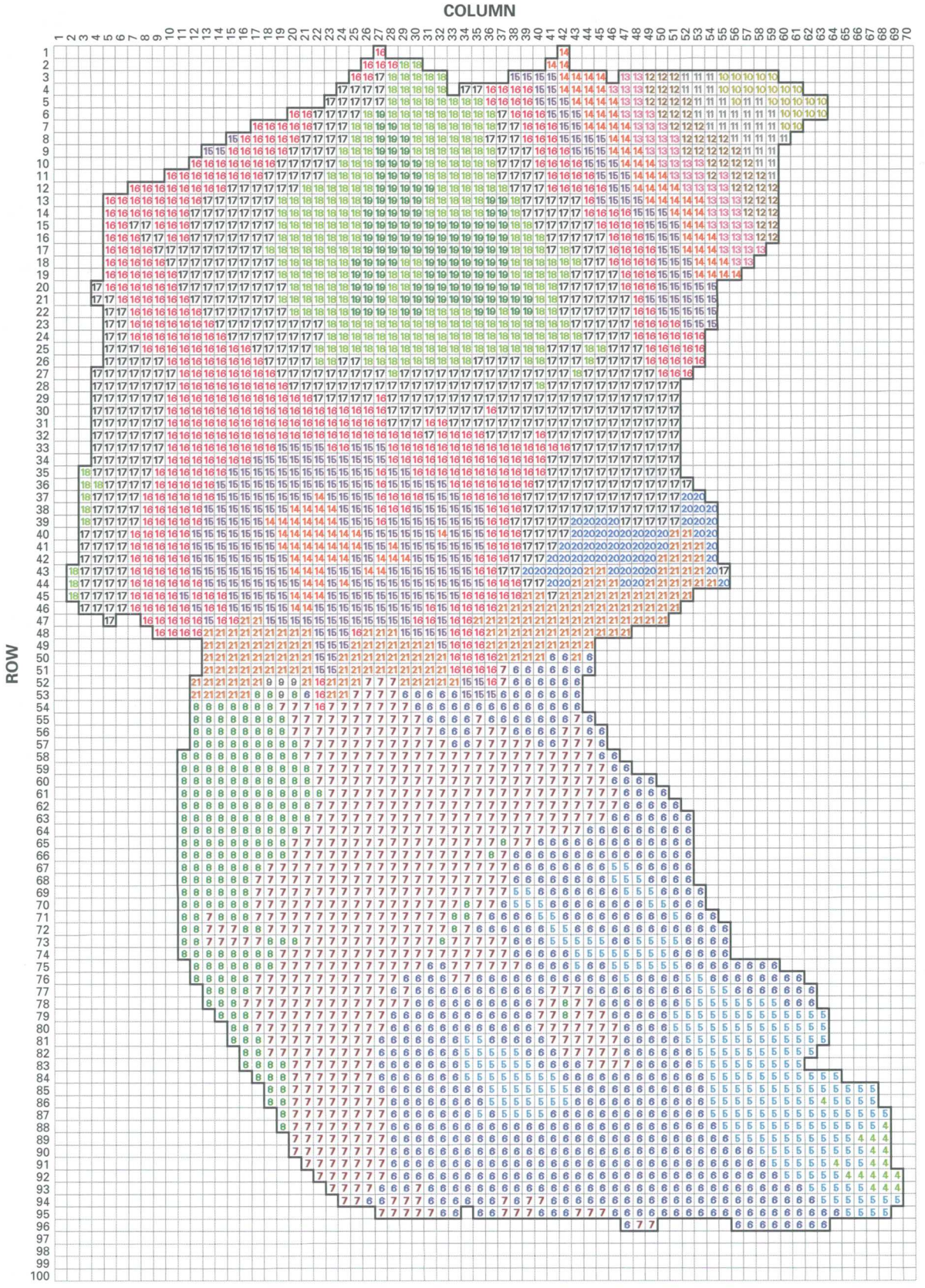

Figure 18. Hydraulic-conductivity zones for layer 2 of the flow model. Model-grid location is shown in figure 2.

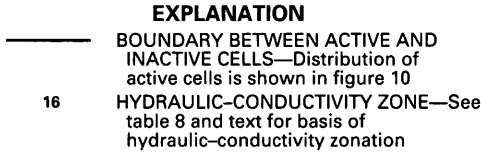

Figure 18. Hydraulic-conductivity zones for layer 2 of the flow model. Model-grid location is shown in figure 2—Continued.

the transfer of contaminants between the aqueous phases and the solid phases, contaminant transport was modeled in two dimensions over the study area using a version of SUTRA (Voss, 1984) modified to simulate rate-limited sorption and desorption (see the "Supplemental Information" section at the end of the report for description and validation of SUTRA modifications); the modified version is referred to as DKSUTRA in this report.

Because the code used to model contaminant transport was limited to two dimensions, whereas the flow model was three dimensional, generalization of model parameters in the vertical direction was required. As discussed in the "Geochemistry of Uranium and Molybdenum" section, concentrations of uranium and molybdenum in wells completed in zones more than 100 ft below land surface were small. Because weathering and fracturing are the most well developed in the near-surface materials (table 2), hydraulic conductivities of rocks above 100 ft generally are larger than hydraulic conductivities of rocks below 100 ft. The calibrated flow model has small values of hydraulic conductivity for the deepest two layers (parameters L5K and L6K in tables 11 and 12). Because of (1) the small hydraulic conductivities assigned to flow-model layers 5 and 6, (2) the relative lack of fracturing and weathering in the materials corresponding to flow-model layers 5 and 6, and (3) the apparent relative lack of transport of uranium and molybdenum in rocks represented by these model layers, the (one-layer) transport model was conceptualized as corresponding to layers 1 through 4 of the flow model. Simulated flow through layers 5 and 6 was small compared to flow through the upper four layers and was ignored in the transport model, except that discharge from the ground-water system simulated in the flow model through the Littell mine shaft was specified as a constant flux in the transport model. As a result of this generalization, the simulated flow system is simplified. The three-dimensional aspect of flow paths of the contaminants is not simulated.

For simulating solute transport in the study area, ground-water flow was assumed to be at steady-state equilibrium at any point in time. In the history of the operation of the uranium mill, substantial changes were made to hydraulic stresses on the ground-water system and to the ground-water system itself in the upgradient area (see the "Physical Ground-Water System" section). During periods between substantial changes, however, hydraulic stresses on the ground-water system in the upgradient area were essentially constant. Solute transport was simulated using a series of steady-state flow-model simulations corresponding to a series of four periods between substantial changes to the ground-water system and its hydraulic stresses. The solute-transport model was calibrated using uranium and molybdenum concentration data for three sites. Predictive runs of the solute-transport model were based on one, two, or four steady-state flow-model simulations representing hydraulic stresses of the proposed remediation alternatives.

Model Description

Areal discretization of the modeled area for the transport model was identical to the areal discretization for the flow model; the quadrilateral elements required for the transport model exactly coincided with the active cells of the flow model. Nodes in the transport-model mesh coincided with grid-cell corners in the flow model. Transmissivities for the transport-model elements were calculated as the sum of the transmissivities for the corresponding cells in layers 1 through 4 of the calibrated flow model.

The SUTRA model code and the models derived from it (KSUTRA, DKSUTRA; see the "Supplemental Information" section.) calculate hydraulic pressure and water flow, given boundary conditions, stresses, and other input to the models, then simulate the transport of solutes in the resulting simulated flow field. To force the transport model to have a two-dimensional approximation of the (three-dimensional) flow field predicted by the flow model, constant-pressure nodes were specified at nodes in the transport model corresponding to the outside corners of cells in the flow model that were

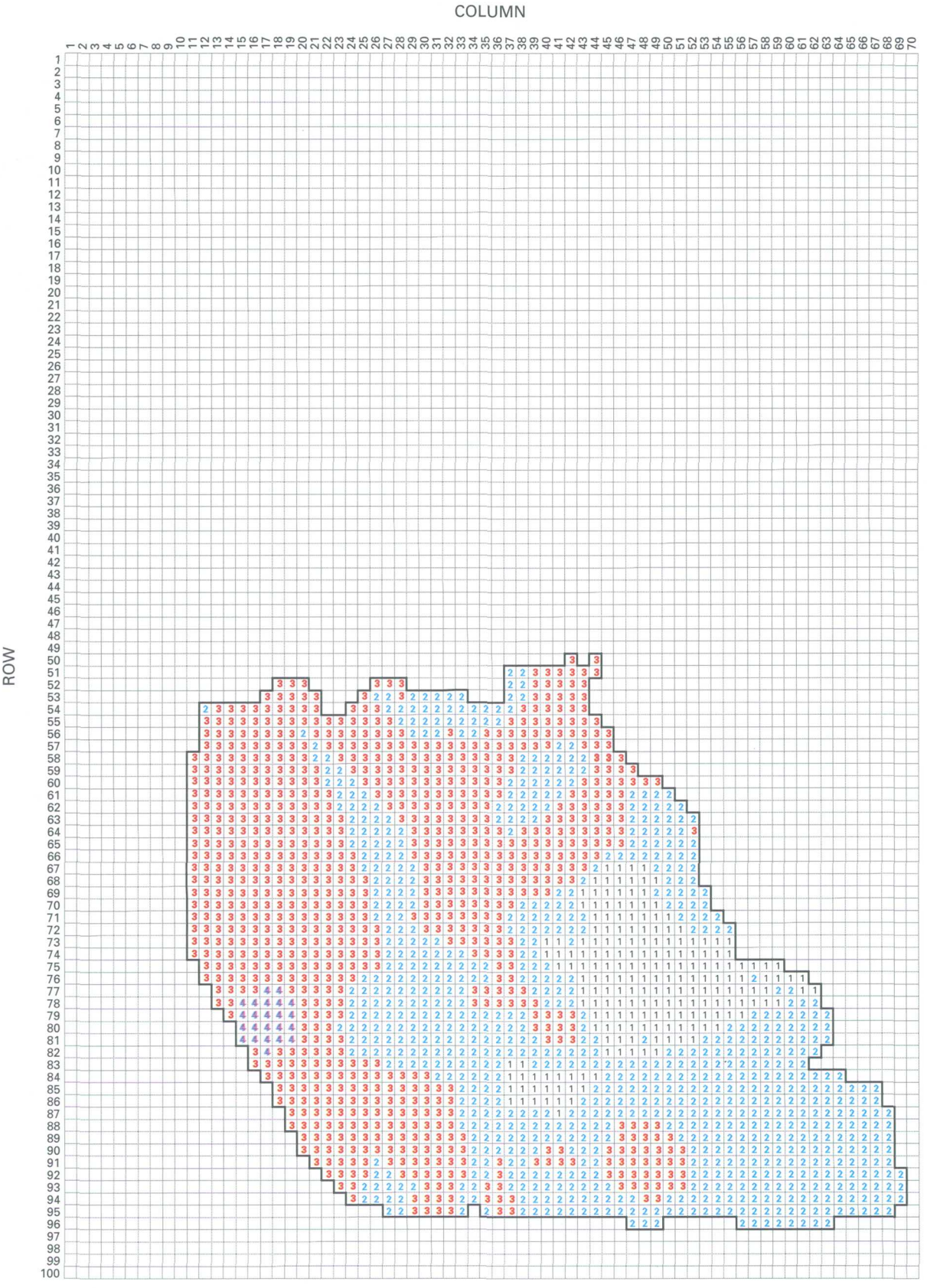

Figure 19. Hydraulic-conductivity zones for layer 3 of the flow model. Model-grid location is shown in figure 2.

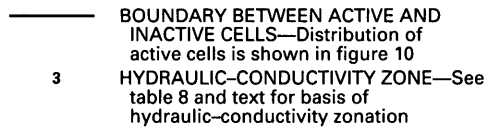

Figure 19. Hydraulic-conductivity zones for layer 3 of the flow model. Model-grid location is shown in figure 2—Continued.

specified as drain cells along the northern edge of the model area and were points of simulated discharge. Other points where water was simulated as entering or leaving the system in the flow model were coded as specified-flux nodes in the transport model. For groups of flow-model cells representing reaches of creeks or irrigation ditches or other areas where flow was simulated into or out of the modeled system, the simulated flow was distributed equally to corresponding groups of nodes representing the same features in the transport model. For each set of hydraulic stresses to be simulated by the transport model, a steady-state flow-model simulation was made to provide fluxes into and out of the system for the transport model.

Model Calibration

The transport model was calibrated using a parameter-estimation method similar to the method used in calibration of the flow model. Contaminant-concentration data potentially useful as observations are available for samples from a small number of wells in the downgradient area that date as early as 1962. However, increases in uranium concentration at well 144 as early as 1968 (Goode and Wilder, 1987) likely were caused, in part, by surface-water transport of tailings particles from the upgradient area to the downgradient area prior to the construction of the SCS dam in 1971 and by air transport of ore-stockpile particles (Geotrans, Inc., and others, 1986). In this report, it is assumed that, by 1978, the effects in the downgradient area of surface-water- and air-transported contaminants were less important than the effects of contaminants transported by ground water. For this reason, concentrations of uranium and molybdenum in water samples collected between 1978 and 1994 were used as observations; where possible, for each year, one sample for each observation location was selected that most closely represented the median concentrations for the year for uranium and molybdenum. The model-independent parameter-estimation program PEST (Watermark Computing, 1994) was used to control the DKSUTRA model runs; to calculate the value of an objective function, defined as the sum of squared, weighted residuals; and to adjust parameters to minimize the objective function. In input to PEST, each observation is assigned a weight, which is inversely proportional to the estimated standard deviation (square root of the variance) of the observation (Watermark Computing, 1994).

The assignment of observations and weights is problematic when contaminant concentrations range over three orders of magnitude, as in the case for the study area. Several methods of assigning observations and weights based on contaminant concentration were considered. If untransformed concentrations had been used as observations and had been assigned equal weights, equal differences between observed and model-calculated concentrations, whether the observed concentration is large or small, would have contributed equally to the objective function. To give appropriate emphasis to observations of small concentrations, however, observations of small concentrations need to be weighted more than observations of large concentrations. In one attempt to weight the concentration observations appropriately, weights were assigned as the reciprocal of the observed concentration. The problem with this approach is that, if a calculated concentration is very small compared to the corresponding measured concentration, the weighted residual is close to 1. However, if the calculated concentration is very large compared to the measured concentration, the weighted residual is a large negative value, and its square contributes disproportionately to the objective function. Appropriate weighting of observations of large and small concentrations was achieved by using log-transformed concentrations and equal weights. By log transforming the concentrations and setting the weights equal, the magnitude of each residual depended on the ratio of the observed value to the model-calculated value. All (log-transformed) concentration observations were assigned weights equal to 1.

Table 8. Hydraulic-conductivity zones of the flow model

[Distribution of hydraulic-conductivity zones in model is shown in fig. 17 for layer 1, in fig. 18 for layer 2, and in fig. 19 for layer 3. See text for explanation of lithology codes]

Hydraulic-conductivity zone	Basis for hydraulic-conductivity zone
	Layer 1 (fig. 17)
1	Lithology code = –8 in upgradient area
2	Lithology code = –7 in upgradient area
3	Lithology code = –6 in upgradient area
4	Lithology code = –5 in upgradient area
5	Lithology code = –4 in downgradient area
6	Lithology code = –3 in downgradient area
7	Lithology code = –2 in downgradient area
8	Lithology code = –1 in downgradient area
9	Lithology code = 0 in downgradient area
10	Lithology code = 1 in downgradient area
12	Quaternary alluvium along Sand Creek in downgradient area
13	Quaternary alluvium along Sand Creek downstream from mouth of west tributary of Sand Creek in upgradient area
14	Quaternary terrace alluvium near west tributary of Sand Creek in upgradient area
15	Vicinity of well 333 in upgradient area
16	Quaternary alluvium along Sand Creek in upgradient area
17	Quaternary alluvium along unnamed drainage upstream from west SCS dam in upgradient area
18	Quaternary alluvium along unnamed drainage downstream from west SCS dam in downgradient area
19	Quaternary alluvium along west tributary of Sand Creek in upgradient area
20	Quaternary alluvium along unnamed creek where the Willow Lakes are located in downgradient area
21	Quaternary alluvium in vicinity of SCS dam in downgradient area
22	Lithology code = –5 or –4 in downgradient area, near north edge of study area
23	Lithology code = –5 in downgradient area, between SCS dam and DeWeese Dye Ditch
	Layer 2 (fig. 18)
4	Lithology code = –9 in upgradient area
5	Lithology code = –8 in upgradient area
6	Lithology code = –7 in upgradient area
7	Lithology code = –6 in upgradient area
8	Lithology code = –5 in upgradient area
9	Lithology code = –4 in upgradient area
10	Lithology code = –11 in downgradient area
11	Lithology code = –10 in downgradient area
12	Lithology code = –9 in downgradient area
13	Lithology code = –8 in downgradient area
14	Lithology code = –7 in downgradient area
15	Lithology code = –6 in downgradient area
16	Lithology code = –5 in downgradient area
17	Lithology code = –4 in downgradient area
18	Lithology code = –3 in downgradient area
19	Lithology code = –2 in downgradient area
20	Lithology code = –3 or –2 in downgradient area between DeWeese Dye Ditch and Raton ridge
21	Vermejo Formation along Raton ridge
	Layer 3 (fig. 19)
1	Lithology code = –8
2	Lithology code = –7
3	Lithology code = –6
4	Lithology code = –5

Table 9. Transient-state stress periods and stresses used in calibration of the flow model

[Simulated injection is indicated by a positive number; simulated withdrawal is indicated by a negative number]

Transient-state stress period	Stress-period begin date and military time	Stress-period length (days)	Stress						
			Irrigation ditches and ponds	Dam-to-ditch flush injection (cubic feet per day)	North-test-area injection (cubic feet per day)	North-test-area withdrawal (cubic feet per day)	South-test-area injection (cubic feet per day)	South-test-area withdrawal (cubic feet per day)	Third-test-area injection (cubic feet per day)	Well 333 (cubic feet per day)
1	05–01–1978 0000	153	On	0	0	0	0	0	0	0
2	10–01–1978 0000	212	Off	0	0	0	0	0	0	0
3	05–01–1979 0000	153	On	0	0	0	0	0	0	0
4	10–01–1979 0000	213	Off	0	0	0	0	0	0	0
5	05–01–1980 0000	153	On	0	0	0	0	0	0	0
6	10–01–1980 0000	212	Off	0	0	0	0	0	0	0
7	05–01–1981 0000	153	On	0	0	0	0	0	0	–2,800
8	10–01–1981 0000	212	Off	0	0	0	0	0	0	–2,800
9	05–01–1982 0000	153	On	0	0	0	0	0	0	–2,800
10	10–01–1982 0000	212	Off	0	0	0	0	0	0	–2,800
11	05–01–1983 0000	153	On	0	0	0	0	0	0	–2,800
12	10–01–1983 0000	213	Off	0	0	0	0	0	0	–2,800
13	05–01–1984 0000	153	On	0	0	0	0	0	0	–2,800
14	10–01–1984 0000	212	Off	0	0	0	0	0	0	–2,800
15	05–01–1985 0000	153	On	0	0	0	0	0	0	–2,800
16	10–01–1985 0000	212	Off	0	0	0	0	0	0	–2,800
17	05–01–1986 0000	153	On	0	0	0	0	0	0	–2,800
18	10–01–1986 0000	212	Off	0	0	0	0	0	0	–2,800
19	05–01–1987 0000	153	On	0	0	0	0	0	0	–2,800
20	10–01–1987 0000	213	Off	0	0	0	0	0	0	–2,800
21	05–01–1988 0000	153	On	0	0	0	0	0	0	–2,800
22	10–01–1988 0000	212	Off	0	0	0	0	0	0	–2,800
23	05–01–1989 0000	153	On	0	0	0	0	0	0	–2,800
24	10–01–1989 0000	163	Off	0	0	0	0	0	0	–2,800
25	03–13–1990 0000	202	On	11,650	0	0	0	0	0	–2,800
26	10–01–1990 0000	79	Off	11,650	0	0	0	0	0	–2,800
27	12–19–1990 0000	15	Off	0	0	0	0	0	0	–2,800

Table 9. Transient-state stress periods and stresses used in calibration of the flow model—Continued

[Simulated injection is indicated by a positive number; simulated withdrawal is indicated by a negative number]

Transient-state stress period	Stress-period begin date and military time	Stress-period length (days)	Stress							
			Irrigation ditches and ponds	Dam-to-ditch flush injection (cubic feet per day)	North-test-area injection (cubic feet per day)	North-test-area withdrawal (cubic feet per day)	South-test-area injection (cubic feet per day)	South-test-area withdrawal (cubic feet per day)	Third-test-area injection (cubic feet per day)	Well 333 (cubic feet per day)
28	01–03–1991 0000	75	Off	0	385	–254.9	963	–94.9	0	–2,800
29	03–19–1991 0000	115	On	5,775	385	–1,222.9	963	–344.1	0	–2,800
30	07–12–1991 0000	88	On	5,775	963	–1,556.9	963	–410.2	0	–2,800
31	10–08–1991 0000	56	Off	0	963	–1,731	963	–463.3	0	–2,800
32	12–03–1991 0000	31	Off	0	770	–1,499	963	–482.7	0	–2,800
33	01–03–1992 0000	31	Off	0	770	–1,615.9	963	–370.8	0	–2,800
34	02–03–1992 0000	24	Off	0	770	–1,448.9	963	–802.2	4,655.9	–2,800
35	02–27–1992 0000	69	Off	0	770	–760.8	193	–833.4	1,083.9	–2,800
36	05–06–1992 0000	14	On	5,775	770	–847.5	193	–286	1,083.9	–2,800
37	05–20–1992 0000	69	On	5,775	0	0	0	0	1,083.9	–2,800
38	07–28–1992 0000	70	On	5,775	0	0	0	0	5,201	–2,800
39	10–06–1992 0000	57	Off	0	0	0	0	0	5,201	–2,800
40	12–02–1992 0000	150	Off	0	0	0	0	0	0	–2,800
41	05–01–1993 0000	153	On	5,775	0	0	0	0	0	–2,800
42	10–01–1993 0000	213	Off	0	0	0	0	0	0	–2,800
43	05–02–1994 0000	152	On	5,775	0	0	0	0	0	–2,800
44	10–01–1994 0000	224.5	Off	0	0	0	0	0	0	–2,800
45	05–13–1995 1200	2	On	0	0	0	0	0	0	–2,800
46	05–15–1995 1200	19.5	Off	0	0	0	0	0	0	–2,800
47	06–04–1995 0000	58	On	0	0	0	0	0	0	–2,800
48	08–01–1995 0000	61	On	5,775	0	0	0	0	0	–2,800
49	10–01–1995 0000	213	Off	0	0	0	0	0	0	–2,800

Table 10. Sites used for hydraulic-head observations in calibration of the flow model

[Site locations are in Banta (1997); --, no observation(s) used]

Site identifier	Steady-state head (feet above sea level)	Number of transient observations	Minimum head (feet above sea level)	Maximum head (feet above sea level)	Date of first transient-state observation	Date of last transient-state observation
0001	5,602.17	10	5,600.33	5,603.64	04/24/1990	01/26/1993
0003	5,505.33	10	5,504.87	5,506.26	04/09/1990	04/19/1993
0007	5,369	10	5,359.45	5,373.54	06/22/1990	11/05/1992
0009	5,517.36	10	5,515.34	5,518.88	04/19/1990	04/19/1993
0010	5,346.05	10	5,337.74	5,351.77	06/22/1990	03/23/1993
0014	5,520.41	10	5,519.21	5,520.6	04/19/1990	04/20/1993
0015	5,443.67	1	5,443.67	5,443.67	01/28/1992	01/28/1992
0016	5,491.56	10	5,478.2	5,491.9	03/29/1990	04/08/1993
0017	5,475.68	4	5,475.68	5,476.2	07/29/1992	04/08/1993
0019	5,400.91	27	5,384.24	5,411.8	04/24/1990	09/26/1995
0020	5,390.28	27	5,376.38	5,398.96	04/24/1990	09/26/1995
0021	5,474.74	10	5,470.11	5,478.72	04/09/1990	04/20/1993
0022	5,475.53	10	5,473.46	5,476.69	04/10/1990	04/20/1993
0114	5,361.39	0	--	--	--	--
0119	5,407.02	29	5,394.63	5,416.58	08/27/1992	10/31/1995
0120	5,387.74	0	--	--	--	--
0121	5,395.09	41	5,390.87	5,415	05/15/1995	10/31/1995
0122	5,373.42	0	--	--	--	--
0124	5,360.11	0	--	--	--	--
0129	5,334.9	0	--	--	--	--
0130	5,332.23	0	--	--	--	--
0145	5,408.45	0	--	--	--	--
0166	5,319.34	1	5,319.34	5,319.34	07/19/1995	07/19/1995
0174	5,360.08	0	--	--	--	--
0179	5,418.05	29	5,416.61	5,419.49	05/15/1995	10/17/1995
0303	5,507.1	0	--	--	--	--
0309	5,536.12	0	--	--	--	--
0312	5,480.58	0	--	--	--	--
0313	5,480.55	0	--	--	--	--
0314	5,474.6	1	5,474.6	5,476.66	03/11/1993	03/11/1993
0318	5,523.49	0	--	--	--	--
0324	5,455.	19	5,455	5,473.73	08/31/1982	06/17/1994
0325	5,581.63	10	5,577.08	5,582.34	03/27/1990	04/26/1993
0326	5,421.95	17	5,420.06	5,422.7	11/02/1992	10/31/1995
0329	5,431.84	29	5,426.84	5,435.25	03/12/1990	10/31/1995
0331	5,429.92	27	5,428.13	5,443.41	03/12/1990	10/31/1995
0333	5,484.89	0	--	--	--	--
0334	5,490.88	6	5,489.46	5,491.71	04/17/1990	09/10/1990
0335	5,575.06	12	5,575.06	5,579.32	05/18/1990	03/05/1993
0336	5,494.37	10	5,492.28	5,494.37	05/11/1990	02/08/1993

Table 10. Sites used for hydraulic-head observations in calibration of the flow model—Continued

[Site locations are in Banta (1997); --, no observation(s) used]

Site identifier	Steady-state head (feet above sea level)	Number of transient observations	Minimum head (feet above sea level)	Maximum head (feet above sea level)	Date of first transient-state observation	Date of last transient-state observation
0337	5,514.48	10	5,514.01	5,515.11	03/12/1990	04/27/1993
0338	5,487.7	10	5,487.26	5,488.85	03/16/1990	04/28/1993
0350	5,546.88	0	--	--	--	--
0351	5,559.3	9	5,557.3	5,562.42	04/09/1990	04/07/1993
0352	5,560.69	9	5,558.6	5,561.46	04/09/1990	04/07/1993
0353	5,563.57	9	5,562.33	5,563.57	04/09/1990	04/07/1993
0354	5,599.15	9	5,594	5,603.55	04/09/1990	04/07/1993
0357	5,523.57	9	5,522.29	5,524.29	04/09/1990	04/07/1993
0358	5,520.82	9	5,518.46	5,524.21	04/09/1990	04/07/1993
0359	5,448.63	0	--	--	--	--
0360	5,570.27	14	5,566.15	5,578.79	04/09/1990	04/07/1993
0367	5,549.56	10	5,547.36	5,550.42	03/16/1990	04/28/1993
0802	5,582.16	10	5,581.73	5,582.55	03/16/1990	04/26/1993
0803	5,553.23	10	5,551.89	5,554.44	03/16/1990	04/26/1993
0804	5,529.82	10	5,529.5	5,530.67	03/16/1990	04/26/1993
0805	5,520.62	10	5,519.52	5,521.1	03/16/1990	04/19/1993
0806	5,516.73	10	5,516.62	5,517.3	03/16/1990	04/19/1993
0807	5,488.62	9	5,487.74	5,489.81	04/17/1990	04/08/1993
0808	5,490.14	9	5,487.55	5,490.39	04/17/1990	04/08/1993
0809	5,400.03	19	5,383.8	5,409.08	04/24/1990	10/31/1995
0810	5,398.76	19	5,384.12	5,410.25	04/24/1990	10/31/1995
0811	5,393.63	18	5,380.07	5,402.88	04/24/1990	10/24/1995
0812	5,385.71	12	5,376.08	5,393.17	04/24/1990	10/17/1995
0813	5,489.47	9	5,489.47	5,489.84	04/19/1990	04/08/1993
0814	5,426.9	15	5,426.9	5,432.8	03/16/1990	10/30/1995
0815	5,429.98	15	5,429.98	5,433.76	11/03/1992	10/29/1995
0817	5,424.65	11	5,422.58	5,426.1	11/02/1992	10/31/1995
0818	--	14	5,430.81	5,433.94	10/02/1995	10/30/1995
0821	5,387.33	0	--	--	--	--
0822	5,387.5	0	--	--	--	--
1000	5,518.7	0	--	--	--	--
1001	5,506.8	4	5,506.43	5,507.06	01/15/1993	04/22/1993
1002	5,504.71	0	--	--	--	--
1003	5,501.16	0	--	--	--	--
1004	5,507.08	4	5,506.8	5,507.38	01/15/1993	04/22/1993
1005	5,503.89	4	5,503.4	5,504.22	01/15/1993	04/22/1993
1006	5,506.02	0	--	--	--	--
1007	5,501.65	0	--	--	--	--
1010	5,497.12	0	--	--	--	--
1011	5,522.58	0	--	--	--	--

Table 10. Sites used for hydraulic-head observations in calibration of the flow model—Continued

[Site locations are in Banta (1997); --, no observation(s) used]

Site identifier	Steady-state head (feet above sea level)	Number of transient observations	Minimum head (feet above sea level)	Maximum head (feet above sea level)	Date of first transient-state observation	Date of last transient-state observation
1012	5,525.9	4	5,515.16	5,528.3	01/15/1993	04/22/1993
1014	5,505.9	0	--	--	--	--
1015	5,498.61	0	--	--	--	--
1016	5,502.15	0	--	--	--	--
1017	5,501.1	4	5,500.92	5,501.1	01/15/1993	04/22/1993
1300	5,469.25	28	5,467.35	5,480.46	01/07/1991	07/01/1992
1301	5,543.45	31	5,536.25	5,549.55	12/17/1990	07/01/1992
1302	5,547.86	27	5,547.75	5,554.24	12/17/1990	07/01/1992
1303	5,535.26	39	5,504.32	5,537.12	12/17/1990	06/19/1992
1304	5,549.5	0	--	--	--	--
1305	5,554.35	0	--	--	--	--
1306	5,538.72	0	--	--	--	--
1307	5,537.82	0	--	--	--	--
1308	5,545.91	0	--	--	--	--
1309	5,550.31	0	--	--	--	--
1310	5,551.66	27	5,551.47	5,558.45	12/17/1990	07/01/1992
1311	5,537.26	0	--	--	--	--
1312	5,527.92	0	--	--	--	--
1314	5,550.56	0	--	--	--	--
1315	5,551.51	35	5,551.28	5,557.43	12/17/1990	07/01/1992
1316	5,545.85	0	--	--	--	--
1317	5,535.76	20	5,516.68	5,539.3	12/17/1990	07/01/1992
1318	5,539.75	14	5,537.13	5,551.86	12/17/1990	07/01/1992
1319	5,590.07	0	--	--	--	--
1320	5,588.47	0	--	--	--	--
1321	5,591.61	0	--	--	--	--
1322	5,601.14	33	5,593.61	5,606.89	12/17/1990	07/01/1992
1323	5,601.22	0	--	--	--	--
1324	5,582.81	17	5,562.69	5,583.85	12/17/1990	07/01/1992
1325	5,581.97	27	5,570.98	5,596.16	12/17/1990	07/01/1992
1326	5,583.85	0	--	--	--	--
1327	5,600.27	21	5,596.01	5,605.83	12/17/1990	07/01/1992
1328	5,600.37	27	5,597.08	5,606.91	12/17/1990	07/01/1992
1329	5,568.3	0	--	--	--	--
1330	5,583.27	0	--	--	--	--
1331	5,580.74	0	--	--	--	--
1332	5,597.94	0	--	--	--	--
1333	5,599.09	24	5,596.32	5,603.59	12/17/1990	07/01/1992
1334	5,566.14	0	--	--	--	--
1335	5,577.4	0	--	--	--	--

Table 10. Sites used for hydraulic-head observations in calibration of the flow model—Continued

[Site locations are in Banta (1997); --, no observation(s) used]

Site identifier	Steady-state head (feet above sea level)	Number of transient observations	Minimum head (feet above sea level)	Maximum head (feet above sea level)	Date of first transient-state observation	Date of last transient-state observation
1336	5,579.66	0	--	--	--	--
1339	5,550.53	0	--	--	--	--
1340	5,535.24	13	5,527.93	5,535.95	12/17/1990	07/01/1992
1341	5,599.63	0	--	--	--	--
1342	5,589.57	0	--	--	--	--
1343	5,597.04	17	5,576.85	5,601.14	12/17/1990	07/01/1992
1344	5,601.06	20	5,597.48	5,604.41	12/17/1990	07/01/1992
1345	5,519.9	25	5,519.82	5,547.29	12/17/1990	07/01/1992
1346	5,546.18	0	--	--	--	--
1347	5,515.26	0	--	--	--	--
1348	5,514.52	0	--	--	--	--
1349	5,514.99	0	--	--	--	--
1350	5,514.97	29	5,514.73	5,550.91	12/17/1990	07/01/1992
1351	5,524.68	28	5,524.23	5,557.66	12/17/1990	07/01/1992
1352	5,517.8	0	--	--	--	--
1353	5,524.4	0	--	--	--	--
1354	5,510.68	0	--	--	--	--
1355	5,503.67	0	--	--	--	--
1356	5,525.28	0	--	--	--	--
1357	5,551.71	0	--	--	--	--
1358	5,551.77	0	--	--	--	--
1359	5,553.82	0	--	--	--	--
1360	5,555.14	27	5,554.99	5,598.71	12/17/1990	07/01/1992
1361	5,561.09	26	5,560.35	5,603.24	12/17/1990	07/01/1992
1362	5,563.01	0	--	--	--	--
1363	5,565.22	0	--	--	--	--
1364	5,566.53	0	--	--	--	--
1365	5,574.88	0	--	--	--	--
1366	5,597.61	37	5,567.49	5,601.24	12/17/1990	07/01/1992
1367	5,555.24	28	5,555.2	5,598.09	12/17/1990	07/01/1992
1368	5,585.84	0	--	--	--	--
1369	5,534.77	0	--	--	--	--
1382	5,525.26	24	5,525.26	5,581.06	01/03/1992	12/18/1992
1383	5,534.54	15	5,532.28	5,535.88	01/03/1992	12/18/1992
1384	5,530.57	0	--	--	--	--
1385	5,567.47	0	--	--	--	--
1386	5,566.86	0	--	--	--	--
1387	5,566.1	0	--	--	--	--
1388	5,562.26	0	--	--	--	--

Table 10. Sites used for hydraulic-head observations in calibration of the flow model—Continued

[Site locations are in Banta (1997); --, no observation(s) used]

Site identifier	Steady-state head (feet above sea level)	Number of transient observations	Minimum head (feet above sea level)	Maximum head (feet above sea level)	Date of first transient-state observation	Date of last transient-state observation
1389	5,566.1	22	5,566.1	5,585.03	01/03/1992	12/18/1992
1390	5,567.46	0	--	--	--	--
1391	5,565.14	22	5,565.14	5,583.5	01/03/1992	12/18/1992
1392	5,566.12	24	5,565.68	5,577.22	01/03/1992	12/18/1992
1393	5,566.2	19	5,566.2	5,582.96	01/03/1992	12/18/1992
1394	5,567.46	25	5,567.33	5,597.45	01/03/1992	12/18/1992
1395	5,568.57	26	5,568.5	5,601.03	01/03/1992	12/18/1992
1396	5,569.19	30	5,569.01	5,583.49	01/03/1992	12/18/1992
1397	5,562.15	27	5,562.07	5,581.84	01/03/1992	12/18/1992
1398	5,568.05	39	5,567.97	5,604.74	01/03/1992	12/18/1992
1399	5,570.24	29	5,570.24	5,592.72	01/03/1992	12/18/1992
1400	5,563.63	34	5,563.58	5,581.33	01/03/1992	12/18/1992
2107	5,389.38	1	5,389.38	5,389.38	07/20/1995	07/20/1995
2116	5,354.04	0	--	--	--	--
DH-1	5,591.21	0	--	--	--	--
DH-11	5,554.43	0	--	--	--	--
DH-12	5,610.08	0	--	--	--	--
DH-13	5,610.43	0	--	--	--	--
DH-14	5,535.47	0	--	--	--	--
DH-16	5,523.16	0	--	--	--	--
DH-1A	5,591.49	0	--	--	--	--
DH-5	5,596.56	0	--	--	--	--
DH-6	5,608.06	0	--	--	--	--
DH-7	5,585.09	0	--	--	--	--
DH-9	5,592.96	0	--	--	--	--
LP85-1S	--	9	5,404.05	5,411.77	07/14/1995	10/31/1995
LP85-3	5,389.3	11	5,389.3	5,409.74	05/15/1995	10/31/1995
OW-10	5,559.5	0	--	--	--	--
OW-1B	5,508.76	0	--	--	--	--
OW-1C	5,514.17	0	--	--	--	--
OW-2A	5,479.26	0	--	--	--	--
OW-2B	5,473.67	0	--	--	--	--
OW-2C	5,485.51	0	--	--	--	--
OW-3A	5,486.36	0	--	--	--	--
OW-3B	5,545.31	0	--	--	--	--
OW-4A	5,528.71	0	--	--	--	--
OW-4B	5,538.69	0	--	--	--	--
OW-6A	5,517.42	0	--	--	--	--
OW-7	5,582.73	0	--	--	--	--
OW-8	5,462.47	0	--	--	--	--

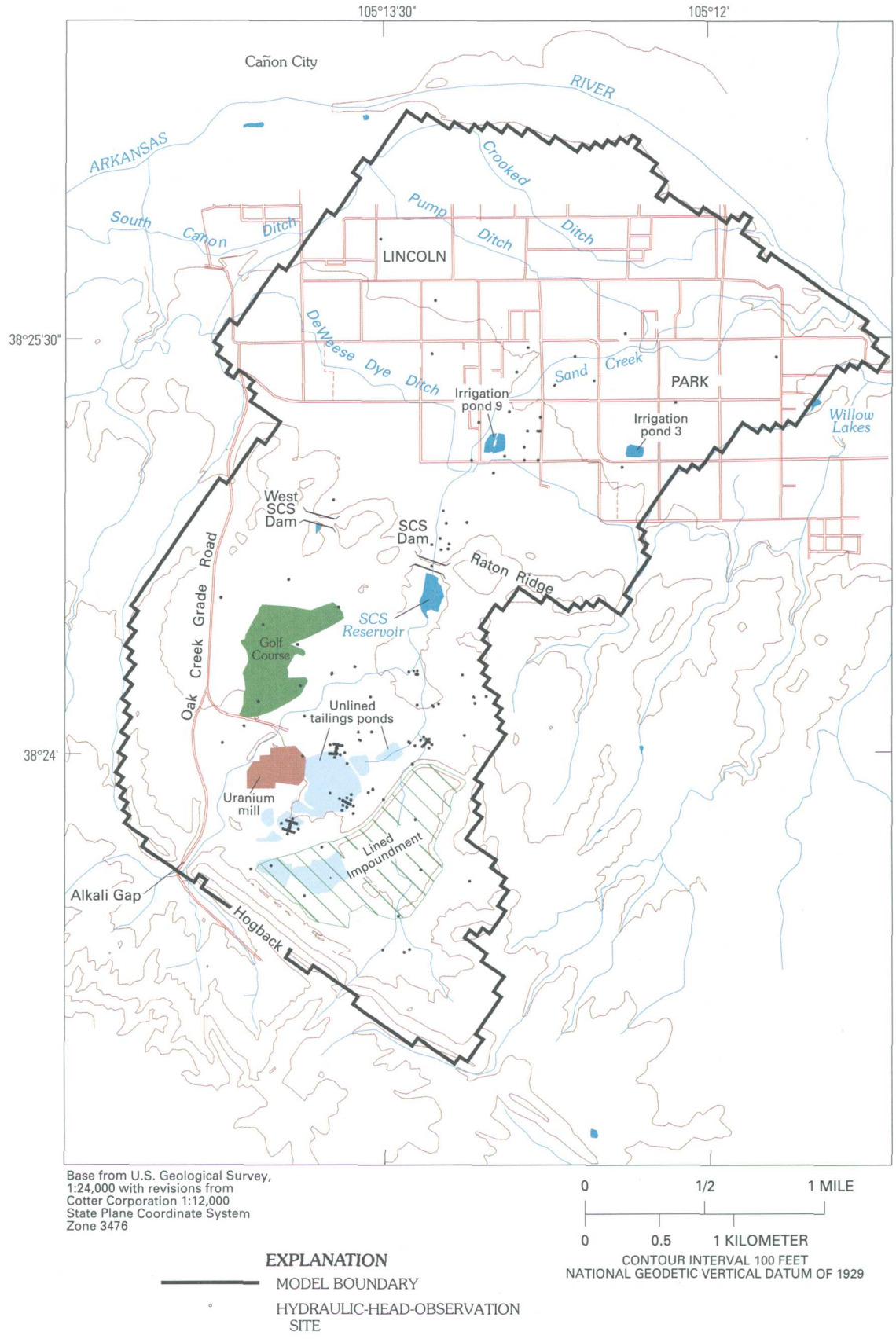

Figure 20. Locations of hydraulic-head observations used in calibration of the flow model.

Table 11. Parameters used in calibration of the flow model. Hydraulic-conductivity zones are shown in figures 17–19; recharge zones are shown in figure 16

[ft/d, feet per day; ft^{-1}, inverse foot; ft^2/d, square feet per day; in/yr, inches per year]

Parameter identifier	Model input (units)
	Head-dependent-boundary conductance
KD3RD	Drain conductance[1] for drain cells in the third test area (ft^2/d)
KDCR	Drain conductance for drain cells representing Sand Creek and the unnamed creek where the Willow Lakes are located (ft^2/d)
KDSP	Drain conductance for drain cells representing seeps near Arkansas River (ft^2/d)
KRDSP0	River-bed conductance[2] for river cells representing irrigation ditches during steady-state stress period (ft^2/d)
KRDIRR	River-bed conductance for river cells representing irrigation ditches during transient-state stress periods in which irrigation is simulated (ft^2/d)
KRPSP0	River-bed conductance for river cells representing irrigation ponds during steady-state stress period (ft^2/d)
KRPIRR	River-bed conductance for river cells representing irrigation ponds during transient-state stress periods in which irrigation is simulated (ft^2/d)
	Hydraulic conductivity
L1K1–2	Hydraulic conductivity for layer 1, hydraulic-conductivity zones 1 and 2 (ft/d)
L1K3–4	Hydraulic conductivity for layer 1, hydraulic-conductivity zones 3 and 4 (ft/d)
L1K5	Hydraulic conductivity for layer 1, hydraulic-conductivity zone 5 (ft/d)
L1K6	Hydraulic conductivity for layer 1, hydraulic-conductivity zone 6 (ft/d)
L1K7	Hydraulic conductivity for layer 1, hydraulic-conductivity zone 7 (ft/d)
L1K8	Hydraulic conductivity for layer 1, hydraulic-conductivity zone 8 (ft/d)
L1K9–10	Hydraulic conductivity for layer 1, hydraulic-conductivity zones 9 and 10 (ft/d)
L1K12	Hydraulic conductivity for layer 1, hydraulic-conductivity zone 12 (ft/d)
L1K13	Hydraulic conductivity for layer 1, hydraulic-conductivity zone 13 (ft/d)
L1K14	Hydraulic conductivity for layer 1, hydraulic-conductivity zone 14 (ft/d)
L1K15	Hydraulic conductivity for layer 1, hydraulic-conductivity zone 15 (ft/d)
L1K16	Hydraulic conductivity for layer 1, hydraulic-conductivity zone 16 (ft/d)
L1K17	Hydraulic conductivity for layer 1, hydraulic-conductivity zone 17 (ft/d)
L1K18	Hydraulic conductivity for layer 1, hydraulic-conductivity zone 18 (ft/d)
L1K19	Hydraulic conductivity for layer 1, hydraulic-conductivity zone 19 (ft/d)
L1K20	Hydraulic conductivity for layer 1, hydraulic-conductivity zone 20 (ft/d)
L1K21	Hydraulic conductivity for layer 1, hydraulic-conductivity zone 21 (ft/d)
L1K22	Hydraulic conductivity for layer 1, hydraulic-conductivity zone 22 (ft/d)
L1K23	Hydraulic conductivity for layer 1, hydraulic-conductivity zone 23 (ft/d)
L2K4–5	Hydraulic conductivity for layer 2, hydraulic-conductivity zones 4 and 5 (ft/d)
L2K6	Hydraulic conductivity for layer 2, hydraulic-conductivity zone 6 (ft/d)
L2K7	Hydraulic conductivity for layer 2, hydraulic-conductivity zone 7 (ft/d)
L2K8–9	Hydraulic conductivity for layer 2, hydraulic-conductivity zones 8 and 9 (ft/d)
L2K10–17	Hydraulic conductivity for layer 2, hydraulic-conductivity zones 10 through 17 (ft/d)
L2K18–19	Hydraulic conductivity for layer 2, hydraulic-conductivity zones 18 and 19 (ft/d)
L2K20	Hydraulic conductivity for layer 2, hydraulic-conductivity zone 20 (ft/d)
L2K21	Hydraulic conductivity for layer 2, hydraulic-conductivity zone 21 (ft/d)
L3K1	Hydraulic conductivity for layer 3, hydraulic-conductivity zone 1 (ft/d)
L3K2	Hydraulic conductivity for layer 3, hydraulic-conductivity zone 2 (ft/d)
L3K3–4	Hydraulic conductivity for layer 3, hydraulic-conductivity zones 3 and 4 (ft/d)
L4K	Hydraulic conductivity for layer 4 (ft/d)
L5K	Hydraulic conductivity for layer 5 (ft/d)
L6K	Hydraulic conductivity for layer 6 (ft/d)

Table 11. Parameters used in calibration of the flow model. Hydraulic-conductivity zones are shown in figures 17–19; recharge zones are shown in figure 16—Continued

[ft/d, feet per day; ft^{-1}, inverse foot; ft^2/d, square feet per day; in/yr, inches per year]

Parameter identifier	Model input (units)
	Storage
L1S1–2	Specific yield for layer 1, hydraulic-conductivity zones 1 and 2 (dimensionless)
L1S3–10	Specific yield for layer 1, hydraulic-conductivity zones 3 through 10 (dimensionless)
L2–6S	Specific storage for layers 2 through 6 (ft^{-1})
	Recharge
R1SP0	Recharge rate for recharge zone 1 during steady-state stress period (in/yr)
R1IRR	Recharge rate for recharge zone 1 during transient-state stress periods in which irrigation is simulated (in/yr)
R2–3	Recharge rate for recharge zones 2 and 3 for all stress periods and for recharge zone 8 prior to construction of lined impoundment (in/yr)
R4–6	Recharge rate for recharge zones 4 through 6 (in/yr)
R7	Recharge rate for recharge zone 7 (in/yr)
R9–10	Recharge rate for recharge zones 9 and 10 during use of unlined tailings ponds to receive tailings and fluids (in/yr)

[1]Drain conductance is the constant of proportionality in the relation between simulated discharge to or from a model cell and difference in hydraulic head between the cell and an external sink of water, as specified for the drain package of MODFLOW (McDonald and Harbaugh, 1988).

[2]River-bed conductance is the constant of proportionality in the relation between simulated discharge to or from a model cell and difference in hydraulic head between the cell and an external source or sink of water, as specified for the river package of MODFLOW (McDonald and Harbaugh, 1988).

Table 12. Parameter estimates for the flow model

[See table 11 for explanation of parameter identifiers; ft^2/d, square feet per day; ft/d, feet per day; ft^{-1}, inverse foot; in/yr, inch per year]

Parameter identifier (units)	Estimated value	Composite scaled sensitivity (dimensionless)
	Head-dependent-boundary conductance	
KD3RD (ft^2/d)	3.00×10^3	3.38
KDCR (ft^2/d)	18.1	3.22
KDSP (ft^2/d)	4×10^4	12.7
KRDSP0 (ft^2/d)	1.65×10^3	23.2
KRDIRR (ft^2/d)	5.20×10^3	35.3
KRPSP0 (ft^2/d)	800	4.45
KRPIRR (ft^2/d)	1.27×10^3	3.00
	Hydraulic conductivity	
L1K1–2 (ft/d)	.162	12.4
L1K3–4 (ft/d)	1.14	.592
L1K5 (ft/d)	28	1.01×10^5
L1K6 (ft/d)	279	1.65×10^6
L1K7 (ft/d)	19.38	770
L1K8 (ft/d)	167	1.50×10^4

Table 12. Parameter estimates for the flow model—Continued

[See table 11 for explanation of parameter identifiers; ft^2/d, square feet per day; ft/d, feet per day; ft^{-1}, inverse foot; in/yr, inch per year]

Parameter identifier (units)	Estimated value	Composite scaled sensitivity (dimensionless)
	Hydraulic conductivity—Continued	
L1K9–10 (ft/d)	1.98×10^3	2.81×10^6
L1K12 (ft/d)	317	3.37×10^5
L1K13 (ft/d)	694	1.23
L1K14 (ft/d)	2.48	1.28×10^{-3}
L1K15 (ft/d)	1×10^4	9.99×10^3
L1K16 (ft/d)	.5	.100
L1K17 (ft/d)	694	243
L1K18 (ft/d)	376	32.1
L1K19 (ft/d)	68	137
L1K20 (ft/d)	6.6	.131
L1K21 (ft/d)	11	.679
L1K22 (ft/d)	2.8×10^5	1.11×10^4
L1K23 (ft/d)	1.32	1.16×10^{-2}
L2K4–5 (ft/d)	3.72×10^{-5}	.704
L2K6 (ft/d)	4.7×10^{-2}	330
L2K7 (ft/d)	3.45×10^{-4}	45.0
L2K8–9 (ft/d)	3.56×10^{-3}	12.2
L2K10–17 (ft/d)	5×10^{-2}	1.08
L2K18–19 (ft/d)	132	2.29×10^6
L2K20 (ft/d)	10	19.3
L2K21 (ft/d)	1×10^{-3}	1.07×10^{-4}
L3K1 (ft/d)	3.72×10^{-4}	8.50
L3K2 (ft/d)	2.8×10^{-2}	34.7
L3K3–4 (ft/d)	3.99	20.8
L4K (ft/d)	.322	2.41
L5K (ft/d)	6.8×10^{-5}	.865
L6K (ft/d)	1×10^{-4}	2.66
	Storage	
L1S1–2 (dimensionless)	.199	.384
L1S3–10 (dimensionless)	4.38×10^{-3}	3.84
L2–6S (ft^{-1})	1.6×10^{-6}	39.4
	Recharge	
R1SP0 (in/yr)	6.6	6.60×10^4
R1IRR (in/yr)	15.8	1.04×10^3
R2–3 (in/yr)	.15	1.31
R4–6 (in/yr)	1×10^{-4}	8.64×10^{-2}
R7 (in/yr)	1	3.22×10^3
R9–10 (in/yr)	4	2.97

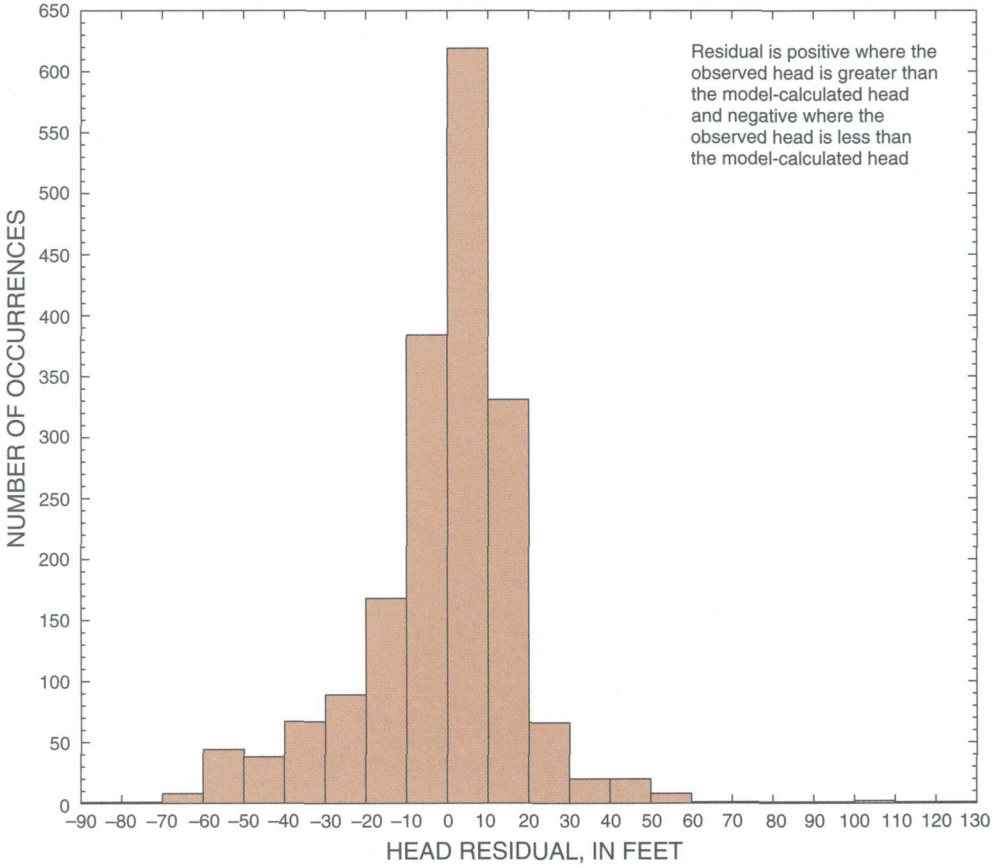

Figure 21. Frequency histogram of hydraulic-head residuals for the calibrated flow model.

When numerous sampling locations were used as observation locations, automated parameter estimation tended to produce model results characterized by long periods of relatively constant concentrations separated by short periods of rapid change in concentrations. Although these model results approximated observed concentrations at a large number of sites, the fit of the model results to observed concentration trends at individual sites was inadequate. Because the objective of the modeling in this study was to simulate time trends in changes in concentrations as an effect of different remediation alternatives, fitting the model to the trends in observed concentrations was of primary importance. To better fit the model to the observed trends in concentrations, concentration observations at three sampling sites were used, one in the upgradient area (well 312) and two in the downgradient area (wells 140 and 144) (fig. 1). These observation locations had (1) a long history of water-quality data for numerous samples, (2) a location in the contaminant plume, and (3) a relatively well-defined trend in concentrations of uranium and molybdenum over time.

Various combinations of values of longitudinal and transverse dispersivities were tested in the uncalibrated solute-transport model to determine how these parameters would affect the stability of the model. Values of longitudinal dispersivity less than 260 ft and values of transverse dispersivity less than 130 ft resulted in instability of the model solution algorithm for the uncalibrated model. Because of the shortage of historical data and to decrease the number of transport-model parameters to be estimated, longitudinal dispersivity and transverse dispersivity were treated as one parameter, and the ratio of longitudinal dispersivity to transverse dispersivity was assumed to be 2:1, which was the ratio of the minimum values found to result in stable model runs.

For distributing transport-model parameters to the model elements, the study area was divided into zones on approximately the same basis as the zonation

of hydraulic conductivity for layer 1 in the flow model (table 14). The geologic unit was the primary variable used to assign zones; the results of the kriging of the lithology codes were used to divide the area of outcrop of the Poison Canyon Formation into two separate zones. In addition, a buffer zone of 500 ft on either side of DeWeese Dye Ditch was used to delineate a zone where the water table was substantially higher than the base of the alluvium and terrace alluvium; transport parameters in this zone were expected to be different from the transport parameters in the areas mapped as terrace alluvium immediately to the south, where transport probably was substantially limited to the weathered and fractured bedrock. Parameters used in calibration of the transport model are listed in table 15; the zonation for the transport-model parameters is shown in figure 25. For each of the two constituents (uranium and molybdenum), four DKSUTRA model runs were made, where each model run represented a specific interval of time corresponding to one of the four periods of relatively constant hydraulic stress. For each time interval, a steady-state flow solution was generated using the calibrated flow model and hydraulic stresses characteristic of the time interval. Stresses for each time interval in the 37-year calibration period are listed in table 16. Initial aqueous-phase concentrations for the model run representing the first time interval were specified as 1.0×10^{-4} mg/L for uranium and 2.5×10^{-3} mg/L for molybdenum; these values approximate the minimum concentrations detected in the study area. Initial solid-phase concentrations for the model run representing the first time interval were specified so that the ratio of solid- to aqueous-phase concentrations represented chemical equilibrium for each cell, based on the distribution coefficient. Initial conditions for the three following model runs were the final aqueous- and solid-phase concentrations from the preceding run.

Table 13. Simulated steady-state water budget from the calibrated flow model

[Values rounded to nearest 10 cubic feet per day]

Simulated feature or process	Flow into model (cubic feet per day)	Flow out of model (cubic feet per day)
Areal recharge	111,700	0
Sand Creek upstream from SCS reservoir	0	2,500
Sand Creek downstream from SCS reservoir	0	288,620
Unnamed creek where the Willow Lakes are located	0	890
Springs and seeps along the Arkansas River	0	455,920
Irrigation ditches and ponds	665,860	4,420
SCS reservoir (pumpage plus evapotranspiration)	0	6,750
Ground-water flow across boundary of modeled system near South Cañon Ditch	0	26,730
Ground-water flow through the Littell mine shaft	0	60
Ground-water flow across the hogback at Alkali Gap	8,330	0
Totals	785,890	785,890

Results of parameter estimation for the contaminant-transport model are listed in table 17. The 95-percent linear confidence limits listed in table 17 for parameters that were optimized indicate how precisely a parameter value was determined by the optimization process. The confidence limits were calculated by PEST. Parameters that had large 95-percent linear confidence intervals were not as precisely determined as parameters that had small 95-percent confidence intervals. For many of the parameters, the model results were insufficiently sensitive to the parameter values to allow optimization. Each parameter in table 17 was varied to assess its effects on the value of the objective function and on the model output in general. The amount by which the sum of squared, weighted residuals is changed by a 10-percent increase in each parameter (table 17) indicates the sensitivity of the model fit to the parameter; large values indicate that the model fit is sensitive to the value of the parameter. The observed concentrations and the calculated concentrations from the optimized transport model for uranium and molybdenum for wells 312, 140, and 144 are shown in figure 26.

Model-calculated concentrations of uranium at well 312 for the calibration period (fig. 26*A*) showed a rapid concentration increase at the beginning of the simulation, followed by a gradual increase through the first two time periods of the calibration period. The rapid decrease that begins at a simulation time of 7,670 days was caused by the simulated decrease in recharge in the old tailing ponds area. After about 8,000 days, the model-calculated concentrations decreased gradually. The fit of the model-calculated concentrations to the observed concentrations was good.

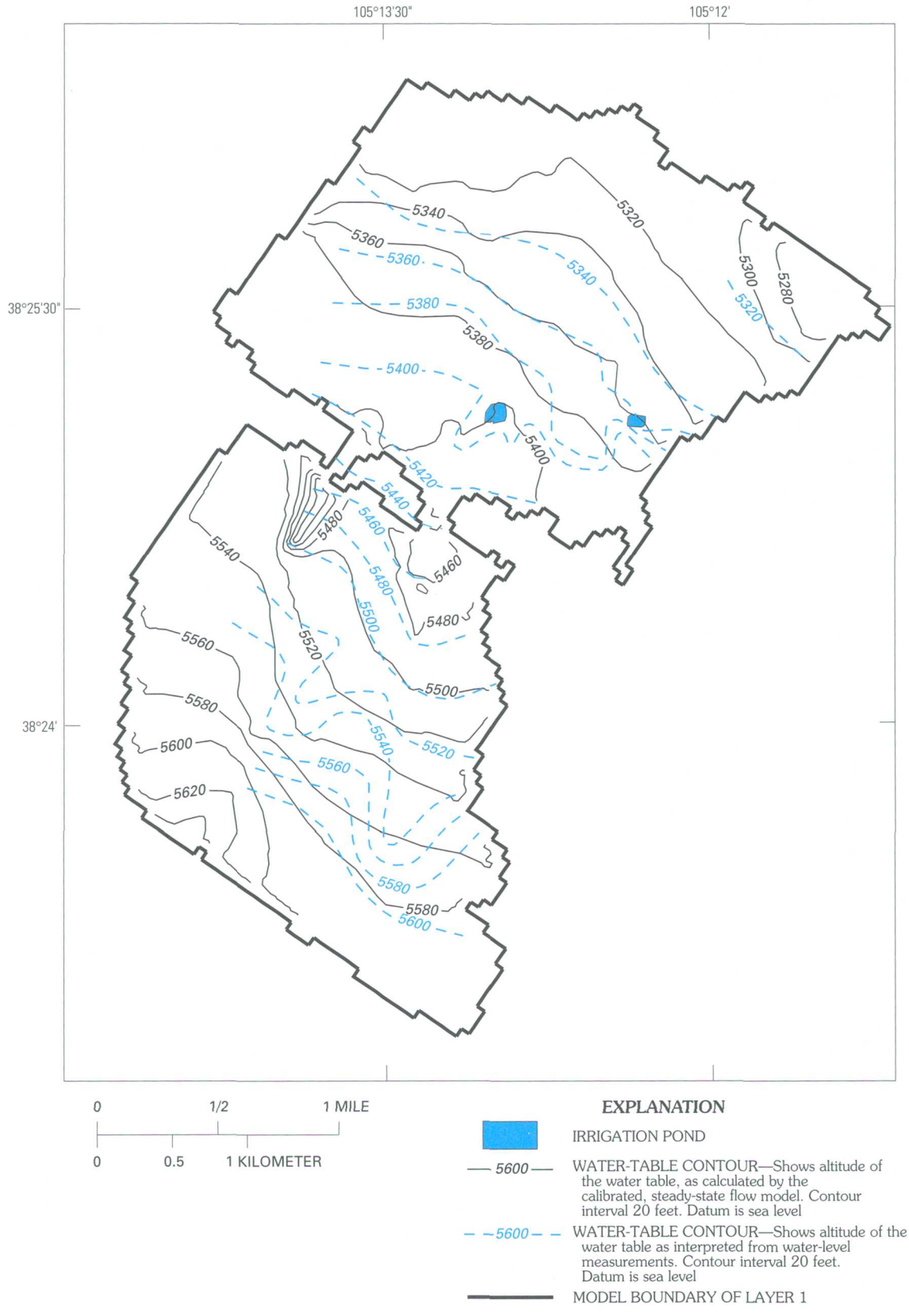

Figure 22. Model-calculated and measured hydraulic-head contours.

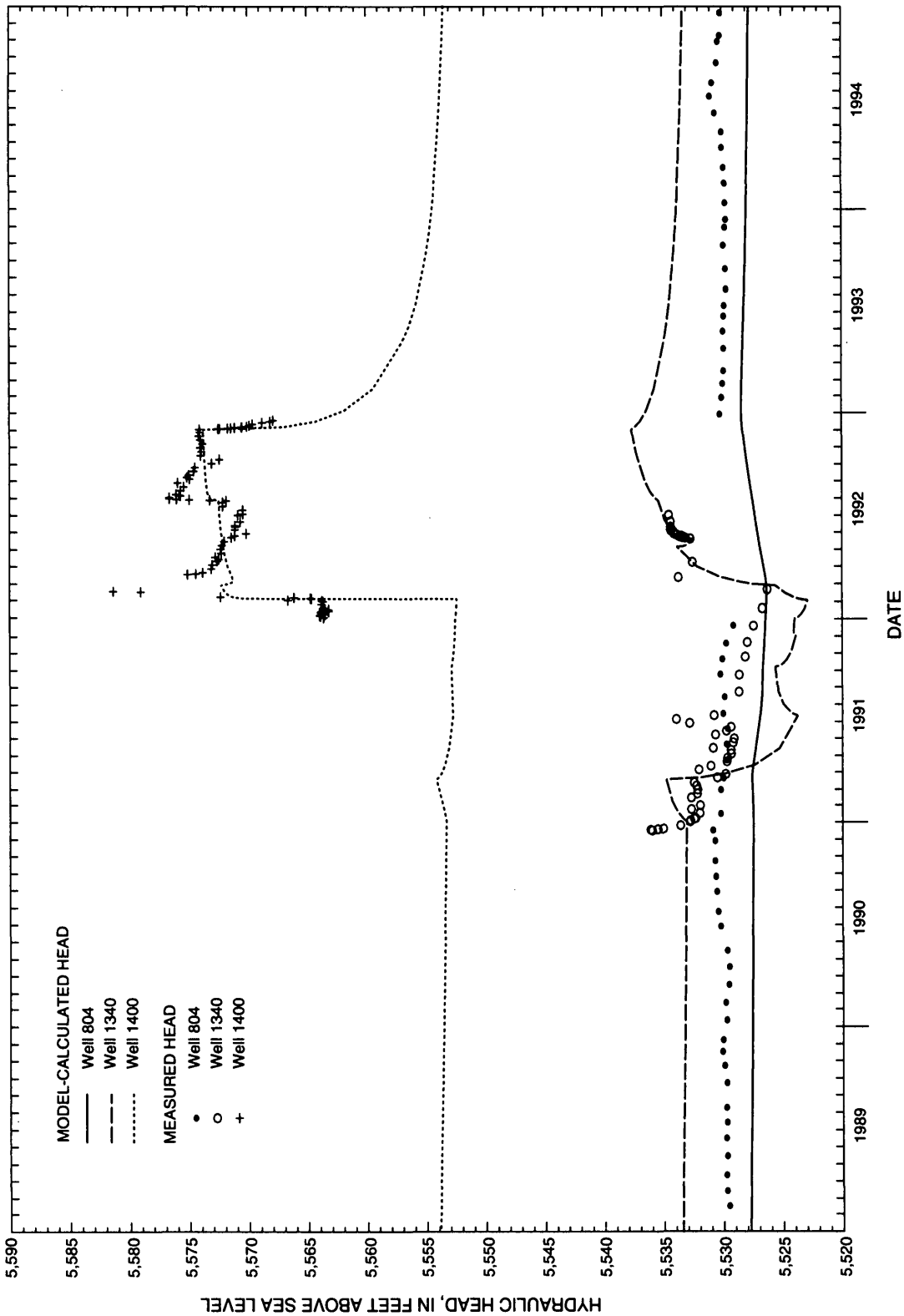

Figure 23. Measured and model-calculated heads for three wells in the upgradient area.

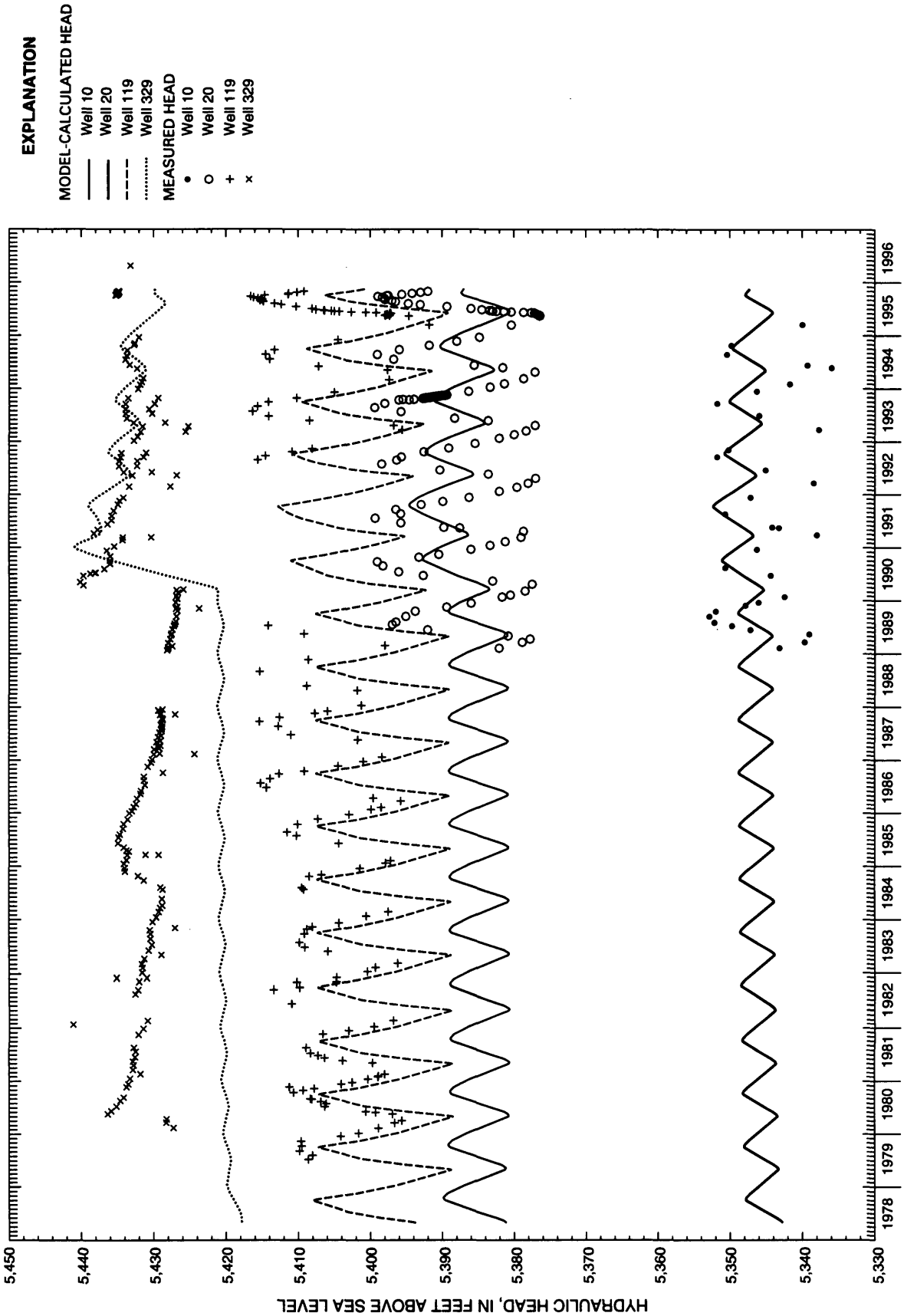

Figure 24. Measured and model-calculated heads for four wells in the downgradient area.

The model-calculated concentrations of uranium at well 140 (fig. 26*B*) show an increase early in the simulation, although the model-calculated concentrations are not as large as the observed concentrations for about the first 9,000 days of the simulation. The model-calculated concentrations for the later part of the simulation fit observed concentrations moderately well. The effect of the simulated construction of the clay barrier at the SCS dam is evident in figure 26*B* as a steepening of the concentration curve at about 11,000 days. Well 144 (fig. 26*C*) is indirectly downgradient from Sand Creek gap, and observed concentrations at well 144 were smaller than at well 140. Model-calculated uranium concentrations fit observed concentrations moderately well, although they were slightly larger than observed concentrations late in the calibration period (fig. 26*C*).

The model-calculated concentrations of molybdenum at wells 312, 140, and 144 (figs. 26*D–F*) produced curves similar in shape to those for uranium. The fit of the model-calculated concentrations to the observed concentrations was good at well 312 (fig. 26*D*). Model-calculated molybdenum concentrations for well 140 tended to be less than observed concentrations (fig. 26*E*). For well 144, model-calculated concentrations were smaller than the observed concentrations before about 10,000 days and larger after that time (fig. 26*F*).

Table 14. Transport-model zones

Transport-model zone	Basis for transport-model zone
1	Terrace alluvium within 500 feet of DeWeese Dye Ditch and north of the ditch in the downgradient area
2	Alluvium in the downgradient area
3	Terrace alluvium more than 500 feet south of DeWeese Dye Ditch in the downgradient area
4	Vermejo Formation along Raton ridge
5	Alluvium and terrace alluvium upgradient from Raton ridge
11	Consolidated rocks, Tertiary and older, layer 1 lithology code = –7 or –8 in upgradient area
12	Consolidated rocks, Tertiary and older, layer 1 lithology code = –5 or –6 in upgradient area

SIMULATIONS OF REMEDIATION ALTERNATIVES

The calibrated ground-water flow and contaminant-transport models described in the preceding sections were used to evaluate five proposed remediation alternatives. The five alternatives are: (1) Simultaneous injection of municipal water derived from the Arkansas River into wells completed at depths of about 10 to 75 ft and withdrawal of water through gravel-filled trenches in the area of the old, unlined tailings ponds; (2) removal of earth materials that have uranium or molybdenum concentrations substantially larger than background concentrations from the unsaturated zone in the area of the old, unlined tailings ponds; (3) injection of water into wells and withdrawal of water through trenches, as in alternative 1, followed by removal of contaminated earth materials, as in alternative 2; (4) installation of a layered cover system in the area of the old, unlined tailings ponds; and (5) application of a reducing agent to decrease the mobility of the contaminants in the area of the old, unlined tailings ponds. Each model run simulated 50 years of implementation of the remediation alternative; ground-water flow was simulated by the calibrated flow model for one, two, or four steady-state periods, depending on the requirements of the remediation alternative being modeled. Initial aqueous- and solid-phase contaminant concentrations were those concentrations calculated by the calibrated transport model at the end of the 37-year calibration period. For each remediation alternative, the results of the simulation were compared to the results of a simulation of a no-action scenario, for which conditions were assumed to be like the conditions in the fourth part of the calibration period.

No-Action Scenario

To provide a basis for comparison for the remediation alternatives, a contaminant-transport simulation was run to represent a (no-action) continuation of the stresses simulated during the fourth part of the calibration period. The concentrations of uranium and molybdenum in water recharging the ground-water system in the area of the unlined tailings ponds were assumed to be constant at the concentrations determined during calibration of the transport model.

Table 15. Parameters used in calibration of the transport model

[Transport-model zones are shown in figure 25. mg/L, milligrams per liter; sec^{-1}, inverse second; $(kg/m^3)/s$, kilograms per cubic meter per second; ft, feet]

Parameter identifier	Model input (units)
	Uranium
URC	Concentration of uranium in recharge water from old tailings ponds (mg/L)
UF1/2	Forward mass-transfer rate coefficient for uranium in transport-model zones 1 and 2 (sec^{-1})
UF3	Forward mass-transfer rate coefficient for uranium in transport-model zone 3 (sec^{-1})
UF4/12	Forward mass-transfer rate coefficient for uranium in transport-model zones 4 and 12 (sec^{-1})
UF11	Forward mass-transfer rate coefficient for uranium in transport-model zone 11 (sec^{-1})
UF5	Forward mass-transfer rate coefficient for uranium in transport-model zone 5 (sec^{-1})
UB1/2	Backward mass-transfer rate coefficient for uranium in transport-model zones 1 and 2 $[(kg/m^3)/s]$
UB3	Backward mass-transfer rate coefficient for uranium in transport-model zone 3 $[(kg/m^3)/s]$
UB4/12	Backward mass-transfer rate coefficient for uranium in transport-model zones 4 and 12 $[(kg/m^3)/s]$
UB11	Backward mass-transfer rate coefficient for uranium in transport-model zone 11 $[(kg/m^3)/s]$
UB5	Backward mass-transfer rate coefficient for uranium in transport-model zone 5 $[(kg/m^3)/s]$
	Molybdenum
MRC	Concentration of molybdenum in recharge water from old tailings ponds (mg/L)
MF1/2	Forward mass-transfer rate coefficient for molybdenum in transport-model zones 1 and 2 (sec^{-1})
MF3	Forward mass-transfer rate coefficient for molybdenum in transport-model zone 3 (sec^{-1})
MF4/12	Forward mass-transfer rate coefficient for molybdenum in transport-model zones 4 and 12 (sec^{-1})
MF11	Forward mass-transfer rate coefficient for molybdenum in transport-model zone 11 (sec^{-1})
MF5	Forward mass-transfer rate coefficient for molybdenum in transport-model zone 5 (sec^{-1})
MB1/2	Backward mass-transfer rate coefficient for molybdenum in transport-model zones 1 and 2 $[(kg/m^3)/s]$
MB3	Backward mass-transfer rate coefficient for molybdenum in transport-model zone 3 $[(kg/m^3)/s]$
MB4/12	Backward mass-transfer rate coefficient for molybdenum in transport-model zones 4 and 12 $[(kg/m^3)/s]$
MB11	Backward mass-transfer rate coefficient for molybdenum in transport-model zone 11 $[(kg/m^3)/s]$
MB5	Backward mass-transfer rate coefficient for molybdenum in transport-model zone 5 $[(kg/m^3)/s]$
	Porosity
P1/2	Porosity of transport-model zones 1 and 2 (dimensionless)
P3	Porosity of transport-model zone 3 (dimensionless)
P4/12	Porosity of transport-model zones 4 and 12 (dimensionless)
P11	Porosity of transport-model zone 11 (dimensionless)
P5	Porosity of transport-model zone 5 (dimensionless)
	Dispersivity
DISP	Longitudinal dispersivity over model domain (ft). Transverse dispersivity always equaled [(1/2) × DISP].

The assumption of constant concentration in recharge water was based on results from an 11.5-month pilot test of remediation alternative 1 (Adrian Brown Consultants, Inc., 1993). In the pilot test for the third test area (Adrian Brown Consultants, Inc., 1993), solid-phase concentrations of uranium and molybdenum before and after the test were approximately equal (fig. 8).

Conditions during the fourth part of the calibration period were simulated for 50 years for the simulation of contaminant transport. Predicted concentrations of uranium and molybdenum for wells 312 and 144 are shown in figure 27. Results of simulation of the no-action scenario indicated substantial decreases in concentrations of uranium and molybdenum at both sites. The decreases in concentrations predicted in this simulation were a continuation of the decreases simulated for the fourth part of the calibration period and were largely a result of the simulated decrease in recharge rate in the area of the unlined tailings ponds, which was introduced at the beginning of the third part of the calibration period.

Remediation Alternative 1: Inject and Withdraw Water

Remediation alternative 1 is the injection of municipal water into wells completed at depths of about 10 to 75 ft and withdrawal of water through gravel-filled trenches constructed with slotted pipes near the bottoms of the trenches and through withdrawal wells at the perimeter of the area of the injection wells. Withdrawn water would be pumped to the lined impoundment or treated to remove contaminants and reused. A pilot test of this alternative is described by Adrian Brown Consultants, Inc. (1993). As simulated, the withdrawal rate equaled the injection rate. The area of injection and withdrawal was assumed to be the area of the unlined tailings ponds that is not overlain by the lined impoundment (fig. 1). The rates of inflow and outflow at the model boundaries for this alternative were the same as the rates from the fourth part of the calibration period (table 16). For the transport simulation, injection and withdrawal were simulated in an alternating pattern in the area of the old tailings ponds that is not overlain by the lined impoundment. Total injection and withdrawal rates of 300 (that is, 300 gal/min injected and 300 gal/min withdrawn) and 600 gal/min for 10 and 20 years were simulated, followed by a period of no injection or withdrawal to complete the 50-year simulation. The effectiveness of each injection and withdrawal phase was evaluated by calculating the ratio of model-predicted solid-phase concentrations of uranium or molybdenum, averaged over the area of injection and withdrawal, at the end of the injection and withdrawal period to the concentrations at the beginning of the period. Concentrations of uranium and molybdenum in water recharging the ground-water system for the part of the simulations following injection and withdrawal were determined by multiplying the concentrations assumed at the beginning of the injection and withdrawal period (which were the concentrations determined during calibration) by that ratio.

This simulation predicted that concentrations of uranium and molybdenum at well 312 (which is near the area where injection and withdrawal was simulated) would decline rapidly during injection and withdrawal (fig. 27). When injection and withdrawal cease, rapid increases in aqueous uranium concentrations as a result of desorption were predicted for well 312.

All simulations of injection and withdrawal were predicted to result in long-term (50-year) decreases in concentrations at well 312, compared to the no-action scenario (fig. 27). However, the decreases in predicted concentrations at well 144 resulting from the injection and withdrawal were small.

Remediation Alternative 2: Remove Contaminated Materials

In this remediation alternative, earth materials in the unsaturated zone in the area of the old, unlined tailings ponds that have uranium or molybdenum concentrations substantially larger than background concentrations would be removed. For the purposes of the simulation, removal of these materials was assumed to result in substantial decreases in concentrations of uranium and molybdenum in recharge water reaching the water table. The simulation included decreases in the recharge-water concentrations in the area of the unlined tailings ponds that is not overlain by the lined impoundment that were 0.5 and 0.1 times the concentrations that were determined during the model calibration. Simulated flows into and out of the ground-water system were the same as flows calculated for the fourth part of the calibration period.

Substantial decreases in concentrations of uranium, compared to the no-action scenario, were predicted for well 312 in these simulations (fig. 28); the decreases in molybdenum concentrations were smaller. The amount of decrease in the predicted concentrations was related to the amount by which the concentrations in recharge water were assumed to change. A decrease in the concentrations in recharge water to one-tenth of the calibration-period concentrations would result in substantially larger decreases in the predicted concentrations than would a decrease to one-half of the calibration-period concentrations. The effects of alternative 2 on contaminant concentrations at well 144 were predicted to be small.

Remediation Alternative 3: Inject and Withdraw Water, Then Remove Contaminated Materials

This remediation alternative is a combination of alternatives 1 and 2. Municipal water would be injected into the ground-water system through injection wells, and water would be withdrawn from trenches and withdrawal wells at the perimeter of the area of injection, as described in alternative 1. Injection and withdrawal of water would be followed

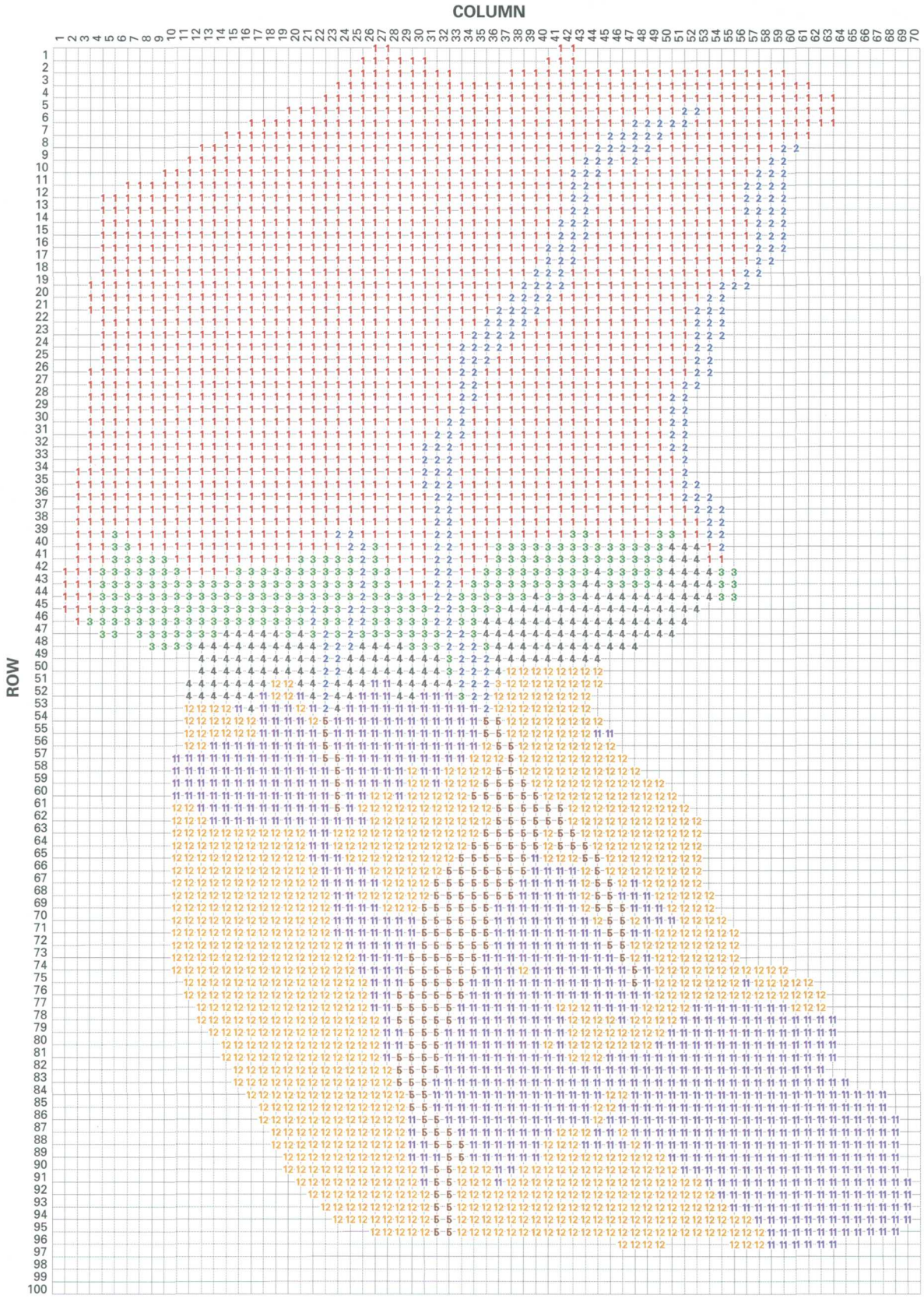

Figure 25. Distribution of transport-model zones. Model-grid location is shown in figure 2.

Figure 25. Distribution of transport-model zones. Model-grid location is shown in figure 2—Continued.

by removal of contaminated materials above the pre-injection water table in the area of the old, unlined tailings ponds. Only the 300-gal/min injection and withdrawal rate was simulated because differences in results between the 300 gal/min and the 600 gal/min injection and withdrawal rates of alternative 1 were predicted to be negligible. Injection and withdrawal were simulated for 10 and 20 years. Effectiveness of injection and withdrawal in decreasing solid-phase concentrations of uranium and molybdenum were the same as for alternative 1. Concentrations of uranium and molybdenum in recharge water in the area of injection and withdrawal following the injection and withdrawal period were determined by multiplying the concentrations used in the post-injection and withdrawal periods of alternative 1 by 0.5 or 0.1 to simulate decreases in concentrations due to removal of contaminated materials above the pre-injection water table.

As in the simulated results for alternative 1, results for alternative 3 indicated rapid declines at well 312 during the injection and withdrawal periods (fig. 29). After the simulated injection and withdrawal periods, predicted aqueous concentrations rapidly increased at well 312 as a result of desorption, although not as much as in alternative 1. The simulated effect of alternative 3 on contaminant concentrations at well 144 were small.

Remediation Alternative 4: Install Cap Over Contaminated Materials

This remediation alternative consists of installation of a layered cover, consisting of locally derived earth materials, to decrease infiltration in areas where materials in the unsaturated zone above the water table were contaminated with uranium-mill-derived uranium and molybdenum. Flux of water through a proposed cover was evaluated by Preston Niesen (Cotter Corporation, written commun., 1995) using the Hydrologic Evaluation of Landfill Performance model, version 3 (HELP–3) of the U.S. Environmental Protection Agency; predicted flux rates ranged from 0.37 to 0.56 in/yr. This range in recharge rates exceeded the recharge rate for the upgradient area determined during calibration of the flow model, which was 0.15 in/yr. Flow-model and transport-model simulations were made to evaluate the possible effects of a decreased rate of recharge. For these simulations, recharge in the area of the unlined tailings ponds that is not overlain by the lined impoundment was specified as one-half the

Table 16. Time periods and stresses used in calibration of the transport model

[in/yr, inches per year; ft^3/d, cubic feet per day]

Period	Time span	Interval length (days)	Description of simulated stresses and changes to system
1	July 1958 through June 1971	4,748	Recharge in area of old tailings ponds, 4 in/yr; recharge in remainder of upgradient area, 0.15 in/yr; discharge (pumpage and evapotranspiration) from SCS reservoir not simulated.
2	July 1971 through June 1979	2,922	Recharge in area of old tailings ponds, 4 in/yr; recharge in remainder of upgradient area, 0.15 in/yr; discharge from SCS reservoir simulated.
3	July 1979 through June 1988	3,288	Recharge in area of lined impoundment, 0 in/yr; recharge in remainder of upgradient area, including area of old tailings ponds, 0.15 in/yr; pumpage from well 333, 2,800 ft^3/d; discharge from SCS reservoir simulated.
4	July 1988 through June 1995	2,556	Stresses unchanged from period 3. Hydraulic conductivity of four cells in the flow model representing vicinity of SCS dam multiplied by factor of 0.0018 to simulate installation of barrier; permeability of corresponding elements in transport model recalculated accordingly.

Table 17. Parameter estimates for the transport model

[See table 15 for explanation of parameter identifiers; mg/L, milligrams per liter; sec^{-1}, inverse second; <, less than; $(kg/m^3)/s$, kilograms per cubic meter per second; --, parameter not optimized]

Parameter identifier (units)	Log-transformed for optimization?	Estimated value	95-percent linear confidence limits on the estimate		Change in sum of squared, weighted residuals due to 10-percent change in parameter (percent)
			Lower	Upper	
		Uranium			
URC (mg/L)	No	163	132	193	0.37
UF1/2 (sec^{-1})	Not optimized	2.24×10^{-11}	--	--	<.01
UF3 (sec^{-1})	Not optimized	4.37×10^{-12}	--	--	<.01
UF4/12 (sec^{-1})	Not optimized	2.69×10^{-12}	--	--	.06
UF5 (sec^{-1})	Not optimized	2.57×10^{-11}	--	--	<.01
UF11 (sec^{-1})	Yes	8.01×10^{-12}	2.25×10^{-12}	2.86×10^{-11}	.10
UB1/2 $[(kg/m^3)/s]$	Not optimized	6.38×10^{-3}	--	--	<.01
UB3 $[(kg/m^3)/s]$	Not optimized	1.43×10^{-9}	--	--	<.01
UB4/12 $[(kg/m^3)/s]$	Not optimized	3.40×10^{-9}	--	--	<.01
UB5 $[(kg/m^3)/s]$	Not optimized	2.46×10^{-3}	--	--	<.01
UB11 $[(kg/m^3)/s]$	Yes	1.06×10^{-5}	4.39×10^{-6}	2.53×10^{-5}	.10
		Molybdenum			
MRC (mg/L)	No	1150	920	1,370	.02
MF1/2 (sec^{-1})	Not optimized	2.55×10^{-10}	--	--	<.01
MF3 (sec^{-1})	Not optimized	3.12×10^{-13}	--	--	<.01
MF4/12 (sec^{-1})	Not optimized	1.07×10^{-12}	--	--	<.01
MF5 (sec^{-1})	Not optimized	1.43×10^{-10}	--	--	<.01
MF11 (sec^{-1})	Yes	5.91×10^{-12}	8.24×10^{-13}	4.25×10^{-11}	<.01
MB1/2 $[(kg/m^3)/s]$	Not optimized	4.56×10^{-3}	--	--	<.01
MB3 $[(kg/m^3)/s]$	Not optimized	1.10×10^{-6}	--	--	<.01
MB4/12 $[(kg/m^3)/s]$	Not optimized	1.60×10^{-4}	--	--	<.01
MB5 $[(kg/m^3)/s]$	Not optimized	6.22×10^{-2}	--	--	<.01
MB11 $[(kg/m^3)/s]$	Yes	1.28×10^{-5}	5.09×10^{-6}	3.22×10^{-5}	.10
		Porosity (dimensionless)			
P1/2	No	.288	.168	.408	.62
P3	Not optimized	2.12×10^{-5}	--	--	<.01
P4/12	No	1.69×10^{-5}	.0	2.46×10^{-3}	<.01
P5	No	1.16×10^{-3}	.0	3.97×10^{-2}	<.01
P11	No	1.80×10^{-4}	.0	8.21×10^{-3}	.01
		Dispersivity (feet)			
DISP	No	220	87.6	353	.06

rate determined during calibration of the flow model. An alternative cover design to the one evaluated by Preston Niesen (Cotter Corporation, written commun., 1995) using the HELP–3 model may be required to achieve this recharge rate. The flow model was run using the decreased recharge rate, and flows of water into and out of the modeled area were used to establish inflow and outflow rates for input to the transport model. Concentrations of uranium and molybdenum were assumed to be the same as concentrations determined during calibration of the transport model.

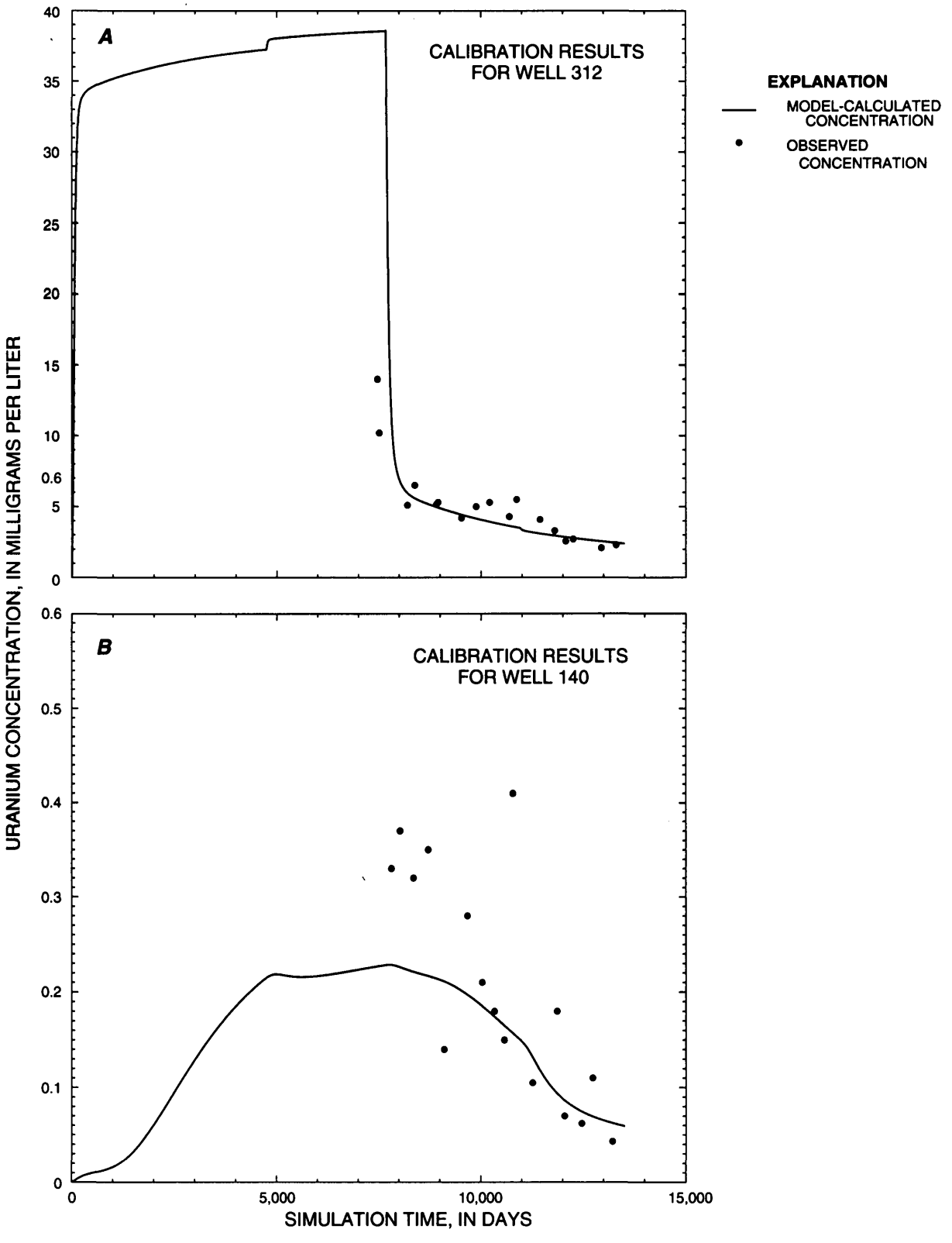

Figure 26. Observed and model-calculated concentrations of uranium and molybdenum.

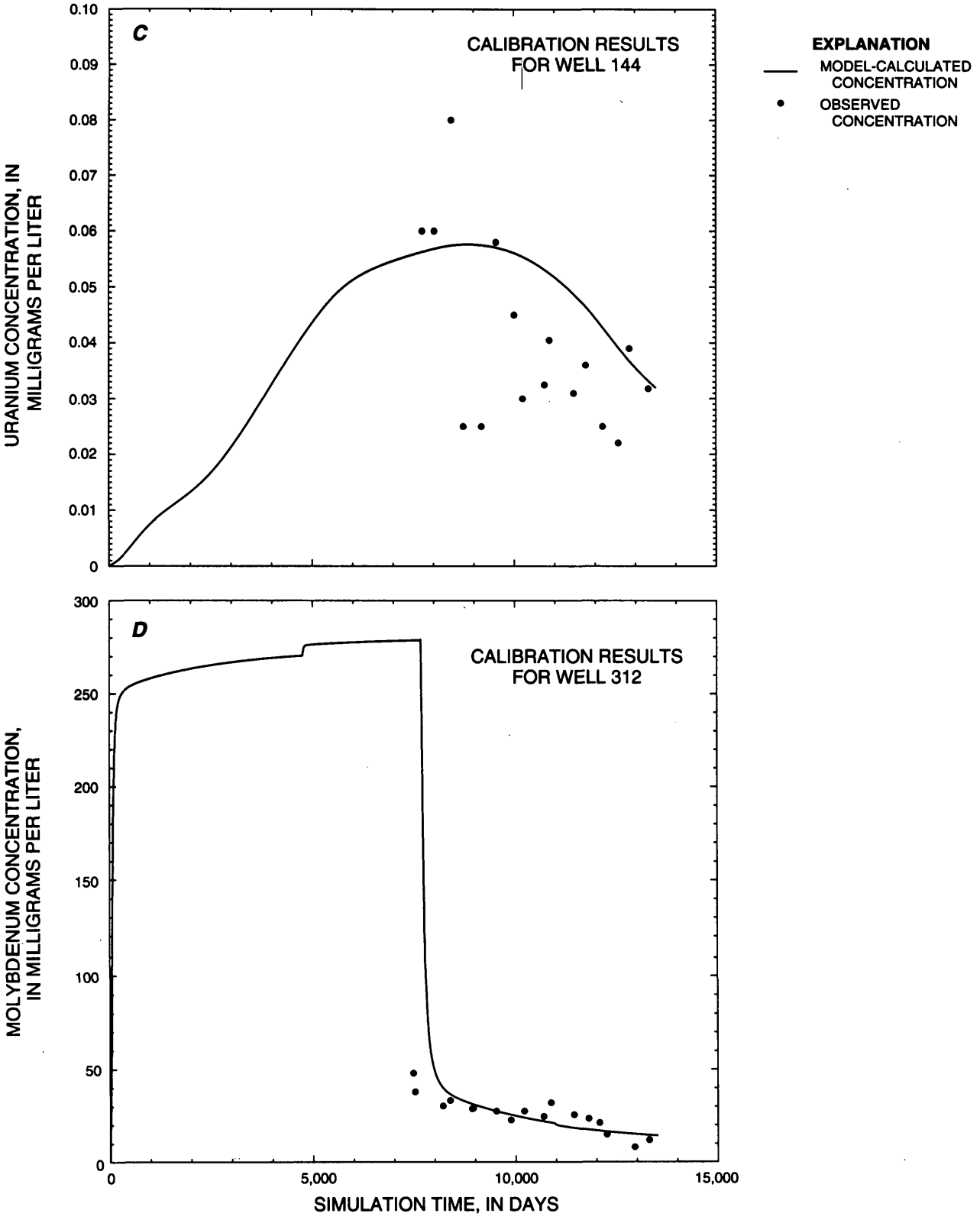

Figure 26. Observed and model-calculated concentrations of uranium and molybdenum—Continued.

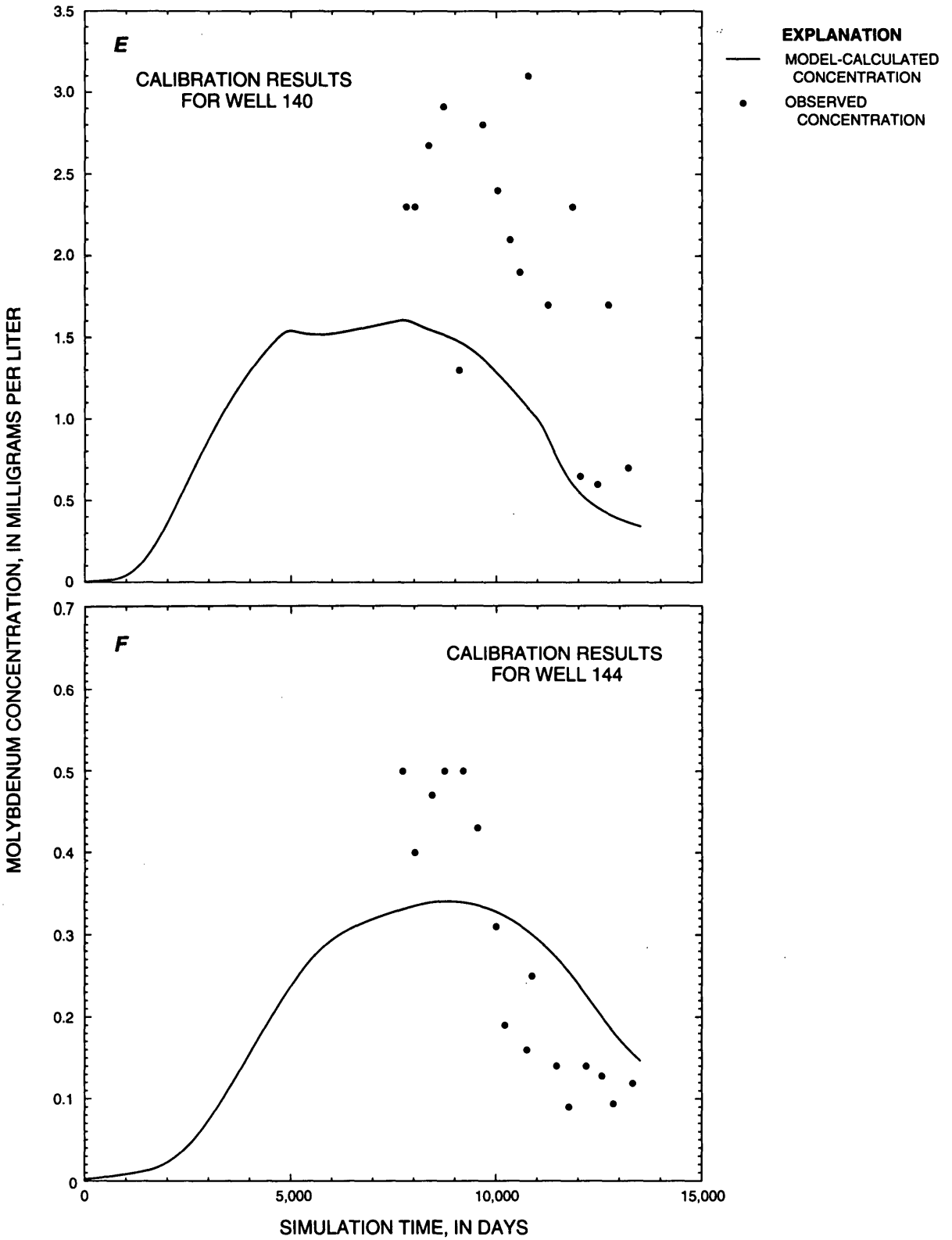

Figure 26. Observed and model-calculated concentrations of uranium and molybdenum—Continued.

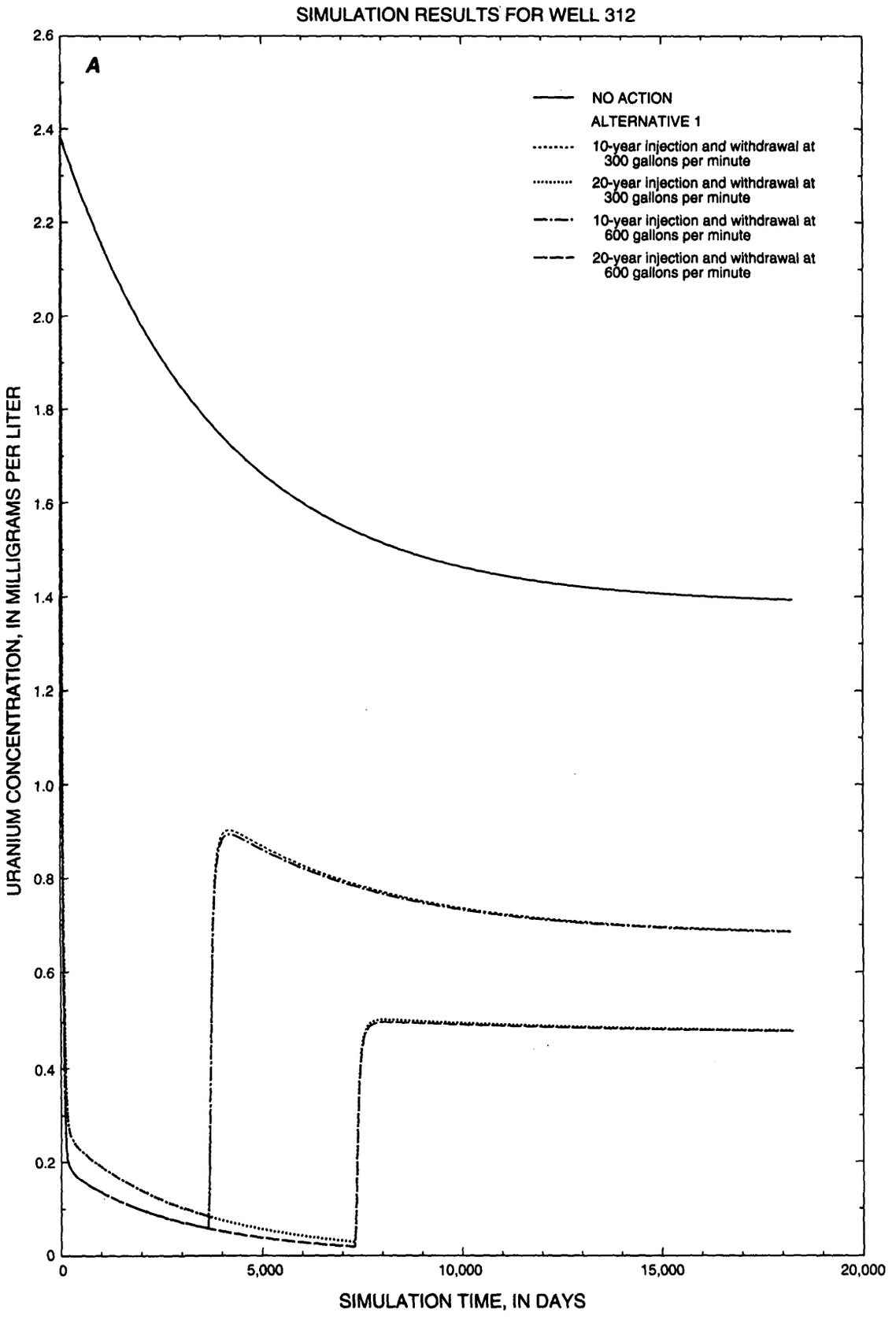

Figure 27. Uranium and molybdenum concentrations predicted for alternative 1.

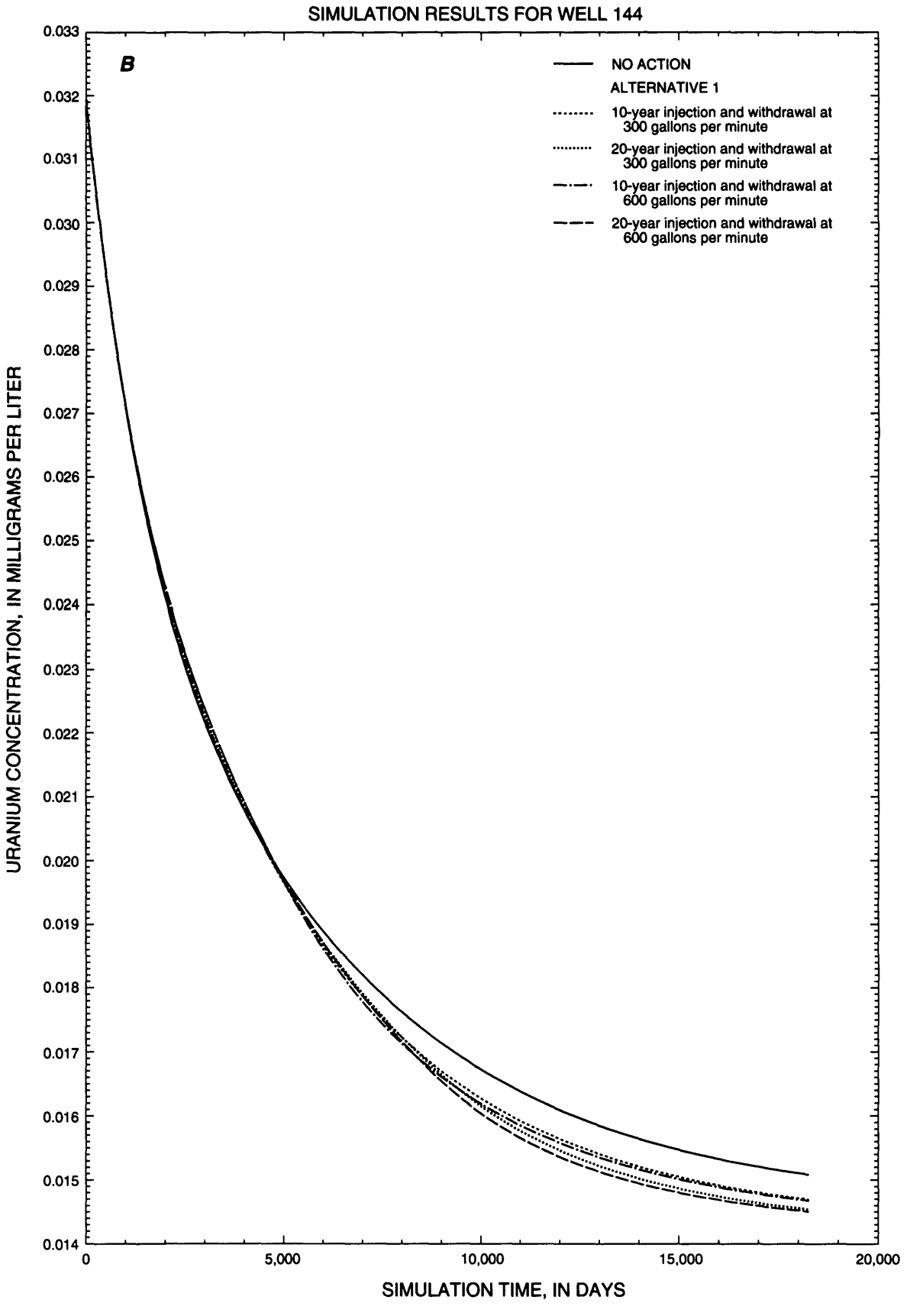

Figure 27. Uranium and molybdenum concentrations predicted for alternative 1—Continued.

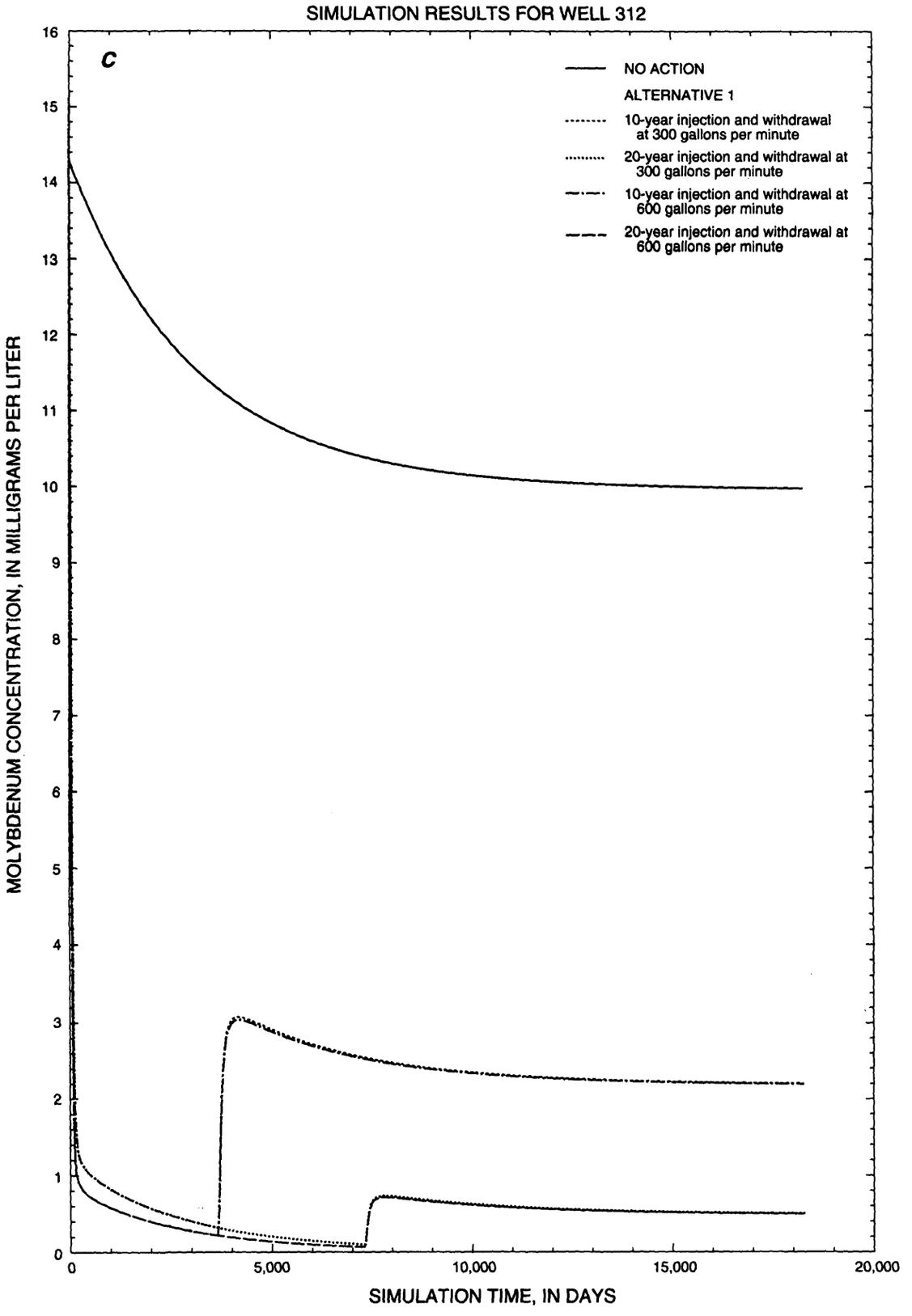

Figure 27. Uranium and molybdenum concentrations predicted for alternative 1—Continued.

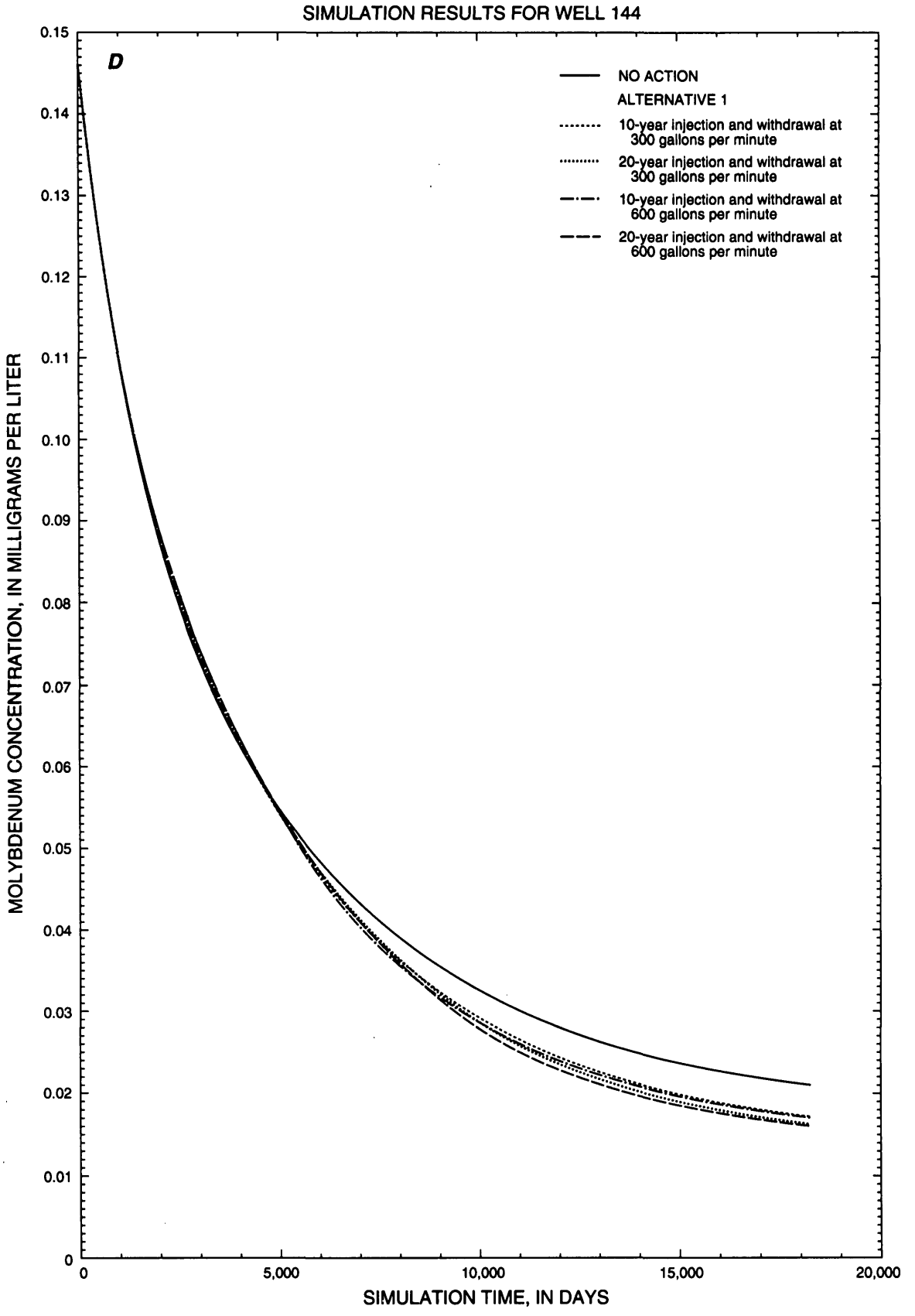

Figure 27. Uranium and molybdenum concentrations predicted for alternative 1—Continued.

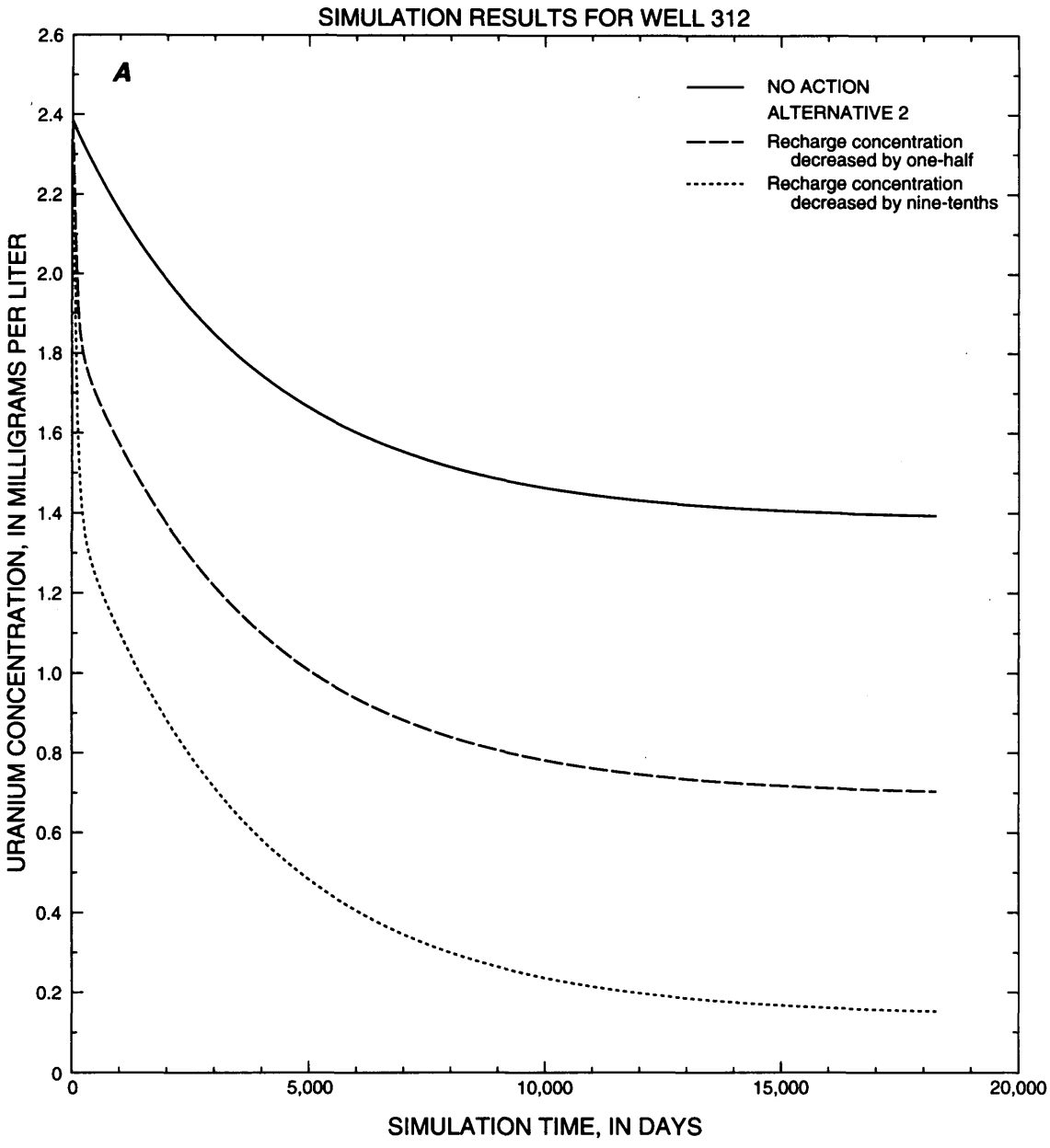

Figure 28. Uranium and molybdenum concentrations predicted for alternative 2.

Simulations of alternative 4 indicated that decreasing the recharge rate in the area of the unlined tailings ponds that is not overlain by the lined impoundment would result in moderate decreases in uranium and molybdenum concentrations at well 312, compared to the no-action scenario (fig. 30). Predicted concentrations at well 144 indicated negligible decreases in uranium and molybdenum concentrations compared to the no-action scenario.

Remediation Alternative 5: Apply Reducing Agent to Decrease Mobility of Contaminants

In this remediation alternative, a mild reducing agent, calcium polysulfide or sodium polysulfide, would be introduced in a series of infiltration cells at the land surface in the area of the unlined tailings ponds that is not overlain by the lined impoundment.

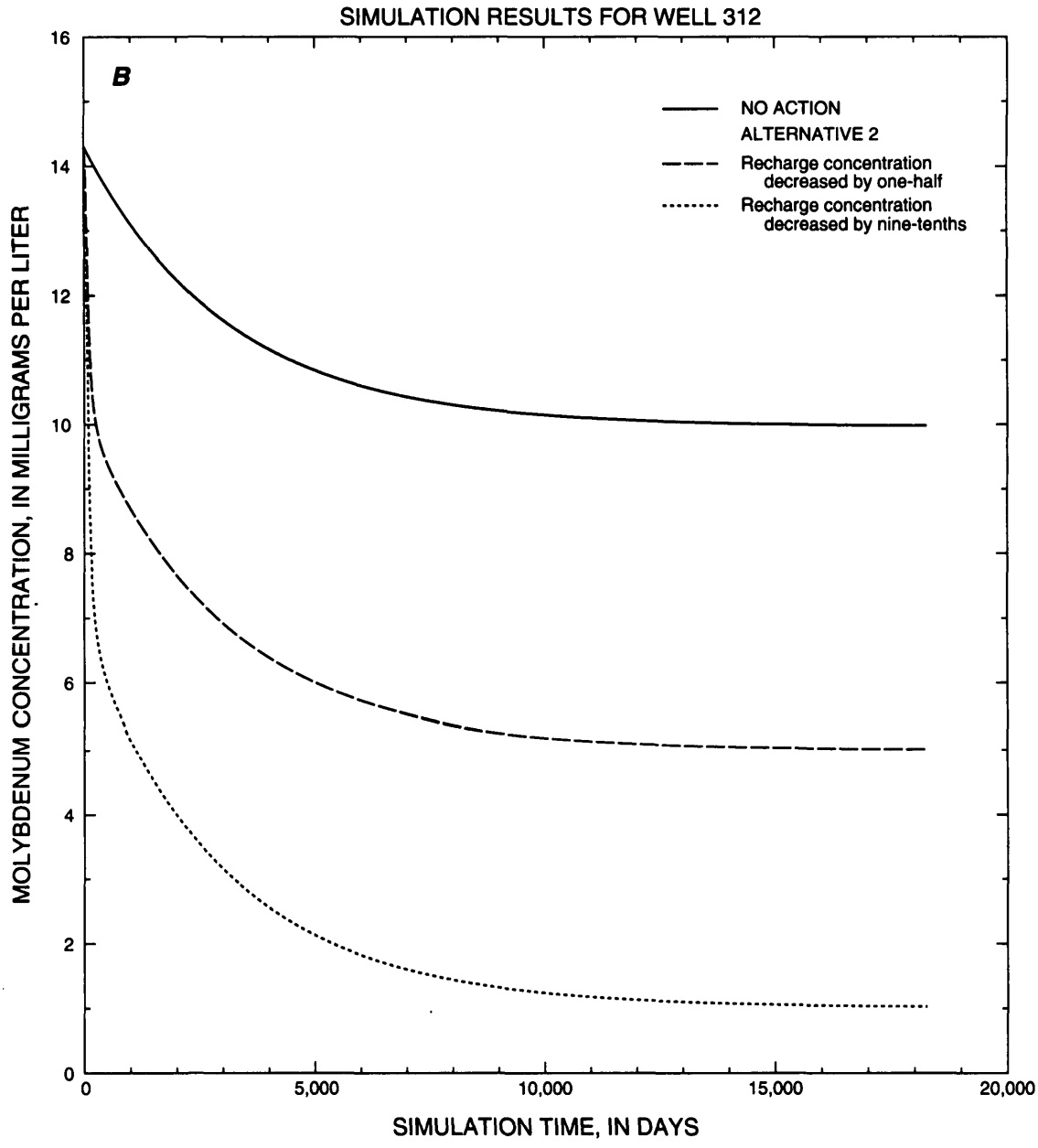

Figure 28. Uranium and molybdenum concentrations predicted for alternative 2—Continued.

The cells would be constructed so that each cell would be level, and the cells would form a series of terraces to conform approximately to the existing land surface; the cells would be filled with about 4 in. of pea gravel. The reducing agent would be added as a dilute aqueous solution and allowed to infiltrate into the ground. The desired effect of the addition of the reducing solution would be initially to flush aqueous uranium and molybdenum from contaminated materials, while creating a reducing environment in the contaminated materials to decrease the rate at which solid-phase uranium and molybdenum would dissolve or desorb. Reduction of uranium from U^{6+} to U^{4+} and of molybdenum from Mo^{6+} to Mo^{4+} has decreased the mobility of uranium and molybdenum in laboratory work using samples of ground water and earth materials from the study area, and the effect on mobility was reported to be relatively persistent even after water not having the reducing

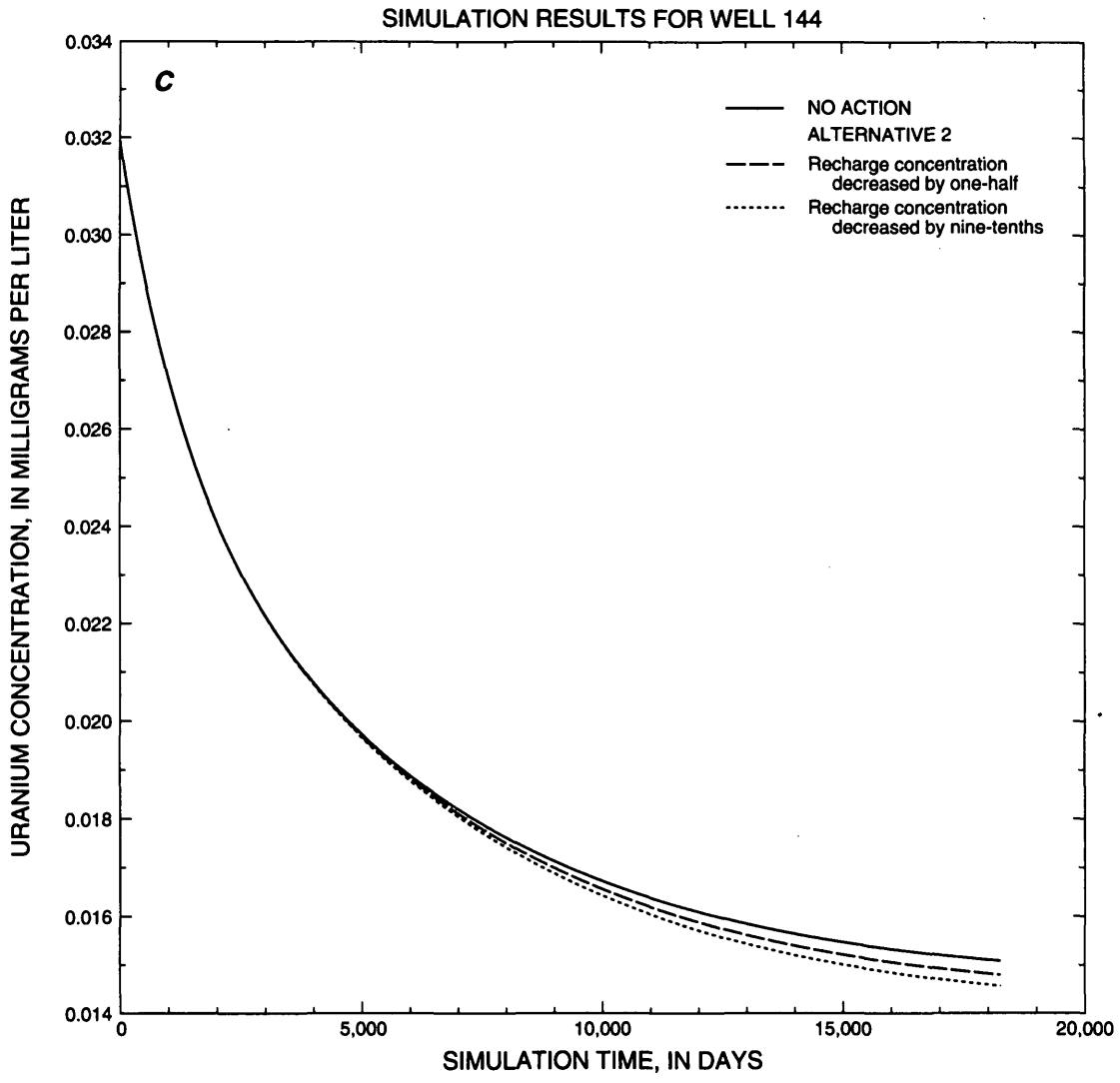

Figure 28. Uranium and molybdenum concentrations predicted for alternative 2—Continued.

agent was applied (Pyrih, 1996). Water samples collected from the unsaturated and saturated zones in field tests of the proposed alternative at the study area indicated decreases in concentrations of dissolved uranium similar to decreases that occurred in the laboratory tests (R.Z. Pyrih, Groundwater Technology, Inc., written commun., 1997), although persistence of the effect in field tests has yet to be demonstrated. Simulations of this alternative depend on the assumption that the decreases in concentrations of uranium and molybdenum observed in the field test are persistent. Application of the reducing solution would be done in segments such that 15 to 20 acres would be treated at a time, and the rate of application would be about 100 gal/min for periods of 3 to 6 months (James Rouse, Groundwater Technology, Inc., oral commun., 1997). Following the infiltration periods, the areas of the infiltration cells would be regraded to approximate the slope and configuration of the original land surface.

This alternative is the only one in which a net increase in inflow of water to the ground-water system was simulated. The reducing solution was assumed to be applied to a series of three 17-acre segments at 100 gal/min for 4 months for each segment. During the time when the addition of reducing solution was simulated in a given segment and thereafter, the concentrations of uranium or molybdenum in recharge water in the segment were assumed to have decreased from the calibration concentrations in proportion to

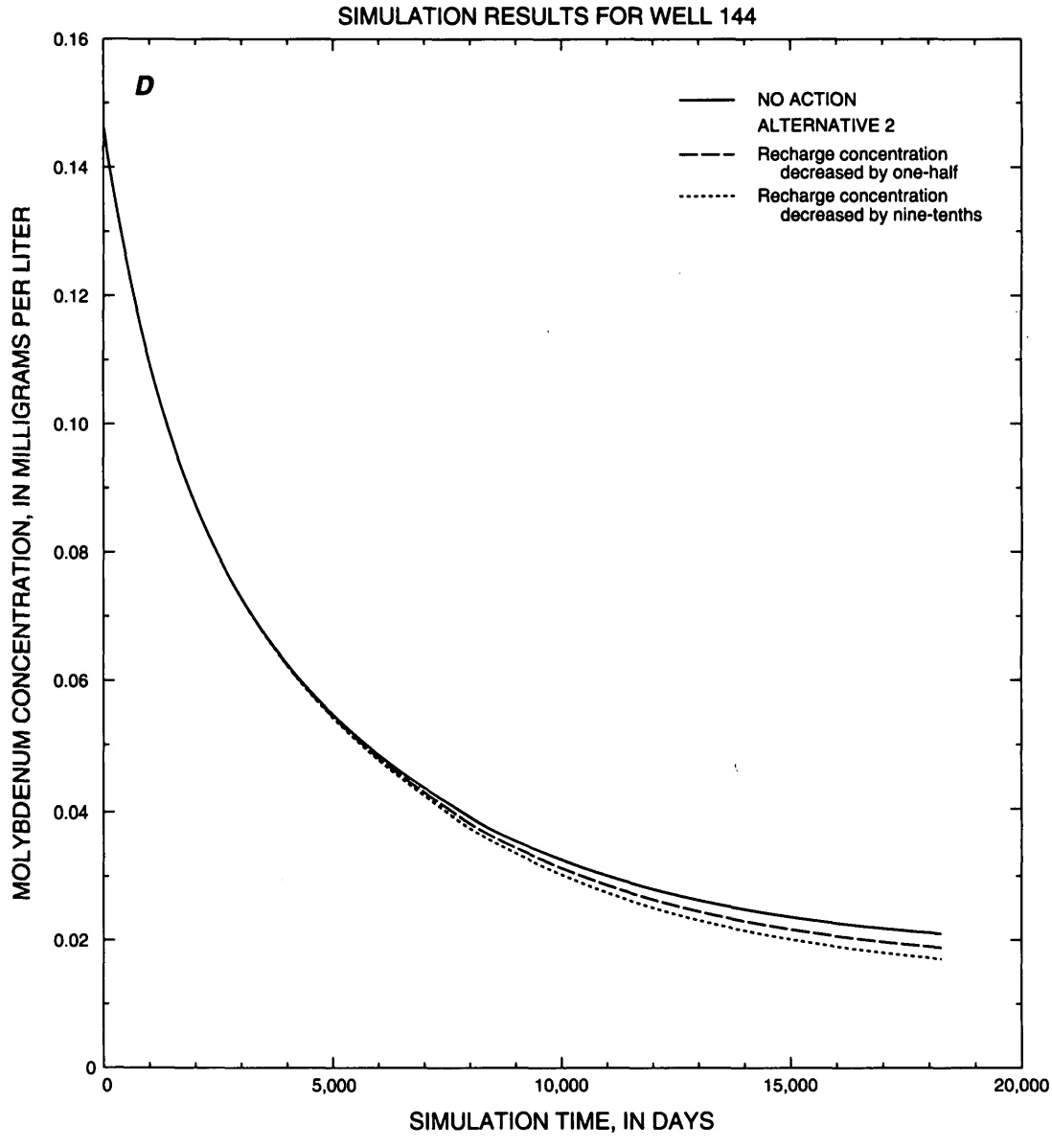

Figure 28. Uranium and molybdenum concentrations predicted for alternative 2—Continued.

the decrease in concentrations that occurred in the field test after application of reducing solution for 4 months. The area of the unlined ponds, except areas overlain by the lined impoundment, was divided into three 17-acre segments separated by boundaries oriented approximately east and west. The segments were numbered with segment 1 at the north end and segment 3 at the south end.

For the simulation, a series of steady-state flow-model runs representing increased recharge in each of three segments was made. Inflows and outflows calculated by the flow model were used to establish inflow and outflow rates for three consecutive 122-day transport-model runs. For the remaining 49 years of the 50-year simulation, recharge was assumed to equal the recharge determined during calibration of the flow model.

In response to the simulated increase in recharge in the area of the old, unlined tailings ponds that is not overlain by the lined impoundment, substantial, short-term increases in uranium and molybdenum concentrations were predicted by the transport model at well 312; these increases were followed by rapid decreases in concentrations (figs. 30*A* and 30*C*).

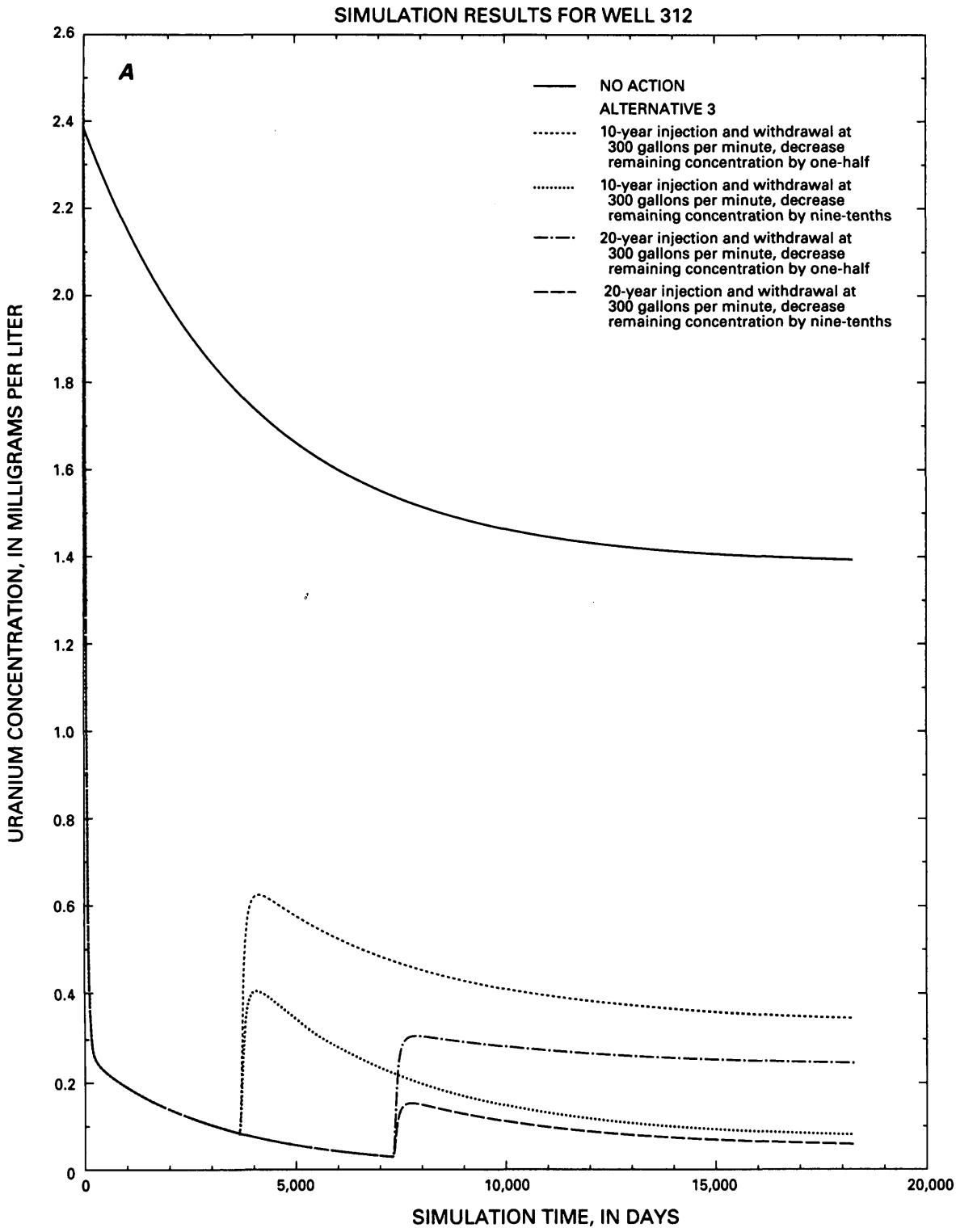

Figure 29. Uranium and molybdenum concentrations predicted for alternative 3.

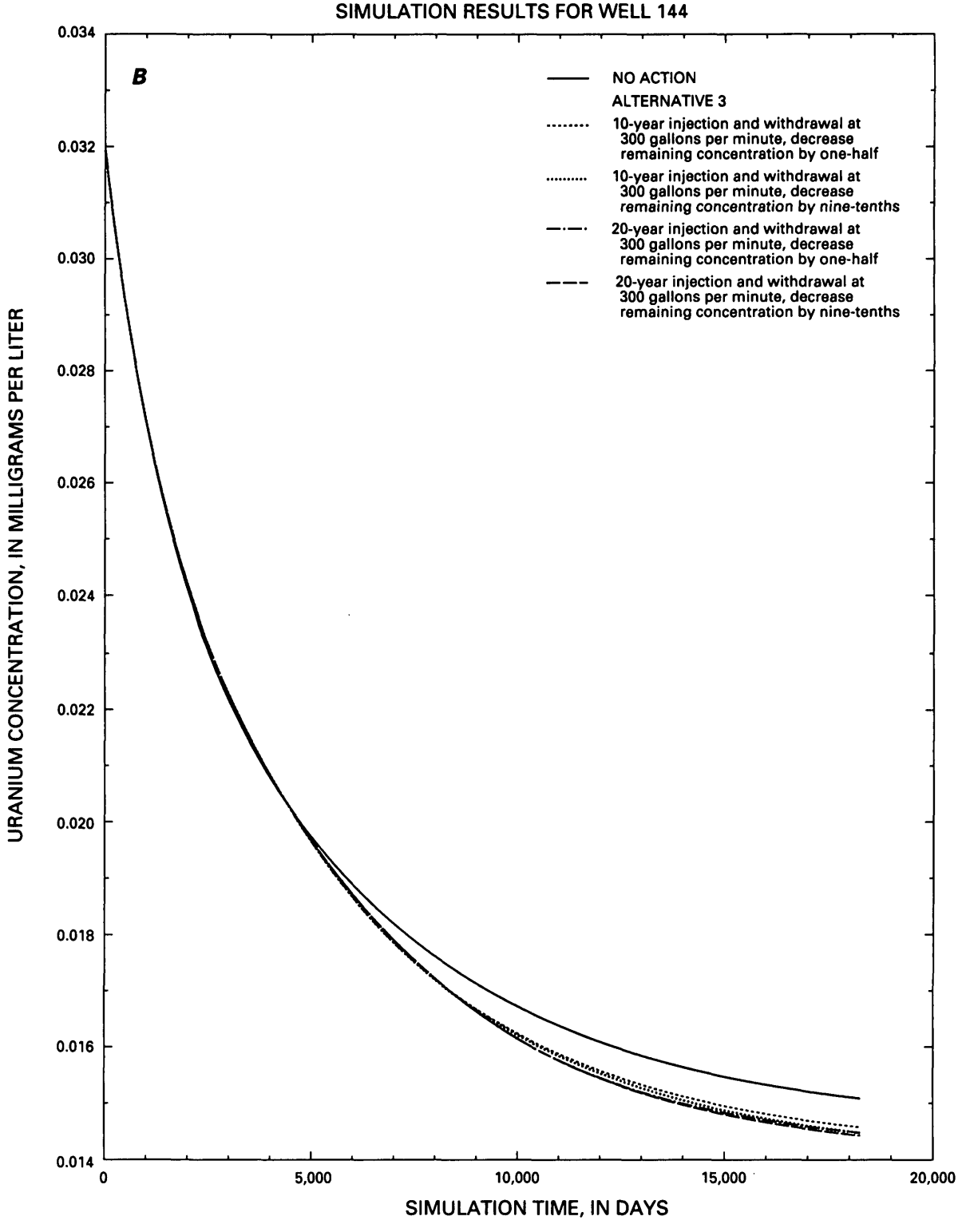

Figure 29. Uranium and molybdenum concentrations predicted for alternative 3—Continued.

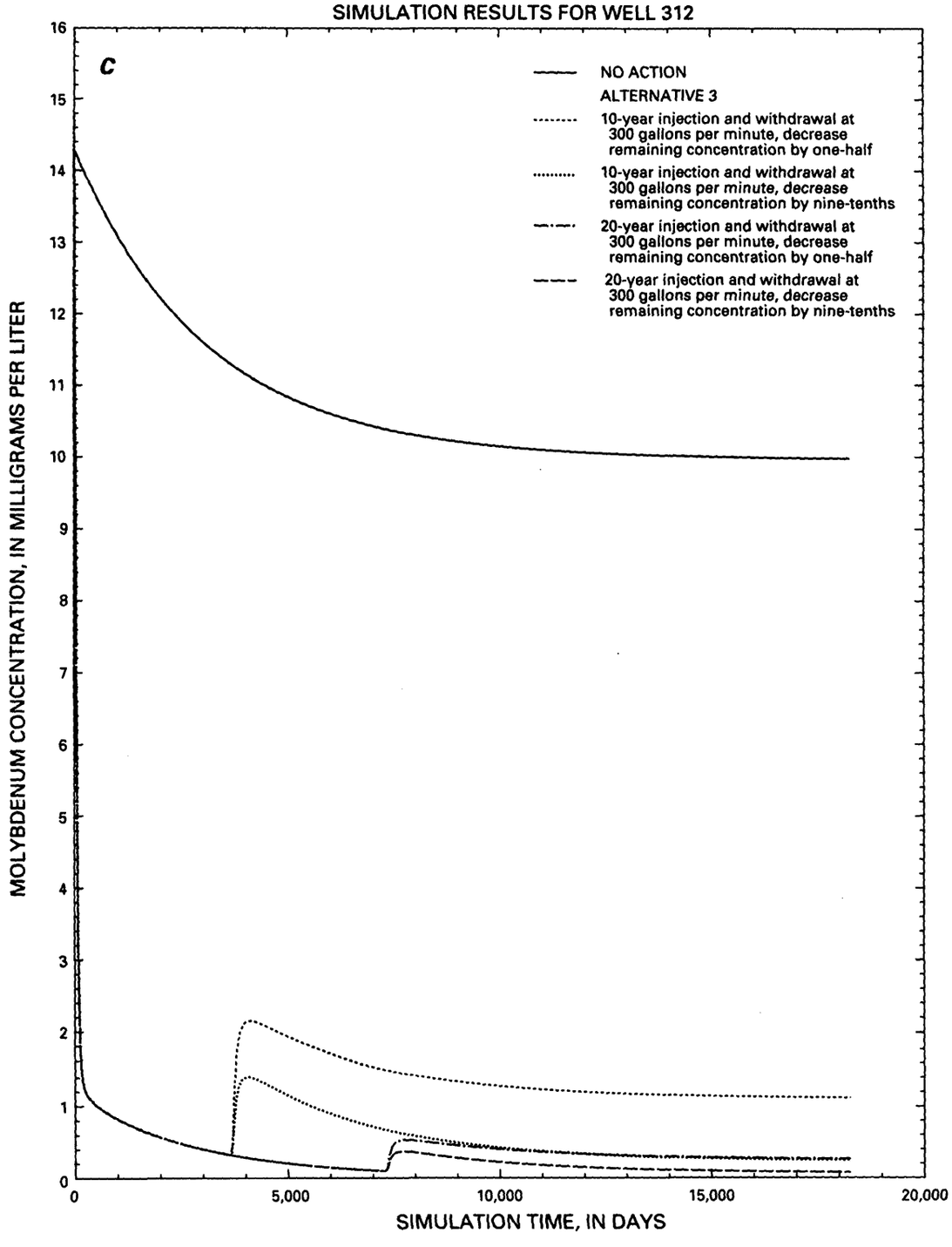

Figure 29. Uranium and molybdenum concentrations predicted for alternative 3—Continued.

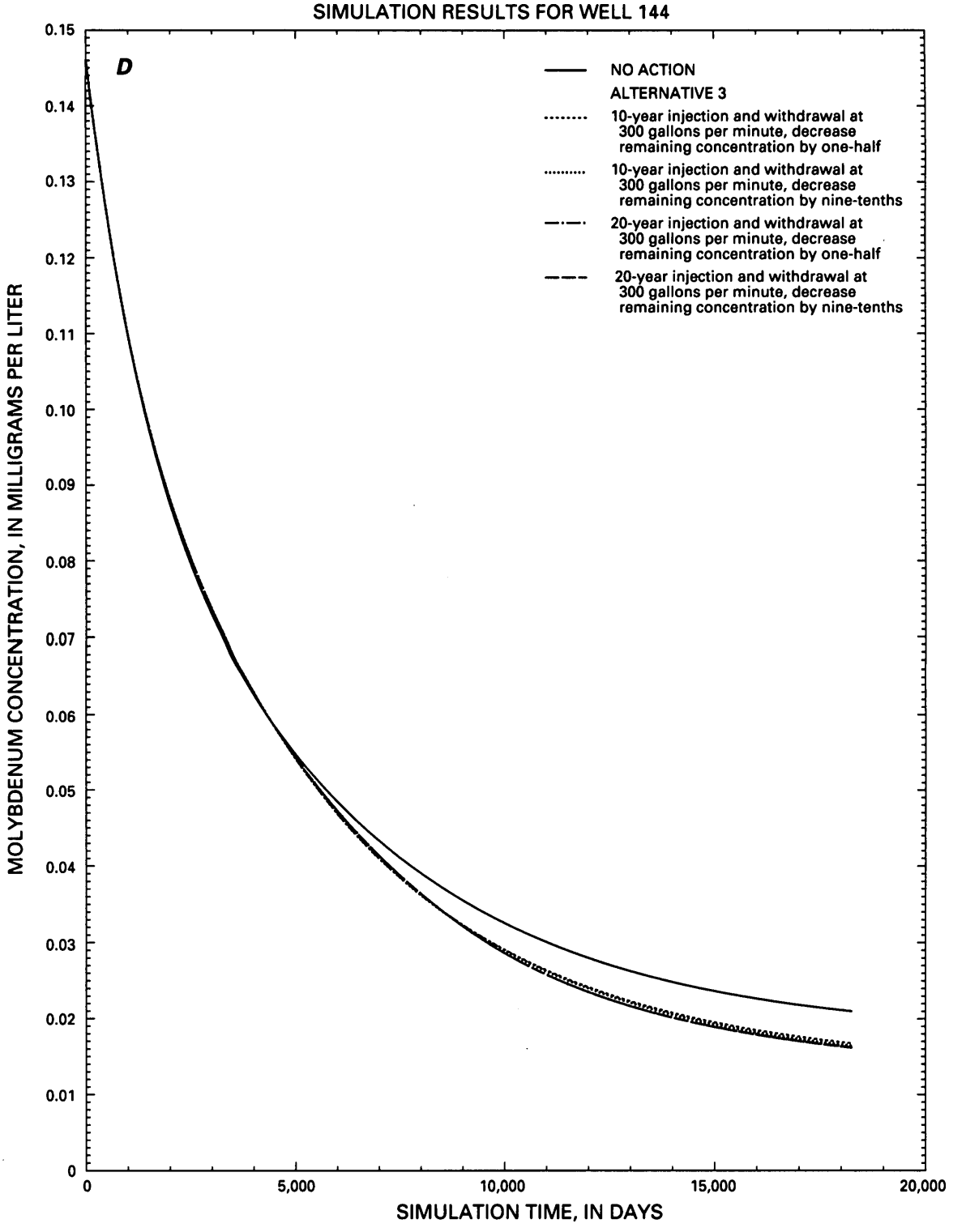

Figure 29. Uranium and molybdenum concentrations predicted for alternative 3—Continued.

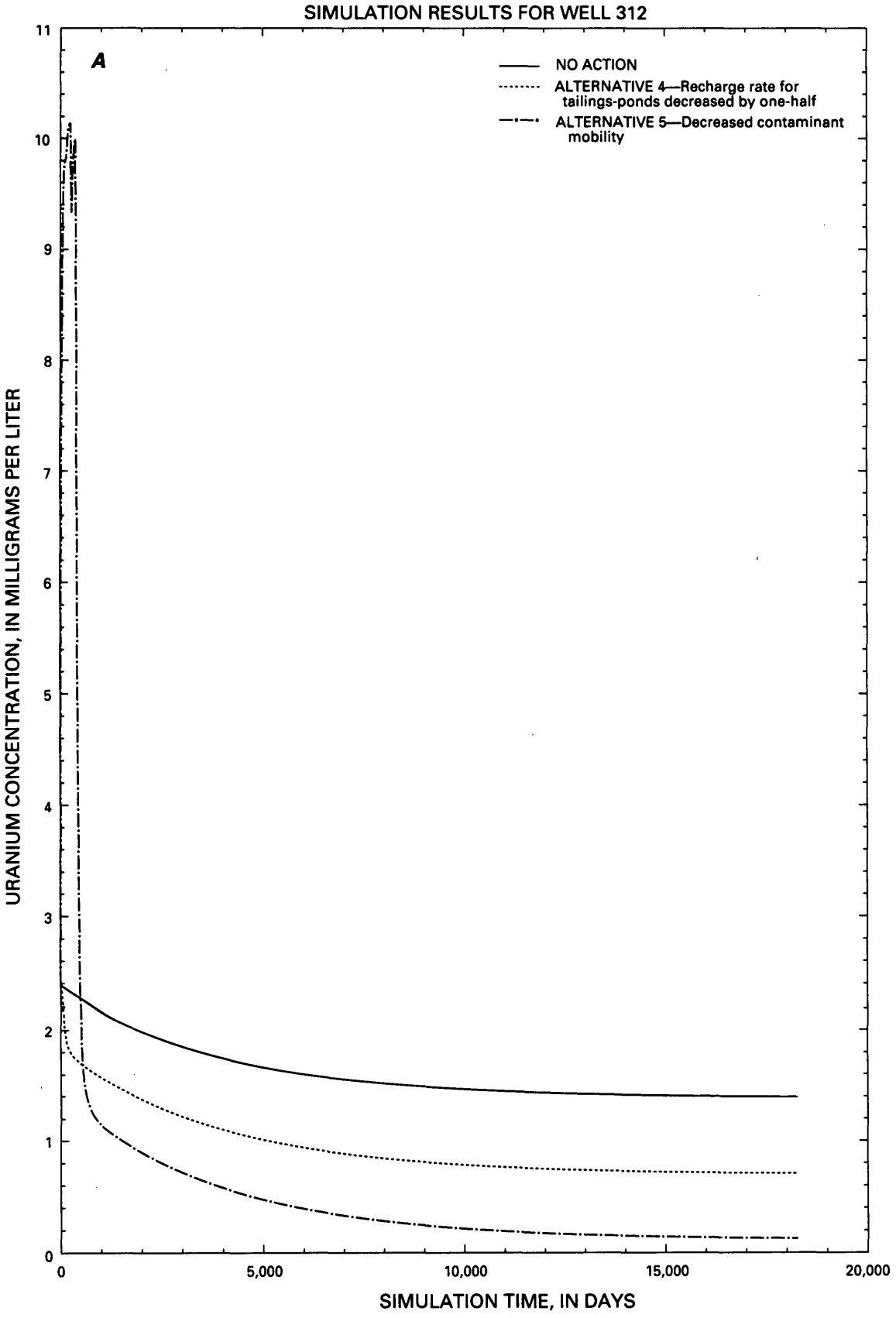

Figure 30. Uranium and molybdenum concentrations predicted for alternatives 4 and 5.

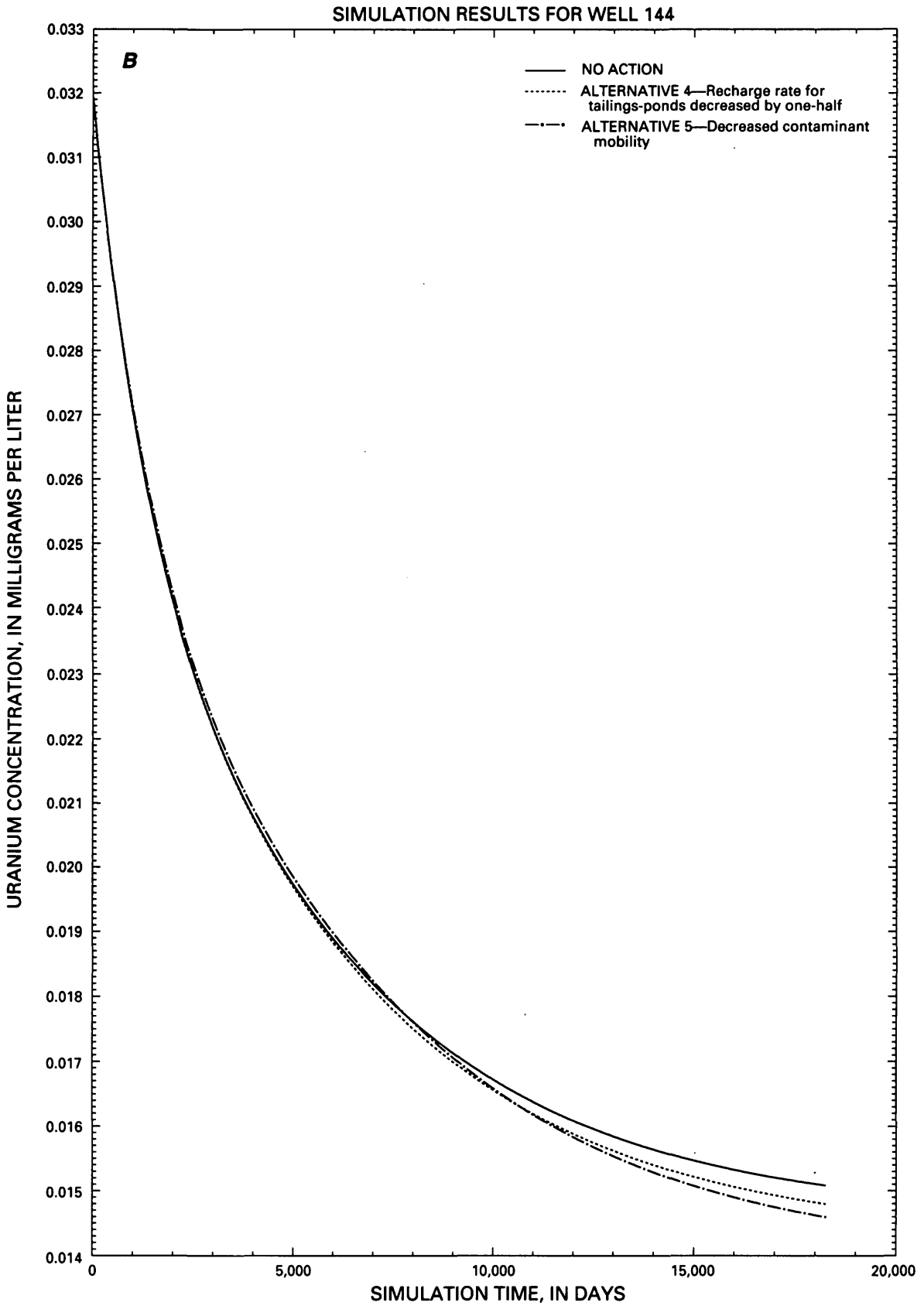

Figure 30. Uranium and molybdenum concentrations predicted for alternatives 4 and 5—Continued.

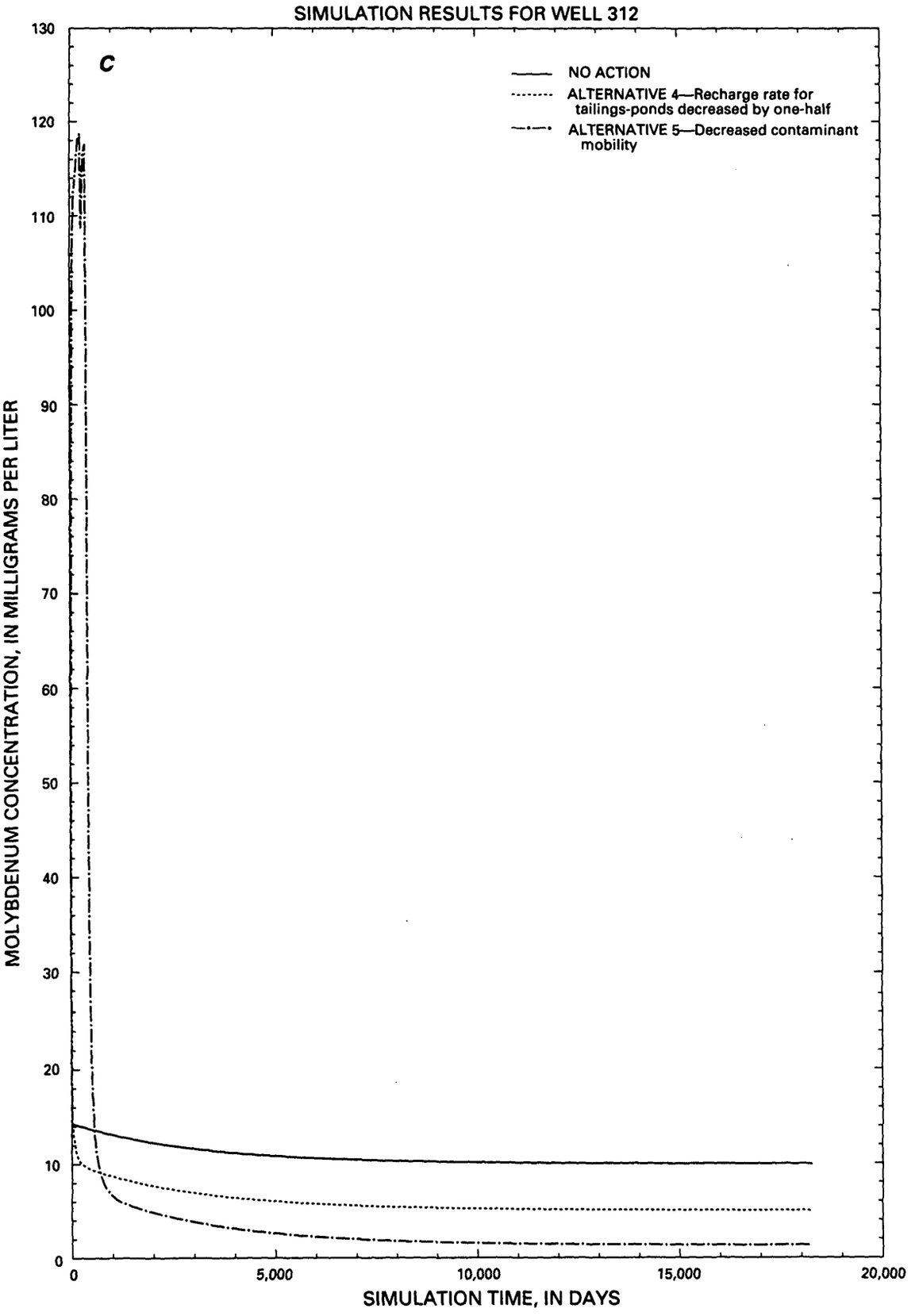

Figure 30. Uranium and molybdenum concentrations predicted for alternatives 4 and 5—Continued.

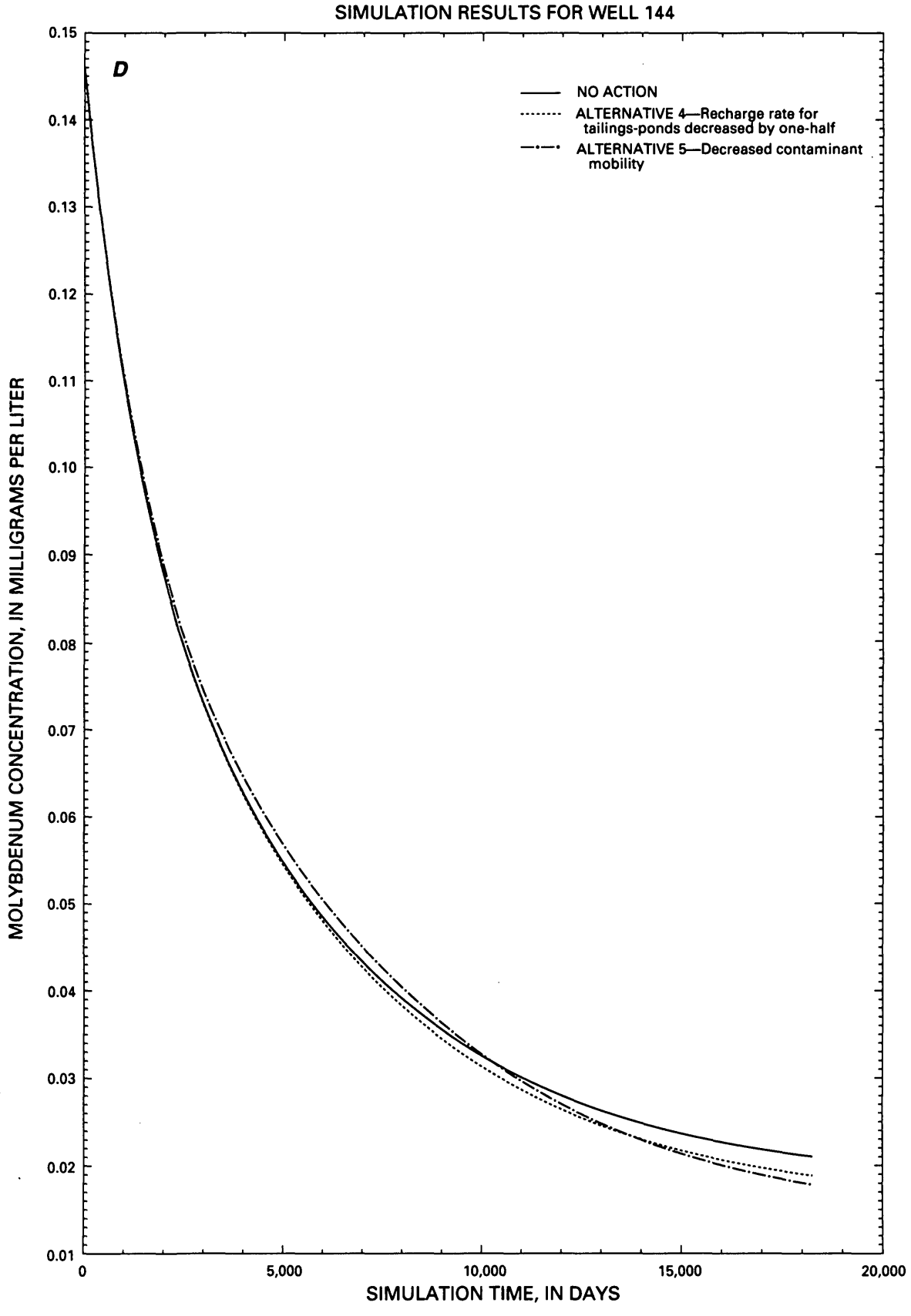

Figure 30. Uranium and molybdenum concentrations predicted for alternatives 4 and 5—Continued.

Predicted concentrations returned to what they were prior to the start of the simulated application of the reducing solution in less than 1,000 days. This spike in concentrations corresponded to the initial flushing discussed earlier in this section. Following the flushing of uranium and molybdenum, predicted concentrations continued to decline to values substantially lower than for the no-action scenario at well 312. Predicted uranium and molybdenum concentrations at well 144 were negligibly different from concentrations predicted for the no-action scenario.

Synopsis of Model Simulations

The predicted effects of the simulated remediation alternatives include short-term increases in concentrations and negligible to substantial long-term decreases in concentrations of dissolved uranium and molybdenum. A comparison of the predicted long-term effects of the no-action scenario and the five remediation alternatives is listed in table 18. The predicted concentrations are based on a contaminant-transport model that was calibrated to observations selected for their representation of trends in concentration over time. Fit of transport-model results to observed concentrations at a large number of wells was of secondary importance because the purpose of the modeling was to evaluate trends in concentration over time, not areal distribution. For these reasons, predicted concentrations listed in table 18 and plotted in figures 27 through 30 are most useful for making comparisons among the remediation alternatives and are less useful for predicting actual concentrations.

Based on the predicted concentrations for a simulation time of 50 years (figs. 27 through 30 and table 18) using models that incorporate numerous simplifying assumptions, some general comments can be made concerning the predicted effects of the remediation alternatives:

1. The choice of remediation alternative had little effect on the predicted concentrations of uranium and molybdenum at well 144 at the end of the 50-year simulations. The implication is that remedial actions that had been implemented prior to 1996 likely would result in long-term decreases in concentrations of uranium in the downgradient area. In particular, the presence of the clay barrier at the SCS dam seems to have substantially enhanced the ability of the Raton ridge to isolate the ground water of the upgradient area from that of the downgradient area.

Table 18. Summary of model simulations

[mg/L, milligrams per liter; gal/min, gallons per minute]

Simulation	Predicted concentration after 50-year simulation (mg/L)			
	Uranium		Molybdenum	
	Well 312	Well 144	Well 312	Well 144
No action	1.39	0.0151	9.98	0.0210
Alternative 1, 300 gal/min, 10-year flush	.686	.0147	2.20	.0172
Alternative 1, 300 gal/min, 20-year flush	.480	.0145	.503	.0163
Alternative 1, 600 gal/min, 10-year flush	.685	.0147	2.20	.0170
Alternative 1, 600 gal/min, 20-year flush	.479	.0145	.499	.0160
Alternative 2, concentration decreased by one-half	.704	.0148	5.01	.0188
Alternative 2, concentration decreased by nine-tenths	.153	.0146	1.03	.0171
Alternative 3, 10-year flush, concentration decreased by one-half	.349	.0146	1.12	.0168
Alternative 3, 10-year flush, concentration decreased by nine-tenths	.0801	.0145	.247	.0164
Alternative 3, 20-year flush, concentration decreased by one-half	.246	.0145	.265	.0162
Alternative 3, 20-year flush, concentration decreased by nine-tenths	.0582	.0144	.0747	.0162
Alternative 4, recharge rate decreased by one-half	.706	.0148	5.02	.0188
Alternative 5, chemical reduction	.126	.0146	1.31	.0178

2. Injection and withdrawal of water at either 300 or 600 gal/min likely would result in similar decreases in uranium and molybdenum concentrations at well 312. However, at either injection and withdrawal rate, a 20-year treatment period likely would result in substantially smaller contaminant concentrations than would a 10-year treatment period.

The predicted concentrations of uranium and molybdenum in the upgradient area, represented by well 312, were substantially affected by the remediation alternative simulated. Results of simulations of alternative 1 indicated that the predicted concentrations at well 312 primarily depend on the duration of injection and withdrawal of water through the contaminated materials. Results of simulations of alternative 2 indicated that substantial decreases in contaminant concentrations at well 312 were predicted when the concentrations of contaminants in water reaching the water table in the area of the old, unlined tailings ponds were decreased to one-tenth of the concentrations used for the no-action scenario. Decreasing the concentrations of contaminants in recharge water to one-half of the concentrations used in the no-action scenario was predicted to result in moderate decreases in concentrations at well 312. The alternative 3 simulation indicated that removal of contaminated materials following injection and withdrawal would have substantial effects on contaminant concentrations, compared to the alternative 1 simulation. The alternative 3 simulation of 20 years of injection and withdrawal followed by decreasing the remaining concentrations by nine-tenths resulted in the smallest contaminant concentrations at well 312 at the end of the 50-year simulation. Decreases in contaminant concentrations at well 312, compared to the no-action scenario, predicted by the alternative 4 simulation were only moderate and were approximately the same as for the alternative 2 simulation, where recharge concentrations in the area of the old, unlined tailings ponds were assumed to be decreased by 50 percent (table 18). Simulation of alternative 5 resulted in substantial decreases in contaminant concentrations, although the effectiveness in decreasing molybdenum concentrations was predicted to be less than the effectiveness in decreasing uranium concentrations.

INTERPRETATION AND USE OF MODEL SIMULATIONS

Assumptions made during the conceptualization of the simulations, particularly for the alternative 5 simulation, to a large degree controlled the model results. Deviations in the behavior of the actual ground-water flow and transport system, including the geochemistry of the contaminants, from the assumed behavior may result in substantially different concentrations from the predicted concentrations. The model simulations are most useful as tools for comparison between remediation alternatives.

A contaminant-transport model that includes the effects of rate-limited sorption and desorption was used to simulate the migration of contaminant species between the fracture system, where contaminants are possibly highly mobile, and blocks of porous medium between fractures, where transport is slower. The effects of rate-limited desorption are indicated by the results of simulation of remediation alternatives 1 and 3 (figs. 27 and 29) at well 312, where large decreases in predicted contaminant concentrations, which were caused by simulated periods of flushing, were followed by rapid increases in predicted contaminant concentrations following cessation of the simulated flushing. The physical explanation for the simulation results is that, during injection of large quantities of small-concentration water into a fractured ground-water system, dilution and flushing of water in high-permeability fractures can produce rapid, large decreases in contaminant concentrations in the fractures, but little effect in the interior of the blocks between the fractures. When injection and withdrawal of water are stopped, the rate of flow of water through the fractures would decline dramatically. When the rate of water flow in the fractures drops, the concentration gradient between the interior of the blocks, where aqueous concentrations are large, and the fractures, where concentrations are now small, can create a situation where diffusion and relatively slow advective transport of contaminants from the blocks to the fractures would produce an increase in contaminant concentrations in the fractures.

The concentrations of uranium and molybdenum at any particular sampling site affected by migration of raffinate were, in general, a result of mixing of waters having different concentrations of the two constituents and of variations in the hydraulics of the ground-water system. Observed concentrations

shown in figure 26 were annual medians; variability of the raw data (Banta, 1997) was even larger than the variability apparent in the plotted points. The models, however, were based on assumptions of uniformity in zones used to assign parameters to the models and were greatly generalized in their simulation of hydraulic stresses. As a result of the generalization and of simplifications made in construction of the models, the model results were not as variable as the observations (fig. 26).

An understanding of the source of the variability in the observed concentrations can help the reader make appropriate use of the model results. For example, contaminant concentrations in the wells downgradient from the DeWeese Dye Ditch that are affected by raffinate from the old, unlined tailings ponds result from mixing of two small-concentration sources, irrigation water and precipitation, and a large-concentration source, raffinate-affected ground water from the area of the old, unlined tailings ponds. Variations in contaminant concentrations in samples from these wells are due to changes in concentrations in the large-concentration source, changes in volumetric rate of recharge in the area of the old, unlined tailings ponds, and changes in other stresses on the flow field. Heterogeneities in the porous medium add another factor that tends to increase variability of concentrations at a particular well in response to changes to the overall flow field. The effect of these factors is to modify the mixing ratio of water from the small- and large-concentration sources with time and, therefore, the concentrations of contaminants in samples. The amount of variation can be an indicator of the difference in contaminant concentrations among the various source waters. If the differences in contaminant concentrations among the source waters were small over a sufficiently long period of time, relatively small variation in contaminant concentrations in samples would be expected. A larger difference in concentrations among the source waters can be expected to produce a proportionately larger variation in concentrations in samples. This principle can be applied conceptually to the problem of predicting the amount of variation that can be expected in response to the various remediation efforts. In the long term, relatively large decreases in contaminant concentrations in the area of the old, unlined tailings ponds can be expected to result in relatively large decreases in the amount of variability that may be measured in water from wells in Lincoln Park.

The discussion in the preceding paragraph is pertinent to the selection of a remediation alternative for contamination at the study area because the contaminant concentrations predicted by the various model simulations represented long-term trends in concentration, whereas the short-term variations were not simulated. Effects of changes in concentrations in the upgradient area on short-term variations in contaminant concentrations in Lincoln Park can be estimated, at least qualitatively, by considering samples from wells in the downgradient area to be mixtures of samples of small- and large-concentration water, where the mixing ratio varies in the short term to produce (unmodeled) variation in contaminant concentrations. The selection of a remediation alternative that was predicted to produce large decreases in contaminant concentrations in the upgradient area, represented by well 312, could increase the likelihood of a stable long-term concentration trend in the downgradient area. By viewing the results of this study in this way, the reader can develop a better understanding of how actual future contaminant concentrations may be expected to vary, whereas the overall trend in concentrations can be expected to approximate the predictions modeled for the various remediation alternatives.

SUMMARY

Wastes from a uranium mill that began operation in 1958 have contaminated ground water in an area in and near Cañon City, Colorado. The affected ground water primarily is in unconsolidated and weathered and fractured consolidated rocks ranging in age from Cretaceous to Quaternary. Ground-water flow and solute transport in the study area are largely controlled by recharge rate, lithology, geologic structure, fractures, and anthropogenic modifications to the ground-water system. Mill wastes were deposited in a series of unlined tailings ponds from 1958 to 1979. The mill and associated tailings ponds are in an upgradient part of the study area, where ground-water flow in fractured consolidated rocks is an important part of the solute-transport process. Contaminants reached wells in a downgradient part of the study area, where transport is mainly in unconsolidated deposits, as early as 1968. Before 1971, when a flood-control dam was constructed at a ridge that separates the upgradient area from the downgradient area, surface water likely transported mill wastes from the

upgradient area to the downgradient area. Some of the contaminants also may have been air transported from the upgradient area to the downgradient area.

The main source of recharge to the ground-water system is water that enters the study area in irrigation ditches and either leaks out of the irrigation ditches and ponds directly to the ground-water system or is applied in excess of the irrigation requirements of crops. Other sources of water recharging the ground-water system are recharge from precipitation and ground-water inflow along a stream channel at the upgradient end of the study area. Infrequent flow in stream channels probably contributes a small amount to recharge of the ground-water system. Ground water is discharged from the system as flow to springs and to a stream at the downgradient end of the study area, pumpage from irrigation wells and wells operated to control the migration of contamination, and ground-water outflow. As an annual average, at least 730,000 ft^3/d of water flows through the ground-water system.

Mobility of uranium and molybdenum in the ground-water system depends, to a large degree, on their oxidation-reduction state. Minerals bearing the reduced form of uranium, U^{4+}, are extremely insoluble. As a result, mobility of uranium in reducing ground-water environments is small. Precipitation of molybdenum sulfide, coprecipitation of iron sulfides, and sorption of the reduced form of molybdenum, Mo^{4+}, limit the mobility of molybdenum in reducing ground-water environments. At depths below about 100 ft in the study area, reducing conditions cause uranium and molybdenum to be reduced. Consequently, most uranium and molybdenum transport is limited to the part of the ground-water system that is at depths less than 100 ft.

Digital ground-water flow and solute-transport models were developed to comparatively evaluate five remediation alternatives that have been proposed for the study area. A three-dimensional finite-difference model was developed to simulate flow in the ground-water system. A two-dimensional finite-element model representing the uppermost 100 ft of the ground-water system was developed to simulate the transport of uranium and molybdenum in the ground-water system. Inflow and outflow rates calculated by the flow model were used to specify inflow and outflow rates in the transport model. Both models were calibrated, in part, by using parameter-estimation techniques. These techniques attempted to provide model-input values that minimize differences between model-calculated values of hydraulic head, flow, or contaminant concentration and corresponding observed values.

Simulations of 50 years of a no-action scenario and of each remediation alternative were used to predict concentration trends over time at two wells, one in the upgradient area and one in the downgradient area. The alternative that was predicted to result in the smallest contaminant concentrations at the upgradient well after 50 years was an alternative that involves injection of water into, and withdrawal of water from, the ground-water system followed by removal of remaining contaminated materials in the area of the unlined tailings ponds. In that alternative, the most important factor in determining contaminant concentrations at the end of the 50-year simulation period was the effectiveness of removal of contaminated materials. For uranium, the second most effective alternative was predicted to be the alternative that involves fixation of contaminants by application of a reducing agent. The contaminant-fixation alternative was predicted to be less effective at decreasing molybdenum concentrations than at decreasing uranium concentrations. For molybdenum, the second most effective alternative was predicted to be the alternative that involves injection and withdrawal of water. For both alternatives that include injection and withdrawal of water, the duration of treatment was predicted to be more important than the rate of injection and withdrawal in determining the effectiveness of remediation. The alternative predicted to be the least effective in decreasing contaminant concentrations at the upgradient well was one in which construction of a layered cover to decrease the recharge rate is proposed. Predicted differences in concentration at the downgradient well at the end of the 50-year simulation, compared to the no-action scenario, were negligible to small for all of the remediation alternatives.

Generalizing assumptions and simplifications made in the model conceptualization and calibration processes cause the model to predict concentrations that are less variable than the historical ground-water data. The variability in data is due, in part, to variability in transient stresses to the ground-water system and to heterogeneity of earth materials. The variable stresses and heterogeneity result in variable mixing ratios of large- and small-concentration water from different parts of the ground-water system in samples obtained from a particular well at different times. In contrast, the models use assumptions of constant hydraulic stress over long periods and of

homogeneity of aquifer properties within each model zone and, therefore, cannot simulate all the variability of the ground-water system. Although the differences in predicted concentration at the downgradient well among the proposed remediation alternatives and the no-action scenario were negligible to small, environmental variability can be expected to produce variability in future samples that was not predicted by the model. Selection of a remediation alternative that is predicted to result in small contaminant concentrations in the upgradient area can be expected to result in a more constant long-term concentration trend in the downgradient area.

REFERENCES CITED

Adrian Brown Consultants, Inc., 1993, Old pond area remediation final report, pilot phase study: Denver, Colo., several loose-leaf volumes.

Banta, E.R., 1994, Statistical analysis of uranium-mill raffinate contamination in water wells in Lincoln Park, south-central Colorado: U.S. Geological Survey Water-Resources Investigations Report 93–4211, 11 p.

Banta, E.R., 1997, Data for water levels, water quality, lithology, and surface-water discharge in the vicinity of Lincoln Park, Colorado, 1961 through 1996: U.S. Geological Survey Open-File Report 97–361, 16 p.

Bertine, K.K., 1972, The deposition of molybdenum in anoxic waters: Marine Chemistry, v. 1, no. 1, p. 43–53.

Bouwer, Herman, and Rice, R.C., 1976, A slug test for determining hydraulic conductivity of unconfined aquifers with completely or partially penetrating wells: Water Resources Research, v. 12, no. 3, p. 423–428.

Brogan, S.D., 1991, Aquifer remediation in the presence of rate-limited sorption: Stanford, Calif., Stanford University, Master's thesis, 238 p.

Brogan, S.D., and Gailey, R.M., 1995, A method for estimating field-scale mass transfer rate parameters and assessing aquifer cleanup times: Ground Water, v. 33, no. 6, p. 997–1009.

Chafin, D.T., and Banta, E.R., 1999, Migration and geochemical evolution of ground water affected by uranium-mill effluent near Cañon City, Colorado: U.S. Geological Survey Water-Resources Investigations Report 98–4228, 62 p.

Cooper, H.H., Jr., Bredehoeft, J.D., and Papadopulos, I.S., 1967, Response of a finite-diameter well to an instantaneous charge of water: Water Resources Research, v. 3, no. 1, p. 263–269.

Cooper, H.H., Jr., and Jacob, C.E., 1946, A generalized graphical method for evaluating formation constants and summarizing well-field history: American Geophysical Union Transactions, v. 27, no. 4, p. 526–534.

D'Agnese, F.A., Faunt, C.C., Turner, A.K., and Hill, M.C., 1997, Hydrogeologic evaluation and numerical simulation of the Death Valley regional groundwater flow system, Nevada and California: U.S. Geological Survey Water-Resources Investigations Report 96–4300, 124 p.

Daniel B. Stephens & Associates, Inc., 1993, Assessment of potential seepage impacts on ground water, Cotter uranium mill, Cañon City, Colorado: Albuquerque, N. Mex., three loose-leaf volumes.

Dunne, Thomas, and Leopold, L.B., 1978, Water in environmental planning: San Francisco, W.H. Freeman and Company, 818 p.

Environ Corp., Radiation Surveillance Associates, Radiant Energy Management, and Western Radiation Consultants, 1991, Health risk assessment of the Cotter uranium mill site, Cañon City, Colorado: Arlington, Va., 336 p.

Environmental Systems Research Institute, Inc., 1994, Grid commands: Redlands, Calif., variously paged.

Freeze, R.S., and Cherry, J.A., 1979, Groundwater: Englewood Cliffs, N.J., Prentice-Hall, 604 p.

Galloway, M.J., 1994, Lincoln Park aquifer test: Lakewood, Colo., Cotter Corporation, variously paged.

Geotrans, Inc., Rocky Mountain Consultants, Inc., and ERI Logan, Inc., 1986, Remedial investigation, Cotter Corporation uranium mill site: Boulder, Colo., Geotrans, Inc., variously paged.

Goode, D.J., and Wilder, R.J., 1987, Ground-water contamination near a uranium tailings disposal site in Colorado: Ground Water, v. 25, no. 5, p. 545–554.

Grim, R.E., 1968, Clay mineralogy: New York, McGraw-Hill, 596 p.

Haggerty, Roy, 1992, Design of multiple containment remediation in the presence of rate limitations: Stanford, Calif., Stanford University, Master's thesis, 72 p.

Haggerty, Roy, and Gorelick, S.M., 1994, Design of multiple contaminant remediation—Sensitivity to rate-limited mass transfer: Water Resources Research, v. 30, no. 2, p. 435–446.

Hearne, G.A., and Litke, D.W., 1987, Ground-water flow and quality near Cañon City, Colorado: U.S. Geological Survey Water-Resources Investigations Report 87–4014, 72 p.

Hem, J.D., 1985, Study and interpretation of the chemical characteristics of natural water: U.S. Geological Survey Water-Supply Paper 2254, 263 p. [Reprinted 1992.]

Hershey, L.A., 1977, Geohydrology of the Cotter mill environment: Cañon City, Colo., Hershey-Wooderson Associates, Inc., 62 p.

Hill, M.C., 1992, A computer program (MODFLOWP) for estimating parameters of a transient, three-dimensional, ground-water flow model using nonlinear regression: U.S. Geological Survey Open-File Report 91–484, 358 p.

Hoog, F.R. de, Knight, J.H., and Stokes, A.N., 1982, An improved method for numerical inversion of Laplace transforms: Journal of Scientific and Statistical Computing, v. 3, no. 3, p. 357–366.

Hsi, C.D., and Langmuir, Donald, 1985, Adsorption of uranyl ferric oxyhydroxides—Application of the surface complexation site-bonding model: Geochimica et Cosmochimica Acta, v. 49, no. 9, p. 1931–1941.

Kaback, D.S., and Runnells, D.D., 1980, Geochemistry of molybdenum in some stream sediments and waters: Geochimica et Cosmochimica Acta, v. 44, no. 3, p. 447–456.

Langmuir, Donald, 1979, The chemistry of uranium in groundwater, *in* Uranium resource/technology; seminar II: Golden, Colorado School of Mines, p. 75–106.

Levinson, A.A., 1980, Introduction to exploration geochemistry (2d ed.): Wilmette, Ill., Applied Publishing, Ltd., 924 p.

McBratney, A.B., and Webster, R., 1986, Choosing functions for semi-variograms of soil properties and fitting them to sampling estimates: Journal of Soil Science, v. 37, no. 4, p. 617–639.

McDonald, M.G, and Harbaugh, A.W., 1988, A modular three-dimensional finite-difference ground-water flow model: U.S. Geological Survey Techniques of Water-Resources Investigations, book 6, chap. A1, 586 p.

National Oceanic and Atmospheric Administration, 1980–96, Climatological data annual summary, Colorado: Asheville, N.C., National Climatic Data Center, v. 85–101.

Neville, C.J., 1992, An analytical solution for solute transport with multiprocess nonequilibrium sorption: Waterloo, Canada, University of Waterloo, Master's thesis, 79 p.

Pyrih, R.Z., 1996, Bench-scale evaluation and field demonstration of in situ flushing and fixation of uranium and molybdenum in old ponds area: Englewood, Colo., Groundwater Technology, Inc., 74 p. plus appendices.

Runnells, D.D., Gerlitz, C.N., Davis, A., Lindberg, R.D., Maglen, R., Swanson, G., Taylor, L., Sistko, R., and McNelly, R., 1983, Contamination of ground and surface water due to uranium mining and milling—v. 3, Experimental studies and analytical techniques: Washington, D.C., U.S. Bureau of Mines, 229 p. [Contract J0295033.]

Scott, G.R., 1977, Reconnaissance geologic map of the Cañon City quadrangle, Fremont County, Colorado: U.S. Geological Survey Miscellaneous Field Studies Map MF–892, scale 1:24,000. [Reprinted.]

Stollenwerk, K.G., 1995, Modeling the effects of variable groundwater chemistry on adsorption of molybdate: Water Resources Research, v. 31, no. 2, p. 347–357.

Theng, B.K.G., 1971, Adsorption of molybdate by some crystalline and amorphous soil clays: New Zealand Journal of Science, v. 14, no. 4, p. 1040–1056.

Ticknor, K.V., 1994, Uranium sorption on geologic materials: Radiochimica Acta, v. 64, nos. 3 and 4, p. 229–236.

U.S. Environmental Protection Agency, 1984, Amendment to national oil and hazardous substance contingency plan; national priorities list, final rule: Federal Register, v. 49, no. 185, September 21, 1984, p. 37070–37090.

Vlek, P.L.G., and Lindsay, W.L., 1977, Thermodynamic stability and solubility of molybdenum minerals in soils: Soil Science Society of America Journal, v. 41, no. 1, p. 42–46.

Voss, C.I., 1984, SUTRA; Saturated-Unsaturated TRAnsport; a finite-element simulation model for saturated-unsaturated, fluid-density-dependent ground-water flow with energy transport or chemically-reactive single-species solute transport: U.S. Geological Survey Water-Resources Investigations Report 84–4369, 409 p.

W.A. Wahler & Associates, 1978, Investigations related to seepage from the existing Cotter tailings impoundments: Palo Alto, Calif., variously paged.

Watermark Computing, 1994, PEST—Model-independent parameter estimation: Oxley, Australia, variously paged.

Zielinski, R.A., Chafin, D.T., Banta, E.R., and Szabo, B.J., 1997, Use of ^{234}U and ^{238}U isotopes to evaluate contamination of near-surface ground water with uranium-mill effluent—A case study in south-central Colorado, U.S.A.: Environmental Geology, v. 32, no. 2, p. 124–136.

SUPPLEMENTAL INFORMATION

The contaminant-transport model described in this report was developed using a modified version of the USGS model code SUTRA (Voss, 1984). The model code SUTRA is a finite-element model that can simulate two-dimensional transport of heat energy or a chemically reactive solute in a saturated or unsaturated ground-water environment; density-dependent ground-water flow also can be simulated. The model domain is divided into a mesh, which consists of quadrilateral elements, where each element represents a given area of the model domain, and nodes, which are points at the corners of the elements. In simulating solute transport, users of SUTRA have the option of specifying one of three types of sorption isotherm to define the mathematical relation between the aqueous (mobile-phase) solute concentration and the solid-phase (immobile-phase) concentration of the sorbed form of the solute. The simplest sorption isotherm is the linear isotherm, where the ratio of solid-phase concentration to aqueous concentration is assumed to be constant. This ratio is called the distribution coefficient. In the other (nonlinear) isotherms, the ratio is a function of the aqueous concentration. For any of the sorption isotherms, the SUTRA method is based on an assumption of equilibrium between the aqueous phase and the solid phase (Voss, 1984).

Brogan (1991) and Haggerty (1992) modified SUTRA to allow simulation of rate-limited (non-equilibrium) sorption of the solute; they called their model code KSUTRA. The mathematical basis for the modifications to SUTRA to allow simulation of rate-limited sorption was described by Haggerty and Gorelick (1994). In KSUTRA, rate-limited sorption is specified by the use of two rate coefficients, the forward mass-transfer rate coefficient (which has units of $time^{-1}$) and the backward mass-transfer rate coefficient (which has units of $mass \times length^{-3} \times time^{-1}$) (Brogan and Gailey, 1995). The ratio of the forward to the backward mass-transfer rate coefficients is equal to the (linear) distribution coefficient (Brogan and Gailey, 1995). Thus, KSUTRA allows only a linear sorption isotherm to be simulated. In KSUTRA, the rate coefficients are specified for the model domain as a whole; no spatial variation of these parameters is possible.

For this study, the ability to specify the rate coefficients of KSUTRA as spatially variable was needed. Minor modifications to the KSUTRA code were made so that the rate coefficients could be specified on a node-by-node basis. The resulting code was called DKSUTRA in this report. To verify that DKSUTRA accurately simulated rate-limited sorption, output of DKSUTRA was compared with an analytical solution for one-dimensional, nonequilibrium solute transport (Neville, 1992).

The one-dimensional transport problem selected contains backward and forward kinetic parameters. The problem is consistent with a laboratory experiment in which a reactive tracer is introduced as a step input into a column. Specifically, the partial differential equation describing the aqueous-phase transport has the form

$$\frac{\partial C}{\partial t} + V\frac{\partial C}{\partial x} - D\frac{\partial^2 C}{\partial x^2} = -\beta\frac{\partial S}{\partial t} - \lambda C \qquad (1)$$

where

$C(x,t)$ is the dissolved-phase concentration;

V is the interstitial water velocity in the x direction;

D is the dispersion coefficient;

$\beta = \rho_b/\phi$, ρ_b is the bulk density, and ϕ is the porosity;

$S(x,t)$ is the sorbed-phase mass; and

λ is the first-order decay coefficient.

In this case, x represents the distance from the inlet end of a column of length L, and t is time since the beginning of the step input. The solid phase, being stationary, is described by the simpler equation

$$\frac{\partial S}{\partial t} = \alpha C + \kappa S \qquad (2)$$

where

$\alpha = \kappa K_d$ is the forward kinetic parameter,

κ is the first-order kinetic desorption coefficient, and

K_d is the distribution coefficient.

A Dirichlet or mixed-type boundary condition is allowed at the inlet ($x = 0$), so that

$$VC - \delta D\frac{\partial C}{\partial x} = VC_0[1 - H(t)] \qquad (3)$$

where $\delta = 0$ for a Dirichlet condition and $\delta = 1$ for a mixed a condition, and $H(t)$ is the Heaviside function [$H(t) = 1$, $t < 0$; $H(t) = 0$, $t \geq 0$]. For the outlet ($x = L$), a Neumann condition is assumed, so that

$$\frac{\partial C}{\partial x} = 0 \tag{4}$$

At the start of the step input ($t = 0$), $C(x,0)$ and $S(x,0)$ were assumed to be zero throughout the domain.

A solution to this system of equations was obtained by Laplace transforming equations 1 and 2 and solving the two transformed equations simultaneously for the Laplace transform of $C(x,t)$ (Neville, 1992). When the Laplace transform of the two boundary conditions is considered, the Laplace transform space solution, $\hat{C}(x,p)$, has the form

$$\hat{C}(\xi,p) = \frac{e^{\xi/(2\bar{D})}}{pd}[(1-\delta\bar{D}\gamma)e^{\gamma(\xi-2)} + (1+\delta\bar{D}\gamma)e^{-\gamma\xi}] \tag{5}$$

where

$\xi = (x/L)$,

p = the Laplace variate,

$\bar{D} = D/(VL)$

$d = (1-\delta\bar{D}\gamma)(1-\delta/2-\delta\bar{D}\gamma)e^{-2\gamma} - (1+\delta\bar{D}\gamma)(1-\delta/2+\delta\bar{D}\gamma)$,

$4\bar{D}^2\gamma^2 = 1+4\bar{D}(p\eta-\bar{\lambda})$,

$\eta = 1+(\beta\alpha L)/(pV+\kappa L)$, and

$\bar{\lambda} = [(\lambda L)/V]$.

For a given relative location ξ, equation 5 can be inverted numerically using the de Hoog algorithm (de Hoog and others, 1982) for any relative time tV/L. For comparison with the equivalent DKSUTRA simulation, λ and δ were set to zero.

For the comparison, a column of porous medium 1 m in length was considered. (DKSUTRA simulations were set up in metric units for the comparison.) Modeled initial conditions were that aqueous- and solid-phase concentrations were equal to zero everywhere and that flow was steady in response to a difference in hydraulic head of 0.1 m between the source end, where water was simulated as entering the column, and the sink end, where water was simulated as leaving the column. Intrinsic permeability of the porous medium was assumed to be 1.0×10^{-15} m^2; porosity was assumed to be 0.1. From Darcy's law, these parameters would produce an interstitial velocity of 1.0×10^{-8} m/s. The distribution coefficient was assumed to be 2.0×10^{-4} m^3/kg, and dispersivity was assumed to be 0.01 m. Starting at time zero, solute concentration at the source end was assumed to go from 0 to 1 (arbitrary units) instantaneously and stay at 1 for the duration of the simulation. Grain density was assumed to be 2.65 g/cm^3.

For the analytical solution, interstitial velocity was specified as 1.0×10^{-8} m/s; dispersivity was specified as 0.01 m; the distribution coefficient was specified as 2.0×10^{-4} m^3/kg; bulk density of the rock matrix was specified as 2,385 kg/m^3 (this is equivalent to a grain density of 2.65 g/cm^3 and porosity of 0.1); and the adsorption-rate coefficient was specified as 3.623×10^{-5} day^{-1} [which is equivalent to a backward mass-transfer rate coefficient of 1.0×10^{-6} (kg/m^3)/s and a bulk density of 2,385 kg/m^3 in DKSUTRA].

For the DKSUTRA model, the domain was represented as a mesh of 200 rectangular elements in a single row lined up in the direction of flow; each rectangle was 0.005 m long in the x direction (parallel to the direction of flow) and 0.01 m long in the y direction (perpendicular to the direction of flow). Specified-pressure nodes were used at the source and sink ends to maintain the difference in head at 0.1 m. The forward mass-transfer rate coefficient was specified as 2.0×10^{-10} sec^{-1} everywhere, and the backward mass-transfer rate coefficient was specified as 1.0×10^{-6} (kg/m^3)/s. The distribution coefficient, calculated as the ratio of the two rate coefficients, was 2.0×10^{-4} m^3/kg. The time step used in the simulation was 5.0×10^4 seconds (0.58 day). The simulation time was 2.5×10^9 seconds (79.2 years) and required 50,000 time steps.

For the analytical solution and the DKSUTRA results, calculated results were plotted for points at distances of 0.1, 0.4, 0.7, and 1.0 m from the source end (fig. 31). The two methods produced similar results, although some of the concentrations calculated using the DKSUTRA model were slightly less than the concentrations calculated by the analytical solution, particularly at the 0.1-m point early in the simulation. Differences between the two methods generally were small, and errors arising from the use of DKSUTRA to simulate nonequilibrium solute transport also can be expected to be small.

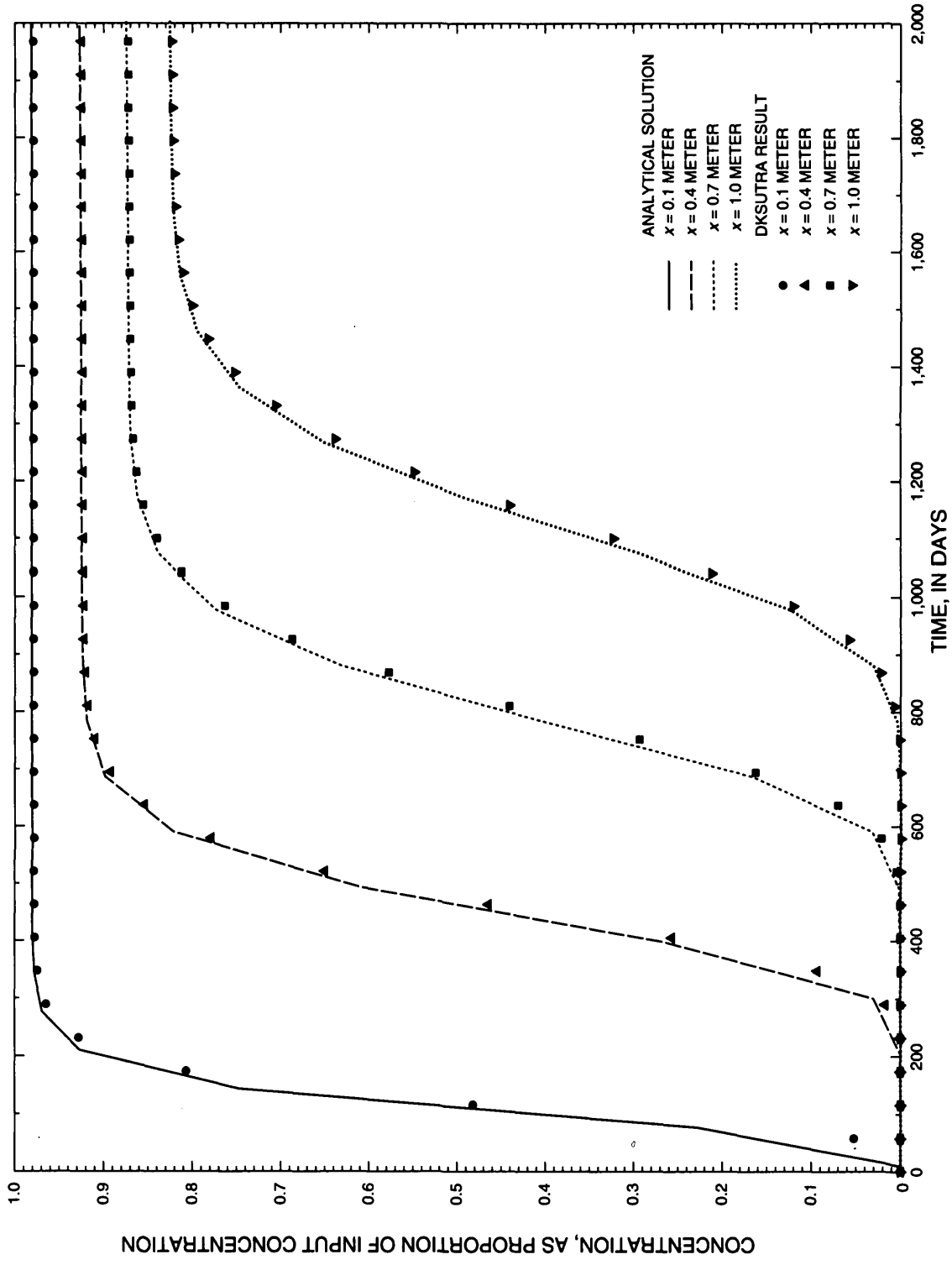

Figure 31. Concentration in a column of porous medium, calculated by DKSUTRA and an analytical solution.

☆ U.S. GOVERNMENT PRINTING OFFICE: 1999 — 773-084 / 20064 Region No. 8